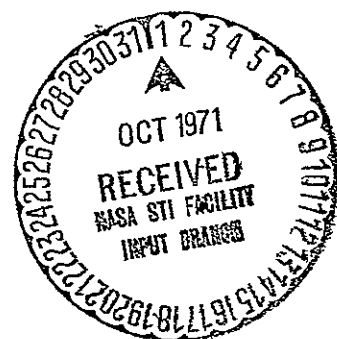
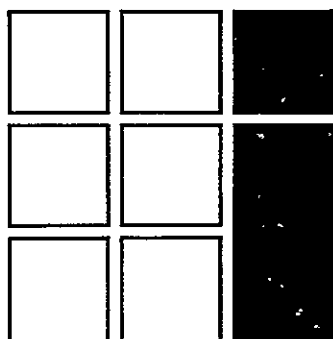


104

FACILITY FORM 602	<u>171-35775</u>	(ACCESSION NUMBER)	(THRU)
	<u>186</u>	(PAGES)	<u>G3</u>
	<u>CR-115138</u>	(NASA CR OR TMX OR AD NUMBER)	<u>21</u>
		(CATEGORY)	



# INTERMETRICS

CR-115138

SPACE SHUTTLE LANDING NAVIGATION  
USING PRECISION DISTANCE-  
MEASURING EQUIPMENT

by

William S. Widnall  
and  
H. Raymond Morth

FINAL REPORT

2 August 1971

Prepared for:

NASA Manned Spacecraft Center  
Houston, Texas  
Under Contract NAS 9-11593

## FOREWORD

This report has been prepared for NASA Manned Spacecraft Center under Contract NAS 9-11593. The technical monitor of this effort has been John F. Hanaway of the MSC Guidance and Control Division.

The principal investigator for this effort has been Dr. William S. Widnall. H. Raymond Morth developed the landing navigation simulation and conducted the simulation parametric studies. James H. Flanders investigated barometric altimeter and radar altimeter performance.

## CONTENTS

	<u>page</u>
1. INTRODUCTION AND SUMMARY	1
1.1 Study Objectives and Key Technical Questions	1
1.2 Navigation Accuracy Required	2
1.3 Landing Navigation System Design	5
1.4 Performance Results and Conclusions	8
2. SUBSYSTEM PERFORMANCE AND SOURCES OF ERROR	11
2.1 DME Performance and Sources of Error	11
2.2 Inertial Navigation Errors	16
2.3 Barometric Altimeter Errors	20
2.4 Radar Altimeter Errors	27
3. ON-BOARD NAVIGATION EQUATIONS DESIGN	31
3.1 Kalman Filter Algorithm	31
3.1.1 Notation and Standard Results	31
3.1.2 Filter Algorithm Selected	33
3.1.3 Approximate Computation of State Transition Matrix	34
3.1.4 Approximate Computation of Noise Covariance Matrix	36
3.1.5 An Advantage of the Discrete Formulation	36
3.2 State Variables: Assumed Dynamics and Disturbances	37
3.2.1 State Variables Chosen for Filter Synthesis	37
3.2.2 Assumed Stochastic Process	39
3.2.3 Transition Matrix and Noise Covariance Matrix	51
3.3 Measurement Incorporation Equations	56
3.3.1 Range-Difference Measurement	56
3.3.2 Delta-Range-Difference Measurement	62

3.3.3	Altitude-Difference Measurement	67
3.3.4	Rectification of Inertial Navigation Errors	69
3.4	Landing Navigation Initialization	70
3.4.1	Concept	70
3.4.2	Position Fix Logic	71
3.4.3	Initial Error-Covariance Matrix	76
4.	TOTAL SYSTEM DESIGN AND PERFORMANCE	81
4.1	Baseline System Performance	81
4.1.1	Landing Trajectory	81
4.1.2	Transponder Locations	84
4.1.3	Measurement Sequence	84
4.1.4	Monte Carlo Simulation	85
4.1.5	Interpretation of Results	87
4.2	Does the Approach Pattern Affect the Results?	98
4.2.1	Landing with Airport Overflight	98
4.2.2	Landing with Approach from Side	107
4.3	How Many Transponders are Required and Where?	107
4.3.1	Geometric Considerations	107
4.3.2	Inner-Approach-Transponder Placement	108
4.3.3	Lateral-Transponder Placement	115
4.3.4	Outer-Transponder Placement	118
4.3.5	Only Two Transponders	121
4.3.6	Failure Tolerance and Recommended Deployment	127
4.4	Are Additional Transponders Required for Distant Initialization?	130
4.4.1	Initialization - Range Requirement	130
4.4.2	Uncertainty After Initial Fix	131
4.4.3	Performance From Distant Initialization Through Touchdown	133

4.5	Effect of Measurement Rate on Performance	139
4.5.1	Performance With a Measurement Pair Every 5 Sec.	139
4.5.2	Recommended Measurement Rates	139
4.6	What Range and Delta-Range Accuracies Are Required?	142
4.6.1	Range-Only Performance	142
4.6.2	Performance For Various Range and Delta-Range Accuracies	145
4.6.3	Should the Delta-Range Be Procured?	149
4.6.4	Recommended Range and Delta-Range Accuracies	149
4.7	Transponder Drop-Out Before Touchdown	149
4.7.1	Simulation Results	149
4.7.2	Recommended Testing	157
4.8	Effect of a Degraded IMU	157
5.	CONCLUSIONS	161
Appendix A	- Error State Formulation of the Estimation Problem	165
Appendix B	- On Treating Delta-Range as a Range-Rate Measurement	169
Appendix C	- Compensation for Nonlinear Elongation of Measured Range	173
REFERENCES		179

## CHAPTER 1

### INTRODUCTION AND SUMMARY

#### 1.1 Study Objectives and Key Technical Questions

The Space Shuttle Vehicle must have an onboard navigation system which can determine vehicle position and velocity during the many mission phases, including. ascent into earth orbit, parking orbit, rendezvous, deorbit, entry, and approach and landing. A possible navigation subsystem to be used in conjunction with an onboard inertial navigation system (INS) is a set of distance measuring equipment (DME). The use of precision DME of the Cubic type CR-100, modified to extend its range to 2800 km (1500 nautical miles) appears quite attractive. By means of range measurements to transponders at known locations on the ground, the onboard navigation can update the state vector after earth orbit insertion (perhaps even during the boost). Precise range measurements to a transponder on the Space Station, can provide the in-plane rendezvous navigation accuracy required. Measurements to the ground transponders can provide the state vector required for the deorbit maneuver.

It is expected that the same onboard equipment, with additional transponders located near the landing site, can be used for the approach and landing navigation. If this is possible, it permits a commonality of navigation equipment that helps minimize cost, weight, volume, and power. A preliminary quantitative estimate of the cost saving is presented by Bettwy of TRW in Ref. [1-1].

The principal objective of this study has been to determine if precision DME, aiding the inertial navigation, can be used to meet the Shuttle landing navigation accuracy requirements. The study approach has been to design alternate navigation configurations, to evaluate the effectiveness of the alternate configurations by means of analysis and simulation, and finally to recommend the best system configuration.

Some of the additional technical questions that have been answered by this study are:

- Can a navigation filter be designed to give satisfactory performance from initial updating (after hypersonic entry) through touchdown and rollout?

- How many transponders are required and what is the best transponder deployment geometry (considering both failure tolerance and performance)?
- Is an independent source of altitude data required (such as derived from air data or from a radar altimeter)? If so, what accuracy specification must be placed on this subsystem?
- What performance is lost if the delta-range ("range-rate") circuits are not included in the DME subsystem?
- Can the Cubic CR-100 DME be modified to meet the 2800-km- (1500-nautical-mile) range requirement, still utilizing omnidirectional antennas and solid-state technology?
- What is a preliminary antenna concept for the Space Shuttle installation?
- What technology risk and procurement costs are associated with the recommended design?

The Cubic Corporation has provided close support to Intermetrics in carrying out this study. Cubic has supplied the models for the CR-100 DME performance used in the total navigation system analyses and simulations. Cubic has carried out a complete preliminary design of the modifications to the CR-100 required to meet the specific Shuttle requirements. The results of the Cubic investigations are presented in a separate volume, Ref. [1-2].

## 1.2 Navigation Accuracy Required

The navigation accuracy required during the approach and landing becomes progressively more stringent as the footprint capability shrinks. Touchdown has the most demanding accuracy specification.

Clark of TRW and Dyer of NASA/MSC in Ref. [1-3] discuss the altitude and downrunway total navigation, guidance, and control (NGC) tolerable dispersions at touchdown. The nominal touchdown sink rate is .9 meter/sec. The maximum tolerable sink rate (beyond which there might be structural failure) is 2.4 m/sec. The minimum acceptable sink rate is .45 m/sec. A smaller sink rate than the minimum would permit the Shuttle to float down the runway an unpredictable distance before landing



gear contact. The difference between the nominal touchdown sink rate and the minimum acceptable sink rate determines the tolerable  $3\sigma$  dispersion in sink rate (or altitude rate) at touchdown: .45 m/sec. The  $1\sigma$  tolerable altitude rate dispersion is .15 m/sec. It is noted that increasing the nominal sink rate would increase the tolerable dispersion.

The nominal speed at touchdown is 90 meters/sec. The touchdown and rollout distance dispersion is a function of the speed error, altitude error and downrunway error. For a wet runway (coefficient of friction 0.2) of 3 km (10,000 ft.) length and no drag chute, Reference [1-3] states that tolerable  $1\sigma$  dispersions are: speed error 3.3 m/sec, altitude error 3 meters, down-runway error 72 meters.

Not discussed in the reference are the cross-runway position and velocity requirements. Let us assume a 45 meter wide runway and a landing gear width of 15 meters. The Shuttle may touchdown no farther than  $\pm 15$  meters from the runway centerline or the landing gear will be off of the runway. This establishes the tolerable  $1\sigma$  dispersion at 5 meters. Furthermore, if there is a cross-runway velocity at touchdown, the Shuttle may roll off the runway. Assume the time required to steer-out any cross-runway velocity after touchdown is of the order of 10 sec. For the rollout peak lateral error to be no greater than the basic 5 meter  $1\sigma$  tolerable lateral error, the lateral velocity must be no greater than .5 m/sec  $1\sigma$ .

The Shuttle touchdown requirements are summarized in Table 1-1. The first column presents the tolerable total NG&C error. It would be desirable to have the navigation error absorb only a small part of the total error budget. If the navigation error component specification is set at one-third of the total budget, then its contribution to the total sum of squared errors will be almost negligible (one-ninth). Accordingly, the navigation specification for altitude, altitude rate, cross-runway position, and cross-runway velocity have been set at one-third of the total tolerable  $1\sigma$  error. The down-runway position and speed navigation specifications have been set tighter than one-third, since no difficulty is anticipated in achieving tighter goals. The navigation touchdown accuracy specifications are summarized in the second column of Table 1-1.

Table 1-1 SHUTTLE TOUCHDOWN REQUIREMENTS

	Tolerable Error ( $1\sigma$ ) Nav. Guid. & Cont.	Navigation Accuracy Required ( $1\sigma$ )
Altitude	3 m	1 m
Altitude Rate	.15 m/sec	.05 m/sec
Cross-runway position	5 m	1.7 m
Cross-runway velocity	.5 m/sec	.17 m/sec
Down-runway position	72 m	10 m
Speed	3.3 m/sec	1 m/sec

### 1.3 Landing Navigation System Design

A functional block diagram of the onboard portion of the landing navigation system is presented in Fig. 1-1. The critical sources of navigation information are the inertial measurement unit and the precision radio distance measuring equipment.

The inertial measurement unit maintains a coordinate system with respect to which the vehicle attitude and non-gravitational acceleration (specific force) are measured. The accelerometer data is corrected according to the known instrument misalignments and scale factor errors. The measured specific force is combined with the assumed gravitational acceleration and is integrated to produce the indicated vehicle velocity and position. This inertial navigation integration is carried out at a high frequency (10 to 20 steps per sec) to provide an accurate nearly continuous indication of velocity and position. The known gyro drift rates and g-sensitive drift-rate coefficients are used to estimate the change in IMU platform alignment. The estimated drift rate plus the computed angular velocity of the computational coordinate system may be used to generate torquing signals to the platform gyros (or the platform may be left untorqued and coordinate rotations are integrated in the software). If the platform is to be torqued, the torquing commands are corrected according to the known gyro input axis misalignments and gyro torquer scale factor errors.

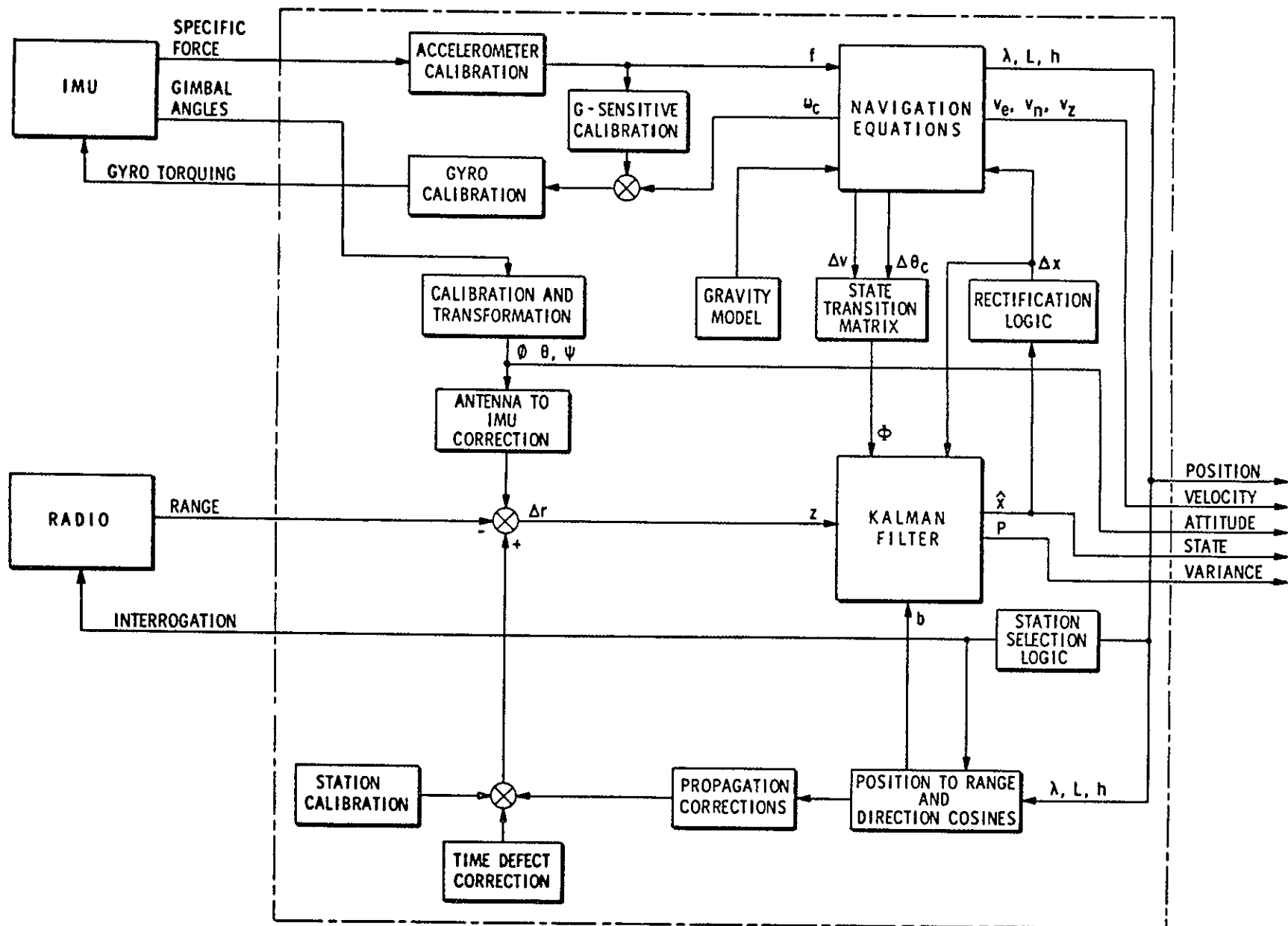
The velocity and position indicated by the inertial navigation is degraded by several sources of error:

- Uncertainty in the calibration of the various accelerometer and gyro instrument errors.
- Error in the assumed gravitational model.
- Initial errors in platform alignment and in indicated velocity and position.

The various sources of inertial navigation error are discussed in Section 2.2. It is the nature of inertial navigation errors (at speeds small compared with orbital velocity) that the horizontal position error grows at a rate of a few kilometers per hour. The vertical errors are unstable.

The touchdown navigation accuracy required is of the order of 1 meter. To obtain this positional accuracy relative to the runway, external position information is mandatory. The precision DME measures the distance between the vehicle and transponders on the ground, whose locations are known. The

Fig. 1-1 DME-AIDED INERTIAL NAVIGATION



measurement is based on the phase delay between the modulation transmitted by the on-board interrogator and the modulation received from the ground transponder. This delay is converted into a range measurement according to the assumed speed of light in the atmosphere. Additional calibration is applied for the known transponder delay characteristics. As accuracy better than one meter is desired, the measurement must also be corrected for the displacement of the vehicle radio antenna with respect to the inertial measurement unit. Also available is a delta-range measuring capability which integrates the Doppler-shift between the transmitted and received carrier frequencies.

The range and delta range measured by the DME is degraded by several sources of error:

- Uncertainty in the propagation corrections.
- Uncertainty in the transponder bias calibration.
- Multipath random error.
- Equipment random error.
- Transponder placement survey error.

These sources of DME error are discussed in Section 2.1.

The most stringent accuracy specifications at touchdown are for the altitude and altitude-rate errors. If the DME-aided inertial navigation alone is not sufficiently accurate to meet the touchdown specification, alternate sources of accurate altitude information would be required. In Sections 2.3 and 2.4 the performance of barometric altimeters and radar altimeters are discussed. It is concluded that barometric altimeters are not sufficiently accurate to help meet the landing navigation accuracy specification. Radar altimeters are found to have excellent accuracy over the runway, but uncertain performance over the terrain preceding the runway.

Kalman filter theory provides an excellent conceptual framework for designing the on-board equations needed to combine the inertial navigation and radio DME data. A review of standard Kalman filter equations is presented in Section 3.1. The choice of navigation errors to be estimated explicitly by the Kalman filter is presented in Section 3.2. In general, the state variables selected are all slowly varying quantities. This permits operating the Kalman filter at a much slower sample rate than the inertial navigation equations, with negligible increase in navigation errors. The information flow is as

illustrated in Fig. 1-1. Based on the position indicated by the inertial navigation equations, the range to the selected transponder is calculated. The difference between the DME-measured range and the onboard-computed range is the actual "measurement" utilized by the Kalman filter. The range-difference measurement is weighted according to the relative size of the navigation uncertainty compared with the assumed measurement random error and is used to improve the estimate of the inertial navigation errors. The estimated navigation errors are used to correct (rectify) the indicated position and velocity of the inertial navigation equations.

Given special attention in Chapter 3 are specific design problems that must be solved to develop a reliable working navigation filter. A low number of filter state variables is selected to minimize the computational requirements. A systematic procedure for modeling the many sources of navigation error is utilized. A compensation for nonlinear difficulties is included.

Section 3.4 presents the landing navigation initialization equations, appropriate for the very large (tens of kilometers) initial position navigation error after hypersonic entry.

#### 1.4 Performance Results and Conclusions

The basic tool utilized to evaluate navigation system performance is a detailed simulation of the various sources of navigation error, the proposed onboard equations design, the vehicle trajectory, and the transponder deployment. The simulated performance results are presented in Chapter 4.

A baseline transponder deployment and system design is presented in Section 4.1. Two transponders are placed under the final approach path and a third transponder is placed to the side. The performance results with the baseline system are excellent. The baseline DME-aided inertial system meets the landing navigation accuracy specification. There is no need for an independent source of altitude data.

Alternate approach paths are tested in Section 4.2 and it is shown that the results at touchdown are not a function of the initial terminal area approach pattern.

Many alternate transponder locations are tested in Section 4.3. It is found that three working transponders are needed for consistent navigation performance. The simulation results with only two transponders showed several difficulties. Because of the very tight altitude and altitude-rate specification, two transponders under the final approach path are required. The lateral transponder delivers the necessary cross-runway accuracy. The best locations for the transponders are presented. Failure tolerance requires some level of deployment redundancy. A recommended deployment of ten transponders is presented which permits landing from either direction on the longest runway and has a satisfactory probability of supporting a successful landing.

The range-from-the-airport at which initial updating must begin is discussed in Section 4.4. For a normal entry, initial updating can be delayed until within 150 km from the airport. Certain aborts however, may require larger initialization ranges. It is shown the radio blackout and radio horizon present no problem. The uncertainty after landing navigation initialization is computed for various points within a 150 km radius of the airport. Two long simulations of the complete landing navigation - from initialization at 150 km from the airport through touchdown and rollout - are presented. The onboard equations as designed deliver completely satisfactory performance.

The effect of measurement rate on performance is presented in Section 4.5. With the exception of the transponder overflights on final approach, the measurement rate requirements are very relaxed. Increasing the measurement rate is shown to do little to improve landing navigation performance.

The performance without the precise delta-rate measurement circuits does not meet the specification, as shown in Section 4.6. Unless the navigation accuracy specification can be relaxed, the delta-range circuits should be included in the radio DME procurement. The recommended specifications for range and delta-range accuracy are presented.

The effect of early transponder dropout before touchdown is presented in Section 4.7. The effect of degraded IMU performance is presented in Section 4.8.

The principal conclusions of this effort are summarized in Chapter 5.

## CHAPTER 2

### SUBSYSTEM PERFORMANCE AND SOURCES OF ERROR

The primary sources of landing navigation information will be the specific-force measurements from the accelerometers in the inertial measurement unit (IMU) and the range plus delta-range measurements from the precision distance measuring equipment (DME). The performance and sources of error in the DME and IMU are discussed in this chapter. Also discussed are the performance of alternate sources of altitude information: barometric altimeters and radar altimeters.

#### 2.1 DME Performance and Sources of Error

The Cubic Corporation Model CR-100 precision range/delta-range measurement set represents the state-of-the-art in highly accurate DME. The CR-100 employs an airborne interrogator and several ground-placed transponders. The interrogators and transponders operate on common frequencies. The transponder whose response is desired is activated by a discrete transmitted address code. Range is determined by continuous-wave phase comparison. As many lower frequency modulation tones are employed as necessary to achieve an unambiguous range measurement at the maximum range. The delta-range measurement is an integration of the carrier-frequency-Doppler shift. The transponder selection, the duration of the delta-range integration interval, the time at which the range and delta-range measurements are taken are all under control of the on-board central computer. This provides maximum flexibility to optimize measurement selection logic, measurement rates, and IMU/DME data synchronization. A CR-100 variation, designed to meet Space Shuttle requirements, is presented in Ref. [2-1].

The most stringent navigation accuracy requirements in the Shuttle entry and landing are associated with the final approach, touchdown, and rollout. The accuracy of the CR-100 during final approach and landing is summarized in Tables 2-1



and 2-2, from Ref. [2-1].

The largest source of random range error is possible multipath error. For the large index of modulation used in the CR-100, it is expected that multipath error will be no larger than 0.9 meter  $1\sigma$ . Analysis and experimental data presented in Ref. [2-1] support this expectation. At high elevation angles, the multipath error should be negligible. The other non-multipath random errors total 0.2 meter  $1\sigma$ .

The retardation of the speed-of-light by the atmosphere is about 300 parts per million at sea level. At higher altitude the retardation is less. Assuming a standard day (temperature, pressure, humidity), the measured range can be corrected such that the residual uncertainty in measured range is 50 ppm  $1\sigma$ . For example, on final approach 10 km from a transponder, the propagation error after correction is 0.5 meter  $1\sigma$ . Even better accuracy (of the order of 10 ppm) can be achieved if the actual temperature, pressure, and humidity in the terminal area is utilized in correcting the measured range. However, the performance results in this study show that this additional accuracy is not required.

The transponders must be carefully placed at known surveyed locations. If the positions of the transponders are determined by survey to an accuracy of 10 ppm of distance from the runway, then the effect of survey error should be negligible compared with the 50 ppm propagation error.

The delta-range measurement performance, shown in Table 2-2, has a total random error of .006 meters. This is based on theoretical analysis. The discussion in Ref. [2-1] adds that high acceleration/high speed tests have shown a somewhat larger random error of .016 meters.

A typical value for the propagation error effect in a delta-range measurement while the vehicle is on final approach may be calculated by assuming a range rate to a transponder of 100 m/sec and a 10 sec delta-range measurement interval. The 50 ppm sea-level propagation error for the change in range of 1000 meters is 0.05 meter.

Not included in the range and delta-range error budgets of Tables 2-1 and 2-2 are: IMU-to-antenna-position correction error, vehicle bending error, inertial navigation position quantization, and measurement-time uncertainty. These effects can be held small compared with the 0.2 meter  $1\sigma$  non-multipath range random error. But they cannot be held small compared

Table 2-1 CR-100 RANGE ERROR BUDGET DURING FINAL APPROACH  
AND LANDING

I. RANDOM ERROR (including rapidly varying error)

<u>Error Source</u>	<u>1σ Magnitude</u>
A. Ranging error due to finite signal-to-noise ratio and equipment added noise	0.09 meter
B. Phase shift over dynamic range of ranging operations	0.15 meter
C. Phase shift of interrogator due to vibration, shock and g-loading	Negligible
D. System error due to craft dynamics (600 m/sec and 300 m/sec <sup>2</sup> )	0.06 meter
E. Multipath error in ground-to-air range links	0.9 cos ε meter
F. Digitization Error	<u>0.09 meter</u>
RSS TOTAL	$[ (.9 \cos \epsilon)^2 + (.2)^2 ]^{1/2}$ meter
where ε = Elevation Angle	

II. BIAS ERROR (including slowly varying error)

A. Calibration (Equipment)	0.3 meter
B. Phase Shift with Temperature	0.15 meter
C. Scale Factor	
1. Stability of crystal oscillators	0.1 ppm
2. Uncertainty in velocity of light	0.5 ppm
D. Propagation	
Sea-level uncertainty after standard correction	50.0 ppm

Table 2-2 CR-100 DELTA-RANGE ERROR BUDGET DURING FINAL APPROACH AND LANDING

I. VELOCITY-INDEPENDENT RANDOM ERROR

<u>Error Source</u>	<u>1<math>\sigma</math> Magnitude</u>
A. Delta-range error due to finite signal-to-noise ratio and equipment added noise	.003 meter
B. System error due to craft dynamics a = 300 meter/sec <sup>2</sup>	.0003 meter
C. Digitization Error	.004 meter
D. Multipath	<u>.003 meter</u>
RSS TOTAL <sup>1</sup>	.006 meter <sup>1</sup>

II. VELOCITY-DEPENDENT ERROR

A. Stability of Crystal Oscillator	1 ppm
B. Uncertainty in Velocity of Light	0.5 ppm
C. Propagation	
Sea-level uncertainty after standard corrections	50.0 ppm

---

<sup>1</sup> Measurement errors under test have been observed at .016 meter 1 $\sigma$ .

Table 2-3 Model for Range and Delta-Range Errors  
Utilized in Simulation

range error = $e_{b_1} + r_1 e_p f(h) + e_m + e_r$		
delta-range error = $\Delta r_1 e_p f(h) + e_{\Delta r}$		
$e_{b_1}$	1-th transponder bias	0.3 meter $1\sigma$
$e_p$	propagation error	$50 \times 10^{-6} \text{ } 1\sigma$
$e_m$	multipath random error	$0.9 \cos \varepsilon \text{ meter } 1\sigma$
$e_r$	other random error	0.2 meter $1\sigma$
$e_{\Delta r}$	delta-range random error	0.1 meter $1\sigma$
$r_1$	actual range to transponder 1	
$\Delta r_1$	actual change-in-range to transponder 1	
$f(h) = (1 - e^{-h/h_s}) / (h/h_s)$		
$h_s$	scale height	6900 meters

with the 0.006 meter  $1\sigma$  delta-range random error. Therefore, the extremely precise delta-range data cannot be fully exploited. A degraded accuracy of 0.1 meter  $1\sigma$  has been utilized in this study as the total delta-range random error from all sources.

The mathematical model utilized in the simulations to represent the range and delta-range measurement errors is summarized in Table 2-3. The decrease in the propagation error with altitude is modelled by the function  $f(h)$  which has maximum value unity at sea level. This exponential model is similar to the error model recommended in Appendix B of Ref. [2-1]. The random errors  $e_m$ ,  $e_r$ , and  $e_{\Delta r}$  are generated for each measurement by a Gaussian random number generator. The transponder biases  $e_{b1}$  and the propagation error  $e_p$  are selected once then held constant through the simulation. The actual evolutions of ranges, delta-ranges, and altitude are utilized.

## 2.2 Inertial Navigation Errors

It is assumed that the Space Shuttle will have three or four inertial measurement units aboard (the total number required is determined by failure considerations). These IMUs will have performance characteristics comparable to present generation "off-the-shelf" equipment. The assumed IMU component errors are as presented in Table 2-4. These data are from Ref. [2-2] (except that a distinction has been made between g-sensitive drift caused by acceleration along the spin axis and the input axis).

A model of an IMU having the baseline component-error uncertainties has been implemented in the landing navigation simulation. Several implementation decisions are necessary to proceed from the component errors of Table 2-4 to a simulated inertial navigation system.

It is assumed that the IMU is a gimballed system (not a strapdown system). Two INS mechanizations are possible: 1) the platform maintains a constant alignment in inertial space, 2) the platform is torqued to maintain level. The first mechanization is usually selected for spaceflight. The inertial navigation equations are very simple in inertial coordinates. The second mechanization is usually selected for ship or aircraft applications. By maintaining level, the IMU components may be kept in the most favorable orientation with respect to the persistent  $1g$  specific force vector. The disadvantage of the level mechanization is the greater arithmetic complexity of the inertial navigation equations in rotating coordinates.

Table 2-4 BASELINE IMU COMPONENT ERRORS

Error	Uncertainty ( $1\sigma$ )
Gyro	
g-insensitive drift rate	.03°/hr
g-sensitive drift (input axis)	.10°/hr/g
g-sensitive drift (spin axis)	.03°/hr/g
torquer scale factor	200 ppm
input axis alignment	1 arc min
Accelerometer	
bias	$5 \times 10^{-4}$ m/sec <sup>2</sup>
scale factor	100 ppm
input axis alignment	15 arc sec

It is not known which implementation will be selected for Shuttle. In the simulation we have assumed a local level implementation with wander azimuth. That is, the platform is torqued to maintain level, but the azimuth gyro is not torqued. The alignment of the platform with respect to north (the wander angle) is calculated in the navigation equations.

There are two different types of IMU platforms: those that rotate some of their components (such as the Delco Carousel IV) and those that do not (such as the Litton LTN-51 or Singer/Kearfott KT-70). It was decided not to utilize a detailed simulation of the Carousel IV available from an earlier program, Ref. [2-3]. The greater complexity of the rotating gyros and accelerometers would complicate the task of relating navigation results to individual instrument errors. The prototype platform selected for simulation in this study was the KT-70.

The KT-70 utilizes two two-degree-of-freedom gyroscopes (rather than three single-degree-of-freedom gyros). When the platform is level, one gyro has its spin-axis horizontal and the other gyro has its spin-axis vertical. The spin-axis-vertical gyro feeds roll and pitch information to the platform stabilization loops, while the other gyro supplies azimuth information. Test data on the performance of the KT-70 gyros (supplied by Singer) indicates that the spin-axis acceleration sensitive gyro drift rate in a 1g field is about the same level as the g-insensitive drift rate. The input-axis acceleration sensitive drift is larger. Hence, the choice of data presented in Table 2-4.

In the Monte-Carlo simulations the IMU component errors are selected at the beginning of each run by a random number generator according to the standard deviations given in Table 2-4. In the single-case simulations, the IMU utilized generally has all error coefficients of value plus 1 $\sigma$ . However, input axis misalignments of all plus 1 $\sigma$  are not used as this maintains input axis orthogonality, which is not realistic. Therefore, both plus and minus 1 $\sigma$  misalignments are utilized such that the gyro and accelerometer input axes are each skewed toward the other two axes.

The azimuth alignment of the platform at the beginning of the simulation is such that the spin axis of the azimuth gyro points north.

The inertial navigation equations have an imperfect mathematical model for the gravitational acceleration. This is an additional source of inertial navigation error. The local variations in the direction of the gravity vector are called the easterly and northerly deflections of gravity. The local variation in gravity magnitude is called the gravity anomaly. The landing navigation simulation utilizes the gravity deflection and anomaly model suggested in Ref. [2-3]. The error in each of the three gravitational acceleration components is modeled by two terms: a local mean value and a local random variation having a certain standard deviation and correlation distance. The data assumed is presented in Table 2-5.

Table 2-5 GRAVITY VARIATIONS IN THE TERMINAL AREA

Component	Mean value (m/sec <sup>2</sup> )	Standard Deviation (m/sec <sup>2</sup> )	Correlation Distance (km)
East deflection	$2 \times 10^{-4}$	$2.6 \times 10^{-4}$	18.5
North deflection	$2 \times 10^{-4}$	$1.7 \times 10^{-4}$	18.5
Anomaly (magnitude)	$2 \times 10^{-4}$	$3.5 \times 10^{-4}$	110

The landing navigation simulations begin after hypersonic entry during the approach to the terminal area. At this point in time it is assumed the platform alignment is in error by 1.5 milliradian  $\sigma$  about each axis. The inertial navigation velocity errors are 10 m/sec  $\sigma$  in each direction. The inertial navigation position errors are 30 km  $\sigma$  in the east and north directions and 3 km  $\sigma$  in altitude. The smaller altitude error assumes that the measured lift and drag acceleration has been used to infer the altitude. It will be shown that the exact values of these assumed initial errors (after hypersonic entry) have little influence on the final approach and touchdown navigation accuracy.



## 2.3 Barometric Altimeter Errors

It is recognized that during final approach, flare, and touchdown, the DME-aided inertial navigation system does not have consistently good radio-altitude-measuring geometry. The navigation must rely on the inertial navigation to extrapolate the altitude and altitude rate from the last transponder overflight. If satisfactory performance cannot be achieved with the DME-aided inertial system, one would seek additional sources of accurate altitude information. One candidate source would be the barometric altitude from the air-data system. What level of accuracy can be obtained from barometric altimeters?

It is helpful to review the basic atmospheric physics that influences barometric altimeter performance. The incremental change in pressure  $dp$  for an incremental change in height  $dh$  is governed by the hydrostatic equation

$$dp = -\rho g dh \quad (2-1)$$

where  $\rho$  is the atmospheric density and  $g$  is the acceleration of gravity. From the ideal gas law, the density may be expressed as

$$\rho = \frac{pW_m}{RT} \quad (2-2)$$

where  $W_m$  is the molecular weight (the mass of one mole) of air,  $R$  is the universal gas constant, and  $T$  is the absolute temperature. Combining Eqs. (2-1) and (2-2) gives

$$d(\ln p) = -\frac{gW_m}{RT} dh \quad (2-3)$$

It is clear that the atmospheric pressure is approximately exponential, because if one neglects the variation of gravity and temperature with altitude, the integral of Eq. (2-3) is

$$p = p_o e^{-\frac{gW_m}{RT} h} \quad (2-4)$$

where  $p_0$  is the sea-level pressure. A more exact tabulation of pressure versus altitude can be constructed by integrating numerically Eq. (2-3) using standard models for the variation of gravity and temperature with altitude. Such tables are presented in Ref. [2-4].

The pressure at the surface of the earth varies from day to day and from location to location. If an altimeter has the wrong value for the sea-level pressure, it will indicate the wrong altitude. Assuming the exponential atmosphere of Eq. (2-4) an altimeter should be a logarithmic detector and should present

$$h = h_s \ln p_0 - h_s \ln p \quad (2-5)$$

where the scale height  $h_s$  is

$$h_s = \frac{RT}{gW_m} \quad (2-6)$$

If the assumed sea-level pressure  $p_0$  is in error by  $\Delta p_0$ , then the indicated altitude will be in error by

$$e_{p_0} = \frac{h_s}{p_0} \Delta p_0 \quad (2-7)$$

Note that for the exponential atmosphere, this error is independent of altitude.

The sea-level pressure deviation-from-standard-pressure varies as one travels from region to region. This is related to the familiar pattern of isobars that one sees on a weather map. Ref. [2-5] shows a typical contour map of the 500 millibar pressure surface over the continental United States and Atlantic. The altitude of this constant-pressure surface varies from 5400 meters in a "low" over Newfoundland to 5880 meters in a "high" over Bermuda. These locations are about 2000 kilometers apart. The average value of the gradient between these locations is therefore 0.2 meters of altitude per kilometer of horizontal distance.

A smaller error effect, also related to the pressure gradient, is due to the motion of the weather system from West to East. At a fixed location (such as the airport) this causes

a variation of the indicated altitude at a rate typically about 10 meters per hour.

It is clear from Eq. (2-3) that the difference in the height of two surfaces of constant pressure is proportional to the mean temperature of the layer of air separating them. Assuming the exponential atmosphere of Eq. (2-4), one can show that the error  $e_{temp}$  in the indicated altitude is

$$e_{temp} = \frac{\Delta T}{T} h \quad (2-8)$$

where  $\Delta T$  is the error in assumed temperature and  $T$  is the standard temperature. Consider a typical temperature error to be  $10^\circ\text{C}$  with standard temperature about  $300^\circ\text{K}$ . In this case the altimeter error is 3% of the indicated altitude.

The exponential atmosphere assumes a constant temperature. Actually the temperature decreases with altitude at a lapse rate of about  $0.6^\circ\text{C}$  per 100 meters. Above the tropopause at 10 km, the temperature holds constant at about  $-40^\circ\text{C}$ . Because of the temperature variation, Eq. (2-8) is not strictly correct. However, it is approximately correct if one defines  $\Delta T$  to be the average deviation of the temperature from the standard lapse rate profile.

In the above discussions of meteorological errors, the pressure under consideration was the static pressure (that is, the pressure at zero aircraft velocity). One must infer this static pressure from measurements taken in the moving aircraft. Because of the variations in the air speed on the surfaces of the aircraft, the actual pressure on the aircraft can be higher or lower than the free-stream pressure. The difference in pressure is called the static defect. Ref. [2-6] discusses this source of error. The static defect at a particular location has been observed to be proportional to the dynamic pressure  $Q$ . Hence, it is convenient to express static pressure errors in coefficient form as

$$C_p = \frac{p - p_s}{Q} \quad (2-9)$$

where  $p$  is the pressure at the static port,  $p_s$  is the free-stream static pressure (quantity to be measured) and  $Q$  is the dynamic pressure. For a properly located port (such as a port on the side of a nose boom) the static pressure coefficient  $C_p$  is of the order of 0.01 for both subsonic and supersonic flight. At Mach 1, however, the fluctuations in  $C_p$  can be as large as 0.3.

It can be shown, assuming the exponential atmosphere, that the altimeter error is of the form  $e_{sp} = C_{sp} v^2$ , where the coefficient  $C_{sp}$  is a constant (not a function of altitude or density). A typical value for  $C_{sp}$  is  $5 \times 10^{-4} \text{ m/(m/s)}^2$ .

Additional sources of static pressure measurement error are discussed in Ref. [2-7]. Quoting from this reference,

"The static pressure source hole is located flush with the aircraft skin in an area of reasonably constant cross-section. In addition to boundary layer effects, the static source hole is extremely sensitive to streamline disturbance caused by the wing and fuselage in different attitudes. The best static source hole was formerly found by flight testing but, for economic reasons, is now determined in the wind tunnel using models of both the aircraft and the wind conditions. Both pitot and static probes are affected by adiabatic temperature change as a result of pressure variations and both are influenced by large pressure changes from ground cushion effect at low altitudes "

One avionics systems manager for a major transport aircraft builder comments [2-8] on a known tendency for  $\Delta p/\Delta h$  at the static source to go momentarily positive during takeoff.

The problem of static source calibration was investigated further by phone conversations with test instrumentation personnel at another major aircraft builder [2-9], [2-10]. The following technique was described. Static sources are evaluated in the wind tunnel. When flight tests being, a master static source is provided by trailing a cone from the test aircraft. This is calibrated stadiametrically by over-flying a vertically-oriented camera on the ground. On-board calibration of static sources is obtained by measuring the  $\Delta p$  between the master source and the proposed operational source. This entire operation yields uncertainties in the region of 1 to 3 meter one sigma, for steady state conditions.

The static pressure is led to the electrical transducer by means of tubing. The static pressure in the cavity of the instrument adjusts to the static pressure at the port by the flow of air through the tubing. Ref. [2-6] indicates that the time constant for a typical aircraft installation is about 0.25 sec. At an altitude rate of 10 meters/sec, the altimeter lag would be 2.5 meters. It is assumed that one can compensate this error source so that the remaining uncertainty is negligible.

The last category of errors are the instrument errors, especially the transducer errors in converting the static pressure in the cavity into an electrical signal. A good pressure transducer has good linearity, good repeatability, and low hysteresis. It must be insensitive to vibration, acceleration, corrosion, humidity, and changes in ambient temperature. An extremely high quality transducer would be required for Shuttle if it is to assist the navigation in meeting the 1 meter  $1\sigma$  altitude accuracy specification at touchdown. It is assumed that instrument accuracy of the order of 1 meter  $1\sigma$  can be obtained.

The typical level of the various sources of error are summarized in Table 2-6.

Table 2-6 BAROMETRIC ALTIMETER ERROR SOURCES

Error Source	Uncertainty ( $1\sigma$ ) (meters of altitude)
Gradient of constant pressure surface	0.2 m/km horiz. dist.
Time-variation	10 m/hour
Non-standard lapse rate	30 m/km altitude
Static pressure defect	$5 \times 10^{-4}$ m/(m/sec) <sup>2</sup>
Instrument error	1 m

Two distinct methods of utilizing barometric altimeter data can be considered for Shuttle landing navigation. In the first method, one estimates the altimeter error bias during the last radio transponder overflight. The change in indicated barometric altitude after the overflight is then hopefully an accurate source of true altitude. Assume the inner approach transponder is located 3 km from touchdown. Assume the gliding Shuttle at this point is at an altitude of 300 meters and a speed of 110 m/sec. Assume at touchdown the speed is 80 m/sec. Then, the navigation accuracy of this method would be as summarized in Table 2-7.

Table 2-7 BAROMETRIC ALTIMETER ERROR AT TOUCHDOWN,  
EXTRAPOLATING RADIO FIX ON FINAL APPROACH

Error Source	Uncertainty ( $1\sigma$ ) (meters)
Radio altitude uncertainty at transponder overflight (bias and random)	.4
Gradient of constant pressure surface	.6
Time variation of pressure-altitude at airport	.1
Non-standard lapse rate	9.0
Static pressure defect	2.8
Instrument errors	<u>1.0</u>
Root sum square all sources	9.5

The largest source of error is due to the non-standard lapse rate. It might be possible to reduce this source of error by telemetering to the Shuttle the actual temperature profile of final approach, based on measurements taken shortly before landing. This would be an undesirable operational procedure. The next largest source of error is the static pressure defect. It is difficult to argue that better horizontal flight test procedures for Shuttle will reduce this source of error. We conclude that the barometric altimeter is not sufficiently accurate for altitude navigation to touchdown by means of the first method.

The second method of utilizing a barometric altimeter is to measure precisely the pressure altitude at the touchdown point and to telemeter the appropriate altimeter setting to the Shuttle shortly before it lands. Assume this is done 6 min before touchdown. The navigation accuracy of this method is summarized in Table 2-8.

Table 2-8 BAROMETRIC ALTIMETER ERROR AT TOUCHDOWN  
WITH TELEMETERED ALTIMETER SETTING

Error Source	Uncertainty ( $1\sigma$ ) (meters)
Time variation of pressure altitude at airport	1.0 m
Static pressure defect	3.2 m
Instrument errors	<u>1.0 m</u>
Root sum square, all sources	3.5 m

The large lapse-rate error of the first method is eliminated. The static defect error associated with the 80 m/sec assumed touchdown speed is the largest source of error. The assumed 1.0 m instrument error is probably optimistic, as this is not the instrument repeatability for a short glide from the inner approach transponder (as in the first method) but is the instrument repeatability since its last preflight calibration.

While the lapse-rate error does not influence the altitude error at touchdown (in the second method), it does influence the altitude-rate error. The 9 meter altitude-error change experienced during the last 30 sec before touchdown (Table 2-7) is a 0.30 m/sec error in altitude rate. This exceeds the altitude-rate specification of 0.05 m/sec.

Reference [2-11] reports flight tests with the barometric altimetry systems aboard a Boeing 720 and a Convair 880 on instrument landing system (ILS) approach paths. Of particular interest was, could barometric altimetry be used as an accurate indication of the 30 meter (100 ft.) decision height? It was concluded that a height of 30 meters could have been determined during descent to an average standard deviation of 1.7 meters for the Boeing 720 and 2.3 meters for the Convair 880, provided the barometric altimetry systems were corrected by the amount of the mean error for each case. With the higher Shuttle landing speed, the larger error shown in Table 2-8 seems consistent with the jet-transport flight test results.

We conclude that the second method of utilizing barometric altimeter data is also not sufficiently accurate for altitude and altitude-rate navigation to touchdown.

## 2.4 Radar Altimeter Errors

Alternate candidates for an independent source of altitude data are radar altimeters. What level of accuracy can be obtained from radar altimeters?

The continuous-wave (CW) radar altimeter is the type widely used in airline transports for approach and landing. It is given a careful specification in ARINC characteristic 552 (Ref. 2-12) and is in production to this specification. Altitude accuracy ( $2\sigma$ ) is specified on page 19 of the basic document to be:

Range:	-6 to +150 meters alt.
Accuracy.	$\pm 1.6$ m or $\pm 2\%$ of the indicated altitude, whichever is greater
Range:	Above 150 m of altitude
Accuracy:	$\pm 5\%$ of indicated altitude.



Supplement 4 calls, however, for tightening of the specification to the values of

Range:           0 - 30 m altitude  
Accuracy:       .45 m. or 1.5% whichever is greater  
Range:           30 - 150 m.  
Accuracy:       .6 m or 2% whichever is greater

ARINC 552 also has a rate specification on page 51. This feature is available but is rarely used [2-13]. The values are

Range.           Ground level to 15 m.  
Accuracy:        $\pm 0.10$  m/sec or  $\pm 10\%$  of the indicated rate  
                  whichever is greater  
Range:           15 m to 150 m  
Accuracy:        $\pm 0.15$  m/sec or  $\pm 10\%$  of the indicated rate, which-  
                  ever is greater.

ARINC 552 calls for filtering to have an effective first order lag time constant not to exceed 0.10 seconds in any case.

There are several types of errors which contribute to the accuracy figures cited above, most of which have known cures. Because of the ARINC 552 CW mechanization, it has certain special characteristics. From 750 meters to 60 meters, it may well be measuring the average of rough terrain below it. From 60 meters to the touchdown, it will track the actual profile below it, although if the antennae are canted forward due to a large angle of attack, it is not clear whether or not, the normal to the aircraft or the normal to the ground will be measured.

There is a type of error known as "double bounce" which has been observed. This occurs when the aircraft is very low over a smooth surface and the receiver circuitry does not lock on to the lowest beat frequency which is the primary return. This error has been eliminated by commercial vendors of ARINC 552 equipment, but there would have to be a specific study made of the multiple-return environment in a shuttle installation.

The pulse type of radio altimeter is the other candidate for this application. An accuracy figure of 0.6 m  $2\sigma$  or 2% was

given [2-14] by a vendor of military equipment of this type. The pulse device always measures the desired normal to the ground and there are no double bounce problems. The above accuracies hold for a wide variety of Mil Spec. environments and are used in configurations where they have demonstrated freedom from the interference of landing gear, pods, etc. The same source cited a typical rate accuracy for these pulse type radars as being around 0.6 m/sec.

Radar altimeters have been used by NASA in the Surveyor spacecrafts and the Apollo Lunar Module. Much larger altitude range was obtained in these altimeters. However, the accuracy was somewhat degraded compared with the above aircraft radar altimeters.

Both the CW and pulse aircraft radar altimeters can deliver excellent altitude accuracy over the runway concrete just before touchdown. The problem is that before reaching the runway, the measured height over the terrain can be significantly different from the altitude with respect to the runway as shown in Fig. 2-1 from Ref. [2-15]. The Shuttle will cross the runway threshold at a high speed (about 100 m/sec). If one needed accurate altitude updates for ten sec before reaching the threshold, one would need to store the terrain profile for the last 1000 meters before the runway. A demonstrated accuracy of about 1 meter RMS error would be required for this tabulated or curve-fitted terrain data at each possible Shuttle landing site.

We do not have terrain data for the proposed Shuttle landing sites, so we cannot make a clear recommendation as to the usefulness of radar altimeters in helping meet the Shuttle landing navigation accuracy specification. Fortunately, it is demonstrated in Chapter 4 that no independent source of altitude data is required to meet the specification. The CR-100 DME-aided inertial system alone can do the job.

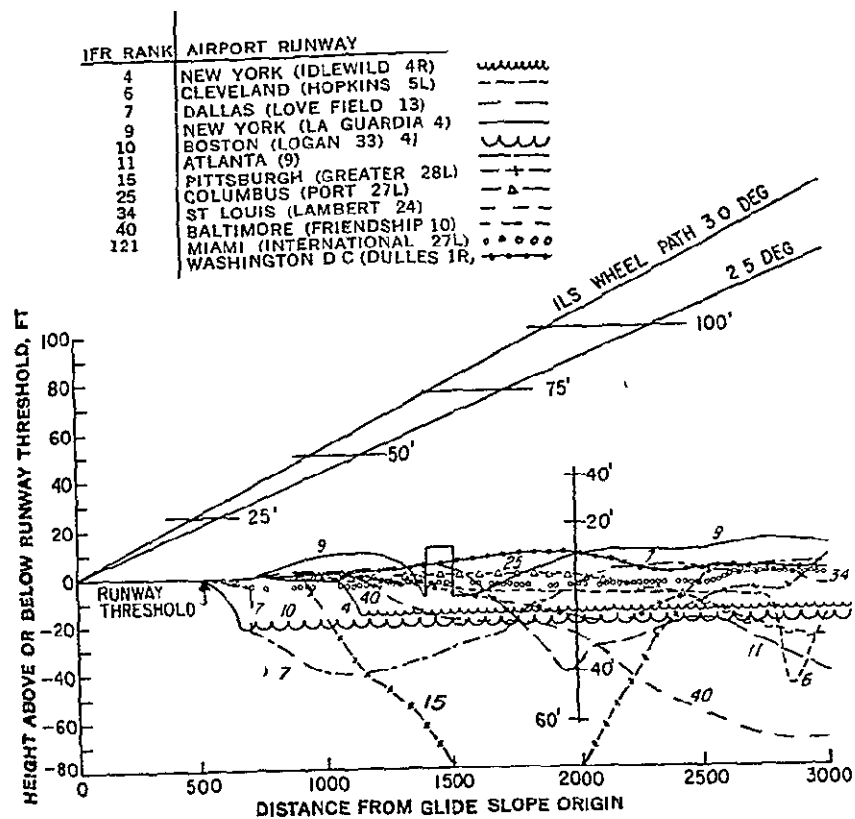


Fig. 2-1 Terrain Height Under Final Approach [2-15]

## CHAPTER 3

### ON-BOARD NAVIGATION EQUATIONS DESIGN

#### 3.1 Kalman Filter Algorithm

Kalman filter theory provides an excellent conceptual framework within which to design the onboard equations for blending the inertial navigation with the radio or other measurement data. A Kalman filter is a real-time recursive data processing algorithm. It automatically computes optimal time-varying gains with which to weight each measurement as a function of the measurement geometry and the relative magnitudes assumed for the navigation error versus the measurement error. The navigation error dynamics and navigation disturbances are also taken into account.

3.1.1 Notation and Standard Results. The navigation error dynamics and navigation disturbances are modeled by a stochastic linear vector differential equation.

$$\underline{\dot{x}} = F(t)\underline{x} + \underline{u} \quad (3-1)$$

where  $\underline{x}$  is the state vector, comprised of various navigation errors,  $F$  is the system fundamental matrix, and  $\underline{u}$  is a white noise vector representing the navigation disturbances. The power spectral density matrix  $N$  of the white noise is

$$E[\underline{u}(t_1) \underline{u}^T(t_2)] = N(t_1) \delta(t_1 - t_2) \quad (3-2)$$

where  $\delta$  is the Dirac delta function. The superscript  $T$  indicates transpose. The state  $\underline{x}$  at one instant of time may be expressed in terms of the state at a previous instant as

$$\underline{x}_{i+1} = \Phi_i \underline{x}_i + \underline{w}_i \quad (3-3)$$

where  $\Phi_i$  is called the state transition matrix and  $\underline{w}_i$  is a random vector. The initial state  $\underline{x}_0$  and the sequence of random vectors  $\underline{w}_i$  have the following statistics

$$\begin{aligned} E(\underline{x}_0) &= \bar{\underline{x}}_0 \\ E(\underline{w}_i) &= \underline{0} \\ E[(\underline{x}_0 - \bar{\underline{x}}_0)(\underline{x}_0 - \bar{\underline{x}}_0)^T] &= P_0 \\ E(\underline{w}_i \underline{w}_j^T) &= Q_i \delta_{ij} \\ E[(\underline{w}_i)(\underline{x}_0 - \bar{\underline{x}}_0)^T] &= 0 \end{aligned} \quad (3-4)$$

where  $\delta_{ij}$  is the Kronecker delta (1 if  $i = j$ , 0 otherwise). The state transition matrix  $\Phi$  for each interval may be computed as the solution to

$$\dot{\Phi}(t, t_1) = F(t) \Phi(t, t_1) \quad (3-5)$$

subject to the initial condition

$$\Phi(t_1, t_1) = I \quad (3-6)$$

The covariance  $Q$  of the random vector  $\underline{w}$  may be computed as the solution to

$$\dot{Q}(t, t_1) = F(t) Q(t, t_1) + Q^T(t, t_1) F^T(t) + N(t) \quad (3-7)$$

Subject to the initial condition

$$Q(t_1, t_1) = 0 \quad (3-8)$$

Each scalar measurement  $z_1$  may be expressed as a linear combination of the elements of the state vector plus noise

$$z_1 = \underline{h}_1^T \underline{x}_1 + v_1 \quad (3-9)$$

where the measurement noise  $v_1$  has the following statistics

$$\begin{aligned} E(v_1) &= 0 \\ E(v_1 v_j) &= r_1 \delta_{1j} \\ E(\underline{w}_1 v_j) &= 0 \\ E(\underline{x}_0 - \bar{\underline{x}}_0) v_1 &= 0 \end{aligned} \quad (3-10)$$

3.1.2 Filter Algorithm Selected. Given the dynamic system and measurements described above, the optimal estimate of the state may be computed in real time as

$$\hat{\underline{x}}_1 = \Phi_{1-1} \hat{\underline{x}}_{1-1} \quad (3-11)$$

$$P_1^- = \Phi_{1-1} P_{1-1}^+ \Phi_{1-1}^T + Q_{1-1} \quad (3-12)$$

$$\underline{k}_1 = P_1^- \underline{h}_1 / (\underline{h}_1^T P_1^- \underline{h}_1 + r_1) \quad (3-13)$$

$$\hat{\underline{x}}_1^+ = \hat{\underline{x}}_1^- + \underline{k}_1 (z_1 - \underline{h}_1^T \hat{\underline{x}}_1^-) \quad (3-14)$$

$$P_1^+ = (I - \underline{k}_1 \underline{h}_1^T) P_1^- (I - \underline{k}_1 \underline{h}_1^T)^T + \underline{k}_1 r_1 \underline{k}_1^T \quad (3-15)$$

This formulation of the Kalman estimator is recommended by Joseph in Ref. [3-1]. It can be shown that Eq. (3-15) is algebraically equivalent to

$$P_1^+ = P_1^- - \underline{k}_1 \underline{h}_1^T P_1^- \quad (3-16)$$

provided  $\underline{k}_1$  is the optimal gain vector as computed by Eq. (3-13). This shorter formula has often been recommended in the literature, including Kalman's fundamental paper Ref. [3-2]. Its principal attraction is it requires far less computation than does Eq. (3-15). Joseph points out, however, that the shorter formula

has a serious practical problem. He considers the possibility that the calculated gains are in error by  $\delta k$ . Then, assuming perfect precision in computing Eq. (3-16), the computed covariance matrix  $P^+$  will be incorrect by an amount

$$\delta P^+ = - \delta \underline{k} \underline{h}^T P^- \quad (3-17)$$

In this unbalanced formulation, a first-order error in the vector  $\underline{k}$  produces a first-order error in the matrix  $P^+$ . Such an error may produce a meaningless non-positive covariance matrix.

With the Joseph formulation, on the other hand, an error in the gain vector  $\delta k$  can be shown to produce zero first-order error in the matrix  $P$ , the actual error being only of second order:

$$\delta P^+ = \delta \underline{k} (\underline{h}^T P^- \underline{h} + r) \delta \underline{k}^T \quad (3-18)$$

Note the error introduced is positive; it cannot produce a non-positive covariance matrix.

Other formulations for the filter have been developed to overcome the numerical difficulties of the original Kalman formulation. A square-root formulation was developed by Potter, and is presented in Problem 9.11 of Ref. [3-3]. The Potter square-root formulation can be used if the noise driving the process state is negligible. This form was used in the onboard space navigation filters in Apollo. Schmidt has recently extended the square-root formulation to include process noise [3-4]. Schmidt suggests the two principal advantages of his formulation are: (1) the covariance matrix is guaranteed to be non-negative; (2) it may be possible to find suitable scaling for fixed point arithmetic, because the square root formulation has a much smaller numerical range. A survey of current square-root filtering techniques may appear shortly in the literature. [3-5]

The Joseph formulation of the Kalman filter has been utilized in the present landing navigation effort.

### 3.1.3 Approximate Computation of State Transition Matrix.

The state transition matrix is the solution to the differential equation

$$\dot{\Phi}(t, t_0) = F(t) \Phi(t, t_0) \quad (3-5)$$

repeat

subject to the initial condition

$$\Phi(t_0, t_0) = I \quad (3-6)$$

repeat

For a sufficiently small  $\Delta t$ , the integral of Eq. (3-5) may be expressed as

$$\Phi(t_1, t_0) = I + F(t_0) \Delta t \quad (3-19)$$

$$\Phi(t_2, t_0) = [I + F(t_1) \Delta t] [I + F(t_0) \Delta t] \quad (3-20)$$

$$\Phi(t_n, t_0) = \prod_{i=1}^n [I + F(t_{i-1}) \Delta t] \quad (3-21)$$

$$\Phi(t_n, t_0) = I + \sum_{i=1}^n F(t_{i-1}) \Delta t + \text{(higher order terms)} \quad (3-22)$$

If the interval from  $t_0$  to  $t_n$  is  $T$ , then  $\Delta t$  is  $T/n$ . This gives the following expression for the state transition matrix (neglecting the higher order terms)

$$\Phi(t_0 + T, t_0) = I + F_{\text{avg}} T \quad (3-23)$$

where

$$F_{\text{avg}} = \frac{1}{n} \sum_{i=1}^n F(t_{i-1}) \quad (3-24)$$

Eq. (3-23) is used to compute the state transition matrix, which is required for filter updates by Eqs. (3-11) and (3-12). The time step  $T$  in the landing navigation filter will be of the order 10 sec or less. Neglecting the higher order terms should be satisfactory because in the error state formulation the state variables each vary slowly (App. A).

Most elements of the fundamental matrix  $F$  vary slowly. For these elements, the value of  $F$  at the end of the interval is used in place of  $F_{\text{avg}}$ . A few of the elements of  $F$  will be shown to be functions of the vehicle acceleration or velocity. These elements can vary rapidly. In these cases



$F_{avg}^T$  is computed by integration of the time varying  $F$  element in parallel with the high frequency inertial navigation equations.

#### 3.1.4 Approximate Computation of Noise Covariance Matrix.

The covariance matrix  $Q$  of the random vector  $w$  is the solution to the differential equation

$$\dot{Q}(t, t_0) = F(t)Q(t, t_0) + Q^T(t, t_0)F^T(t) + N(t) \quad (3-7)$$

repeat

subject to the initial condition

$$Q(t_0, t_0) = 0 \quad (3-8)$$

repeat

Again using the fact that the error variables are all slowly varying, an approximate expression for  $Q$  can be used, namely

$$Q(t_0 + T, t_0) = N(t_0)T \quad (3-25)$$

For certain elements of the noise covariance matrix, one can obtain a suitable formula for the corresponding element of the noise density matrix  $N$ . In most cases, however, it is easier to obtain directly an expression for the error growth  $Q$ , rather than an expression for the fictitious white noise density  $N$ .

3.1.5 An Advantage of the Discrete Formulation. The Kalman filter formulation selected is a discrete formulation which jumps from one measurement time to the next in a single step. An alternate formulation is a continuous formulation which involves the integration of a differential equation governing the propagation of the state error covariance matrix. Integration of a matrix differential equation is often difficult and problems of negative diagonal terms can arise.

The discrete formulation also has matrix differential equations, namely Eqs. (3-5) and (3-7). However, integrating these equations was avoided by using the approximate solutions Eqs. (3-23) and (3-25). The question arises, "Can these approximations cause numerical difficulties?" A distinct advantage of the discrete formulation is that the answer is "No". Consider Eq. (3-12), which is of the form,

$$M = \Phi P \Phi^T + Q \quad (3-26)$$

Now  $Q$  as computed by Eq. (3-25) is clearly non-negative, since the noise density matrix  $N$  is non-negative. Assume that  $P$ , which is the result of previous calculations, is non-negative. If the matrix  $\Phi$  as computed by Eq. (3-23) is grossly in error, can  $M$  be negative? Let  $\underline{v}$  be an arbitrary vector.

$$\underline{v}^T M \underline{v} = \underline{v}^T [\Phi P \Phi^T + Q] \underline{v} \quad (3-27)$$

$$\underline{v}^T M \underline{v} = [\Phi^T \underline{v}]^T P [\Phi^T \underline{v}] + \underline{v}^T Q \underline{v}$$

Since  $P$  and  $Q$  are non-negative, it is proven that for arbitrary  $\Phi$  and  $\underline{v}$

$$\underline{v}^T M \underline{v} \geq 0 \quad (3-28)$$

That is,  $M$  is non-negative.

### 3.2 State Variables: Assumed Dynamics and Disturbances

3.2.1 State Variables Chosen for Filter Synthesis. The state variables to be estimated by the Kalman filter are presented in Table 3-1. The first three state variables are the errors in the inertial-navigation-system indication of vehicle position. The next three state variables are the errors in the inertial-navigation-system indication of vehicle velocity.

The gyro-stabilized platform will be misaligned due to initial alignment errors plus the gyro drift during the entry. Including the platform misalignments as state variables enables the Kalman filter to realign the platform. At speeds small compared with orbital velocity, the vehicle must support itself with a vertical specific force (lift) equal, on the average, to the acceleration of gravity. If the platform is tipped about one of the horizontal axes, the steady vertical specific force is improperly measured as

Variable		Sign Convention
$x_1$	Error in east position	Positive if indicated position is east of actual.
$x_2$	Error in north position	Positive if indicated position is north of actual.
$x_3$	Error in altitude	Positive if INS indicated altitude is above actual.
$x_4$	Error in east velocity	Positive if indicated east velocity exceeds actual.
$x_5$	Error in north velocity	Positive if indicated north velocity exceeds actual.
$x_6$	Error in altitude rate	Positive if indicated up velocity exceeds actual.
$x_7$	Platform tip about east axis	Positive if platform is rotated positive about the east axis.
$x_8$	Platform tip about north axis	Positive if platform is rotated positive about the north axis.
$x_9$	Platform azimuth error	Positive if platform is rotated positive about the up axis.
$x_{10}$	Vertical acceleration error	Positive if it induces a positive altitude-rate error.
$x_{11}$	Altimeter error	Positive if measured altitude exceeds actual.

TABLE 3-1 STATE VARIABLES ESTIMATED BY THE KALMAN FILTER

having a horizontal component. The horizontal acceleration error integrates into a velocity and position error. The position error is discovered by means of the radio distance measurements. The correlation in the covariance matrix, between the platform tip and the horizontal position error, provides the connection whereby the platform misalignment can be estimated and corrected.

Similarly, horizontal specific force, such as in a turn, can provide an input for inferring the azimuth error. The azimuth error has also been included as a state variable to permit this in-flight dynamic alignment, whenever possible. In general, the azimuth accuracy achieved will be less than the level accuracy, because the maneuvering changes-in-velocity are small compared with the integral of the persistent vertical specific force.

The specific force measured by the vertical accelerometer is in error because of the vertical accelerometer bias and scale factor error. In addition, the gravitational model utilized by the inertial navigation equations will be slightly in error due to gravitational anomalies. State variable  $x_{10}$  is the combined vertical accelerometer and magnitude of gravity error. The estimation and correction of this error can reduce the rate at which a good altitude-rate indication would otherwise deteriorate.

Similar state variables are not necessary to account for horizontal acceleration errors. The effect of horizontal acceleration error - due to horizontal accelerometer bias, accelerometer input axis misalignment, or deflection of gravity - is similar to the effect of a platform tip. Therefore, the platform tip state variables can successfully absorb the additional errors.

Barometric altitude, derived from the air data sensors, could provide an alternate source of altitude measurement. The last state variable is the error in the altimeter-indicated altitude. If altimeter measurements are not used, this state variable can be eliminated.

**3.2.2 Assumed Stochastic Process.** Methods for deriving the linearized dynamic equations governing the first nine system state variables are presented in standard texts on inertial navigation systems, such as Refs. [3-6] and [3-7]. In the system of equations presented here, only the significant coefficients are included. Weak coupling terms, such as give rise to 24-hour modes in a pure inertial system, have been deleted. Coriolis error terms have also been deleted; because if the system is operating within the anticipated

accuracies, the effect of these terms is small. The reason for deleting as many terms as possible, of course, is to minimize the arithmetic operations required in the Kalman filter.

Position Errors. The error in east position  $x_1$ , error in north position  $x_2$ , and error in altitude  $x_3$  are governed by

$$\dot{x}_1 = x_4 \quad (3-29)$$

$$\dot{x}_2 = x_5 \quad (3-30)$$

$$\dot{x}_3 = x_6 \quad (3-31)$$

Velocity Errors. The error in east velocity  $x_4$ , error in north velocity  $x_5$ , and error in altitude rate  $x_6$  are governed by

$$\dot{x}_4 = -(g/R)x_1 - a_z x_8 + a_n x_9 + u_4 \quad (3-32)$$

$$\dot{x}_5 = -(g/R)x_2 + a_z x_7 - a_e x_9 + u_5 \quad (3-33)$$

$$\dot{x}_6 = 2(g/R)x_3 - a_n x_7 + a_e x_8 + x_{10} + u_6 \quad (3-34)$$

where  $g$  is the acceleration of gravity;  $R$  is the radius of the earth;  $a_e$ ,  $a_n$ , and  $a_z$  are the time varying components of specific force measured by the inertial navigation system; and  $u_4$ ,  $u_5$ ,  $u_6$  are the white noise disturbances representing other acceleration errors.

Provided the vehicle speed is much lower than orbital velocity, a constant value for  $g/R$  may be used in the coefficients. These  $g/R$  terms give rise to the Schuler oscillations in the east and north errors plus the familiar instability in the altitude errors.

The terms that are products of vehicle specific force times platform misalignments are the acceleration errors that permit inflight alignment.

Note horizontal accelerometer biases, horizontal accelerometer input axis misalignments (toward up or down), and the deflection of gravity do not appear explicitly. Their effect is absorbed into the definition of level ( $x_7 = 0$ ,  $x_8 = 0$ ).

The white noise variables  $u_4$ ,  $u_5$ ,  $u_6$  must account for several other sources of measured acceleration error. During a turn, the scale factor error and input axis misalignments of the horizontal accelerometers produce horizontal acceleration error. The input axis misalignment of the vertical accelerometer causes the same turn to produce a vertical acceleration error. Developing an adequate white noise representation for such physical effects is not discussed in the literature of Kalman filter theory or in the literature of aided-inertial systems. We have developed a practical methodology for approaching such modeling problems.

It is not easy to assign meaningful values to the elements of the power spectral density matrix  $N$  of the white noise. Fortunately, the discrete formulation of the Kalman filter does not require  $N$ . Rather, each cycle a matrix  $Q$  must be added to the estimation-error covariance matrix.  $Q$  must represent the growth in covariance from the last measurement time to the present measurement time. It is easier to compute directly meaningful values for elements of the  $Q$  matrix.

Consider that during a maneuver, such as a  $180^\circ$  turn, the vehicle has experienced horizontal specific forces  $a_e(t)$  and  $a_n(t)$ , the integrals of which are  $\Delta v_{e\text{total}}$  and  $\Delta v_{n\text{total}}$ . The change in east-velocity error due to the maneuver is

$$\Delta x_4 = \Delta v_{e\text{total}} e_{ASF} + \Delta v_{n\text{total}} e_{A\theta} \quad (3-35)$$

where  $e_{ASF}$  is the east-accelerometer scale factor error and  $e_{A\theta}$  is the east-accelerometer input axis misalignment toward north. The mean value of this change in velocity error is zero (the mean is computed over an ensemble of platforms having random instrument errors).

$$E[\Delta x_4] = 0 \quad (3-36)$$

The mean squared value, however, is not zero.

$$E[\Delta x_4^2] = \Delta v_{e_{total}}^2 \sigma_{ASF}^2 + \Delta v_{n_{total}}^2 \sigma_{A\theta}^2 \quad (3-37)$$

where  $\sigma_{ASF}$  is the 1-sigma value of the accelerometer scale factor error, and  $\sigma_{A\theta}$  is the 1-sigma value of the accelerometer input axis misalignment.

One must design an expression for the growth  $Q_{44}$  in east-velocity estimation-error covariance for each Kalman cycle such that the total of the  $Q$ 's added during the maneuver reasonably approximates the total error introduced.

$$\sum_{i=1}^n Q_{44_i} = \Delta v_{e_{total}}^2 \sigma_{ASF}^2 + \Delta v_{n_{total}}^2 \sigma_{A\theta}^2 \quad (3-38)$$

The expression we have selected is

$$Q_{44} = |\Delta v_e| v \sigma_{ASF}^2 + |\Delta v_n| v \sigma_{A\theta}^2 \quad (3-39)$$

where  $|\Delta v_e|$  and  $|\Delta v_n|$  are the magnitudes of the actual  $\Delta v$ 's experienced during the last Kalman cycle (from the previous measurement to the present measurement), and  $v$  is the present vehicle ground speed. If the vehicle is undergoing a 180° turn, the application of Eq. (3-39) each Kalman cycle will yield a reasonable total result.

An alternate expression has been considered, namely

$$Q_{44} = \Delta v_e^2 \sigma_{ASF}^2 + \Delta v_n^2 \sigma_{A\theta}^2 \quad (3-40)$$

This expression gives the correct value for the growth in the error covariance if the maneuver was started and was completed during the present Kalman interval (compare with Eq. (3-37)). However, this expression fails to yield the desired result in a prolonged turn. Because the sum of the squares of the individual  $\Delta v$ 's is not as large as the square of the total  $\Delta v$ , the model for the error growth underestimates the actual error growth. It is dangerous to allow the covariance matrix to be smaller than the actual level of the errors, as the future measurements will fail to receive adequate weighting. Therefore, we have selected the more conservative expression, Eq. (3-39).

For the growth in north-velocity error covariance, a similar expression is used.

$$Q_{55} = |\Delta v_n| \vee \sigma_{ASF}^2 + |\Delta v_e| \vee \sigma_{A\theta}^2 \quad (3-41)$$

The growth in the altitude-rate error covariance is represented by

$$Q_{66} = 2|\Delta v_{hor}| \vee [2\sigma_{A\theta}^2 + (\sigma_{ABIAS}/g)^2 + \sigma_{\delta}^2] \quad (3-42)$$

where  $|\Delta v_{hor}|$  is the magnitude of the horizontal change in velocity,  $\sigma_{ABIAS}$  is the 1-sigma value of an accelerometer bias, and  $\sigma_{\delta}$  is the 1-sigma angular deflection of gravity from the assumed vertical. The platform is considered "level" when in unaccelerated flight the horizontal accelerometers each indicate zero specific force. The block on which the instruments are mounted is then actually not level due to horizontal accelerometer input axis misalignment, horizontal accelerometer bias, and the deflection of gravity. The vertical accelerometer is therefore, not vertical because the block on which it is mounted is not vertical. Furthermore, the input axis of the vertical accelerometer is misaligned from the block, which accounts for the factor of two weighting the input-axis-misalignment variance in Eq. (3-42).

The effect of altitude-rate changes has been neglected.

Platform tips and azimuth error. The platform tip about east  $x_7$ , tip about north  $x_8$ , and azimuth error  $x_9$  are governed by

$$\dot{x}_7 = - (1/R)x_5 - \omega_n x_9 - (\omega_e/R)x_3 + u_7 \quad (3-43)$$

$$\dot{x}_8 = (1/R)x_4 + \omega_e x_9 - (\omega_n/R)x_3 + u_8 \quad (3-44)$$

$$\dot{x}_9 = (\tan L/R)x_4 - \omega_e x_8 + \omega_n x_7 - (v_e \tan L/R^2)x_3 + u_9 \quad (3-45)$$

where  $L$  is latitude,  $v_e$  is the easterly ground speed, and  $\omega_e$  and  $\omega_n$  are the computed east and north components of the



inertial angular velocity of the local vertical coordinate system. In an inertial navigation system that attempts to keep the stable member level,  $\omega_e$  and  $\omega_n$  represent the torquing commands to the east and north gyros. In terms of estimated ground speed, these are

$$\omega_e = -v_n/R \quad (3-46)$$

$$\omega_n = v_e/R + \omega_{1e} \cos L \quad (3-47)$$

where  $\omega_{1e}$  is inertial angular velocity of the earth. It is assumed that inertial navigation equations are implementing a wander-azimuth formulation, in which the azimuth gyro is not torqued. Therefore, no terms proportional to an  $\omega_z$  appear in Eqs. (3-43) and (3-44). In Eq. (3-43), the term  $-\omega_n x_9$  provides the coupling between azimuth error and platform tip about east; this is the coupling that is utilized in conventional gyrocompassing. Including this term, plus a similar term  $\omega_e x_9$  in Eq. (3-44), enables the Kalman filter to perform in-flight gyrocompassing. The azimuth error causes platform tips which are integrated into velocity then position errors. Comparison with the radio distance measurements determines the position error. The correlation in the covariance matrix permits tracing part of this position error back to the azimuth error.

The variables  $u_7$ ,  $u_8$ ,  $u_9$  are the white noise disturbances representing other sources of coordinate-system angular-velocity error. The principal errors are due to bias gyro-drift rate, acceleration-sensitive gyro drift, gyro torquer scale-factor error (if the east and north gyros are being torqued to maintain level), and the rate-of-change of the deflection of gravity. The gravity effect must be included because we are defining the tips  $x_7$  and  $x_8$  with respect to the fluctuating local direction of gravity, and not with respect to the normal to the reference ellipsoid.

One certainly must stress his imagination to model bias gyro-drift rate as a white noise. However, this is necessary, if one is to avoid adding additional bias state variables to the Kalman filter design. Since the arithmetic required increases as the cube of the dimension of the state space, one must make every reasonable effort to avoid introducing non-critical state variables.

If gyro drift  $u(t)$  were a white noise, the change in platform tip  $\Delta x$  due to this disturbance would be

$$\Delta x = \int_0^t u(\tau) d\tau \quad (3-48)$$

The mean value would be zero, since the mean of white noise is zero.

$$E[\Delta x] = 0 \quad (3-49)$$

However, the mean squared value is not zero. It can be shown the mean squared value grows linearly with time

$$E[\Delta x(t)^2] = N t \quad (3-50)$$

where  $N$  is the power spectral density of the white noise. This first integral of white noise is called a random walk or Brownian motion. One should choose the value for the assumed density  $N$  so that the total increase in covariance, added during landing navigation, corresponds to the total anticipated integral of bias gyro drift rate. If  $T_B$  is the assumed matching interval (such as  $T_B = 600$  sec), one requires

$$N T_B = (\sigma_{GBIAS} T_B)^2 \quad (3-51)$$

$$N = \sigma_{GBIAS}^2 T_B \quad (3-52)$$

where  $\sigma_{GBIAS}$  is the 1-sigma value of the gyro bias-drift rate. The growth  $Q$  in the platform-misalignment covariance during a single Kalman cycle is then

$$Q = \Delta t T_B \sigma_{GBIAS}^2 \quad (3-53)$$

The steady vertical specific force (of the lift opposing gravity) introduces an additional bias gyro-drift rate for the azimuth gyro due to the acceleration sensitive drift. The total gyro drift rate variance is

$$\sigma_{GB_z}^2 = \sigma_{GBIAS}^2 + \sigma_{ADIA}^2 g^2 \quad (3-54)$$

where  $\sigma_{GBIAS}$  is the 1-sigma value of the g-insensitive drift rate and  $\sigma_{ADIA}$  is the 1-sigma value of the acceleration sensitive drift coefficient due to specific force along the input axis.

In this study we have assumed that the east and north gyros are in fact a single two-degree-of-freedom gyro with spin axis vertical. The steady vertical specific force is therefore assumed to cause drift rates in the east and north directions whose variances are

$$\sigma_{GB_e}^2 = \sigma_{GB_n}^2 = \sigma_{GBIAS}^2 + \sigma_{ADSRA}^2 g^2 \quad (3-55)$$

where  $\sigma_{ADSRA}$  is the 1-sigma value of the acceleration sensitive drift coefficient due to specific force along the spin reference axis.

We neglect the effect of variations in the altitude rate.

Horizontal accelerations also induce acceleration sensitive drift. Again, if we assume that the typical maneuver  $\Delta v$  is that of a 180° turn, appropriate expressions for the growth in covariance during each Kalman cycle are

$$Q_{77_a} = |\Delta v_e| v \sigma_{ADIA}^2 \quad (3-56)$$

$$Q_{88_a} = |\Delta v_n| v \sigma_{ADIA}^2 \quad (3-57)$$

$$Q_{99_a} = |\Delta v_n| v \sigma_{ADSRA}^2 \quad (3-58)$$

The azimuth gyro is assumed to have its spin-reference axis pointed north.

If the platform is torqued to keep it level, the gyro torquer scale-factor errors introduce tip-rate errors. For steady flight velocity, the torquing rates are constant and the tip-rate error is a bias. One can model the statistics of this error in the same manner as the bias gyro-drift rate.

The same time scale  $T_B$  can be used to match the statistics with the anticipated tilt error to be introduced. If the platform has been torqued through angles  $\Delta\theta_e$  and  $\Delta\theta_n$  during the last Kalman interval, it is assumed that during the landing navigation period  $T_B$  the platform will be torqued through a total angle of

$$\Delta\theta_{\text{total}} = (T_B/\Delta t) \sqrt{\Delta\theta_e^2 + \Delta\theta_n^2} \quad (3-59)$$

The appropriate expressions for the growth in tilt covariances during a Kalman cycle are

$$Q_{77_\tau} = |\Delta\theta_e| \Delta\theta_{\text{total}} \sigma_{\text{GSF}}^2 \quad (3-60)$$

$$Q_{88_\tau} = |\Delta\theta_n| \Delta\theta_{\text{total}} \sigma_{\text{GSF}}^2 \quad (3-61)$$

where  $\sigma_{\text{GSF}}$  is the 1-sigma value of the gyro torquer scale-factor error.

In a previous Kalman filter design for a radio-aided inertial system [3-8], the east and north deflections of gravity were included explicitly as state variables. It was shown that an adequate stochastic model for each component of gravity deflection is of the form

$$\dot{\delta} = -\omega_\delta \delta + u_\delta \quad (3-62)$$

The power spectral density  $N$  of the white noise  $u_\delta$  is

$$N = 2\omega_\delta \sigma_\delta^2 \quad (3-63)$$

where  $\sigma_\delta$  is the 1-sigma amplitude of the deflection of gravity. The bandwidth  $\omega_\delta$  of the random process, given by Eq. (3-62), is made a function of the vehicle present ground speed.

$$\omega_\delta = v/d_\delta \quad (3-64)$$

where  $d_\delta$  is the gravity correlation distance. Different

values for both  $\sigma_\delta$  and  $d_\delta$  are appropriate for the easterly and northerly deflections.

In the present landing navigation filter design, the gravity deflections have been deleted as separate state variables. The effect of gravity deflection has been absorbed into the definition of the tilt variables  $x_7$  and  $x_8$ . A shift in the deflection of gravity becomes a system disturbance. Its effect must be included in the statistics of the white noise disturbances  $u_7$  and  $u_8$ .

Assuming a constant bandwidth  $\omega_g$  during a moderate time interval, the solution to Eq. (3-62) is

$$\delta(t) = \delta(0)e^{-\omega_\delta t} + \int_0^t e^{-\omega_\delta(t-\tau)} u(\tau) d\tau \quad (3-65)$$

The change in deflection is

$$\Delta\delta = \delta(0)[e^{-\omega_\delta t} - 1] + \int_0^t e^{-\omega_\delta(t-\tau)} u(\tau) d\tau \quad (3-66)$$

The mean value of the change is zero, since both  $\delta(0)$  and  $u(\tau)$  have zero means.

$$E[\Delta\delta] = 0 \quad (3-67)$$

The mean squared value of the change can be shown to be

$$E[\Delta\delta^2] = 2 \sigma_\delta^2 [1 - e^{-\omega_\delta t}] \quad (3-68)$$

For  $\omega_\delta t$  small compared with unity, this may be approximated by

$$E[\Delta\delta^2] = 2 \sigma_\delta^2 \omega_\delta t \quad (3-69)$$

or

$$E[\Delta\delta^2] = 2(v/d_\delta)\sigma_\delta^2 t \quad (3-70)$$

Appropriate expressions for the growth in tilt covariances during a Kalman cycle are

$$Q_{77\delta} = 2(v/d_{\delta n}) \sigma_{\delta n}^2 \Delta t \quad (3-71)$$

$$Q_{88\delta} = 2(v/d_{\delta e}) \sigma_{\delta e}^2 \Delta t \quad (3-72)$$

Vertical acceleration error. The computed vertical acceleration is in error because of accelerometer bias, accelerometer scale factor error, and error in the onboard computed magnitude of gravity. State variable  $x_{10}$  is this acceleration error. At the beginning of landing navigation the initial variance of this error is

$$P_{10,10} = \sigma_{ABIAS}^2 + \sigma_{ASF}^2 g^2 + \sigma_{gz}^2 \quad (3-73)$$

where  $\sigma_{gz}$  is the 1-sigma value of the gravity anomaly. Eq. (3-73) assumes that the vehicle speed is already small compared with orbital velocity so that 1-g of specific force is being experienced.

It is assumed that the zero-g accelerometer bias plus the effect of accelerometer scale factor error contribute a steady bias during landing navigation. The effect of changes in altitude rate is neglected. The changes in local gravity anomaly, however, do cause shifts in the vertical acceleration error. This is modeled as

$$\dot{x}_{10} = -\omega_{gz} x_{10} + u_{10} \quad (3-74)$$

where

$$\omega_{gz} = v/d_{gz} \quad (3-75)$$

The power spectral density  $N$  of the white noise  $u_{10}$  is

$$N = 2 \omega_{gz} \sigma_{gz}^2 \quad (3-76)$$

The expression for the growth in vertical-acceleration-error

covariance during a Kalman cycle is

$$Q_{10,10} = 2(v/d_{gz})\sigma_{gz}^2 \Delta t \quad (3-77)$$

Altimeter error. There are many diverse sources of barometric altimeter error. The most significant sources of error were discussed in Section 2.3. These are:

- Error due to horizontal gradient of pressure.
- Error due to non-standard temperature.
- Static pressure measurement error.
- Instrument errors.

In the Kalman filter, a first-order random process is used to model the first effect (the geographic pattern of "highs and lows").

$$\dot{x}_{11} = -\omega_{alt} x_{11} + u_{11} \quad (3-78)$$

where

$$\omega_{alt} = v/d_{alt} \quad (3-79)$$

The power spectral density  $N$  of the white noise  $u_{11}$ , supporting the first effect, is

$$N = 2 \omega_{alt} \sigma_{alt}^2 \quad (3-80)$$

The non-standard-temperature error and the static-pressure-measurement error contribute a shift in altimeter error during landing navigation, which can be modeled as

$$\Delta e_h = C_{temp} (h-h_0) + C_{sp} (v^2 - v_0^2) \quad (3-81)$$

The mean value of the shift is zero, since the error coefficients  $C_{temp}$  and  $C_{sp}$  have zero means.

$$E[\Delta e_h] = 0 \quad (3-82)$$

The mean-squared value of the shift is

$$E[\Delta e_h^2] = \sigma_{\text{temp}}^2 (h-h_0)^2 + \sigma_{\text{sp}}^2 (v^2-v_0^2)^2 \quad (3-83)$$

where  $\sigma_{\text{temp}}$  and  $\sigma_{\text{sp}}$  are the 1-sigma values of the error coefficients.

An appropriate expression for the growth in altimeter-error covariance during a Kalman cycle is

$$Q_{11,11} = \Delta t(2v/d_{\text{alt}})\sigma_{\text{alt}}^2 + |\Delta h|h_s \sigma_{\text{temp}}^2 + |\Delta(v^2)|v_s^2 \sigma_{\text{sp}}^2 \quad (3-84)$$

where  $h_s$  and  $v_s$  are the starting altitude and velocity of the landing navigation period; and  $\Delta t$ ,  $\Delta h$ , and  $\Delta(v^2)$  are the changes in time, altitude, and squared velocity during the last Kalman cycle.

The last source of altimeter error - the instrument error - is modeled as an additive noise, uncorrelated from measurement to measurement.

3.2.3 Transition Matrix and Noise Covariance Matrix. In Subsection 3.1.3 it was shown that most elements of the state transition matrix for each Kalman cycle may be computed sufficiently accurately using

$$\Phi = I + F T \quad (3-85)$$

where  $I$  is the identity matrix,  $F$  is the current fundamental matrix, and  $T$  is the length of the current Kalman time step. The exceptions noted were those elements of the state transition matrix for which the corresponding element of the fundamental matrix varied significantly during the Kalman cycle. In these cases the appropriate approximate expression is

$$\Phi = I + F_{\text{avg}} T \quad (3-86)$$



where  $F_{avg}$  is computed by integration of the time-varying  $F$  element in parallel with the high-frequency inertial navigation equations.

The differential equations governing the velocity errors - Eqs. (3-32), (3-33), and (3-34) - each have components of the time-varying specific force as coefficients. Thus, a typical element in the fundamental matrix is

$$F_{4,9}(t) = a_n(t) \quad (3-87)$$

The corresponding element of the state transition matrix is computed as

$$\Phi_{4,9} = \sum_{i=1}^n \Delta v_{n_i} = \Delta v_n \quad (3-88)$$

That is, the element is simply the accumulated  $\Delta v$  in the north direction during the time interval of the present Kalman transition.

The differential equations governing the platform tips and azimuth error - Eqs. (3-43), (3-44), and (3-45), each have the gyro torquing commands  $\omega_e$  and  $\omega_n$  as coefficients. A typical element in the fundamental matrix is

$$F_{8,9}(t) = \omega_e(t) \quad (3-89)$$

The corresponding element of the state transition matrix is computed as

$$\Phi_{8,9} = \sum_{i=1}^n \Delta \theta_{e_i} = \Delta \theta_e \quad (3-90)$$

That is, the element is simply the total angle change commanded about the east axis during the time interval of the present Kalman transition.

The non-zero elements of the state transition matrix are presented in Table 3.2.

$\Phi_{1,1} = 1,$	$\Phi_{1,4} = T$
$\Phi_{2,2} = 1,$	$\Phi_{2,5} = T$
$\Phi_{3,3} = 1,$	$\Phi_{3,6} = T$
$\Phi_{4,4} = 1,$	$\Phi_{4,1} = - (g/R) T$
	$\Phi_{4,8} = - \Delta v_z$
	$\Phi_{4,9} = \Delta v_n$
$\Phi_{5,5} = 1,$	$\Phi_{5,2} = - (g/R) T$
	$\Phi_{5,7} = \Delta v_z$
	$\Phi_{5,9} = - \Delta v_e$
$\Phi_{6,6} = 1,$	$\Phi_{6,3} = 2 (g/R) T$
	$\Phi_{6,7} = - \Delta v_n$
	$\Phi_{6,8} = \Delta v_e$
	$\Phi_{6,10} = T$
$\Phi_{7,7} = 1,$	$\Phi_{7,5} = - (1/R) T$
	$\Phi_{7,9} = - \Delta \theta_n$
	$\Phi_{7,3} = - \Delta \theta_e / R$
$\Phi_{8,8} = 1,$	$\Phi_{8,4} = (1/R) T$
	$\Phi_{8,9} = \Delta \theta_e$
	$\Phi_{8,3} = - \Delta \theta_n / R$
$\Phi_{9,9} = 1,$	$\Phi_{9,4} = (\tan L / R) T$
	$\Phi_{9,8} = - \Delta \theta_e$
	$\Phi_{9,7} = \Delta \theta_n$
	$\Phi_{9,3} = - (v_e \tan L / R^2) T$
$\Phi_{10,10} = 1 - (v/d_{gz}) T$	
$\Phi_{11,11} = 1 - (v/d_{alt}) T$	

TABLE 3-2 NON-ZERO ELEMENTS OF THE STATE TRANSITION MATRIX

$$\begin{aligned}
Q_{4,4} &= |\Delta v_e| v \sigma_{ASF}^2 + |\Delta v_n| v \sigma_{A\theta}^2 \\
Q_{5,5} &= |\Delta v_n| v \sigma_{ASF}^2 + |\Delta v_e| v \sigma_{A\theta}^2 \\
Q_{6,6} &= 2|\Delta v_{hor}| v [2\sigma_{A\theta}^2 + (\sigma_{ABIAS}/g)^2 + \sigma_{\delta e}^2] \\
Q_{7,7} &= \Delta t T_B (\sigma_{GBIAS}^2 + \sigma_{ADSRA}^2 g^2) + |\Delta v_e| v \sigma_{ADIA}^2 \\
&\quad + |\Delta \theta_e| \Delta \theta_{total} \sigma_{GSF}^2 + \Delta t (2v/d_{\delta n}) \sigma_{\delta n}^2 \\
Q_{8,8} &= \Delta t T_B (\sigma_{GBIAS}^2 + \sigma_{ADSRA}^2 g^2) + |\Delta v_n| v \sigma_{ADIA}^2 \\
&\quad + |\Delta \theta_n| \Delta \theta_{total} \sigma_{GSF}^2 + \Delta t (2v/d_{\delta e}) \sigma_{\delta e}^2 \\
Q_{9,9} &= \Delta t T_B (\sigma_{GBIAS}^2 + \sigma_{ADIA}^2 g^2) + |\Delta v_n| v \sigma_{ADSRA}^2 \\
Q_{10,10} &= \Delta t (2v/d_{gz}) \sigma_{gz}^2 \\
Q_{11,11} &= \Delta t (2v/d_{alt}) \sigma_{alt}^2 + |\Delta h| h_s \sigma_{temp}^2 + |\Delta(v^2)| v_s^2 \sigma_{sp}^2
\end{aligned}$$

TABLE 3-3. NON-ZERO ELEMENTS OF THE NOISE COVARIANCE MATRIX

TABLE 3-4 DATA USED IN THE STATE TRANSITION AND NOISE  
MATRICES

$g$	acceleration of gravity	$9.86 \text{ m/s}^2$
$R$	earth radius	6380 km
$\sigma_{ASF}$	accelerometer scale factor error	$1 \times 10^{-4}$
$\sigma_{A\theta}$	accelerometer input axis misalignment	15 arc sec
$\sigma_{ABIAS}$	accelerometer bias	$5 \times 10^{-4} \text{ m/s}^2$
$\sigma_{GBIAS}$	gyro bias drift rate	.03°/hr
$\sigma_{ADIA}$	gyro accel. sensitive drift (input axis)	.10°/hr/g
$\sigma_{ADSRA}$	gyro accel. sensitive drift (spin axis)	.03°/hr/g
$\sigma_{GSF}$	gyro torquer scale factor error	$2 \times 10^{-4}$
$\sigma_{\delta n}$	gravity deflection north	$2.6 \times 10^{-5} \text{ rad}$
$d_{\delta n}$	deflection correlation distance north	44 km
$\sigma_{\delta e}$	gravity deflection east	$3.3 \times 10^{-5} \text{ rad}$
$d_{\delta e}$	deflection correlation distance east	30 km
$\sigma_{gz}$	gravity anomaly (magnitude error)	$4 \times 10^{-4} \text{ m/s}^2$
$d_{gz}$	anomaly correlation distance	146 km
$\sigma_{alt}$	variation in altitude of constant pressure surface	170 m
$d_{alt}$	correlation distance of constant pressure surface	500 km
$\sigma_{temp}$	non-standard temperature altim. error	.03
$\sigma_{sp}$	static pressure altim. error	$5 \times 10^{-4} \text{ m/(m/s)}^2$
$h_s$	assumed starting altitude	20 km
$v_s$	assumed starting speed	300 m/s
$T_B$	assumed navigation duration	600 sec

2 ⊕

The non-zero elements of the noise covariance matrix  $Q$  are summarized in Table 3-3.

The numerical values assumed for the various constants in the state transition matrix and in the noise covariance matrix are presented in Table 3-4. The data on accelerometer and gyro errors are taken from Ref. [3-9]. The data on gravity deflections, gravity anomaly, and altimeter errors are taken from Ref. [3-8].

### 3.3 Measurement Incorporation Equations

Three types of measurements may be processed by the landing navigation Kalman filter. These are range-difference measurements, delta-range-difference measurements, and altitude-difference measurements (if required).

3.3.1 Range-Difference Measurement. At the same instant that the range  $r_M$  to transponder 1 is measured, the vehicle longitude, latitude, and altitude indicated by inertial navigation equations are sampled and held. A calculated range to the transponder is computed: Given the indicated vehicle position  $(\lambda, L, h)$  and the transponder position  $(\lambda_1, L_1, h_1)$  in geocentric coordinates, the earth central angle  $\theta$  between the two positions is

$$\sin^2 \frac{\theta}{2} = \sin^2 \frac{L-L_1}{2} + \cos L \cos L_1 \sin^2 \frac{\lambda-\lambda_1}{2} \quad (3-91)$$

From the law of cosines, the calculated range  $r_C$  is

$$r_C = [(\rho-\rho_1)^2 + 4\rho\rho_1 \sin^2 \frac{\theta}{2}]^{1/2} \quad (3-92)$$

where  $\rho$  is earth radius plus altitude. The range-difference measurement is the calculated range minus the measured range.

$$z_r = r_C - r_M \quad (3-93)$$

It can be shown that for errors in indicated position small compared with the actual range, the range-difference

measurement may be expressed as a linear combination of the navigation-error state vector elements, namely

$$z_r = \underline{h}_r^T \underline{x} + v_r \quad (3-94)$$

where  $v_r$  is the negative of the error in the measured range, and the vector  $\underline{h}_r$  is all zeros except for

$$\begin{aligned} h_{r_1} &= b_e \\ h_{r_2} &= b_n \\ h_{r_3} &= b_z \end{aligned} \quad (3-95)$$

where  $b_e$ ,  $b_n$ ,  $b_z$  are the components of the unit vector directed from the 1-th transponder to the aircraft. The vector  $\underline{h}$  is called the measurement gradient vector, because the elements of  $\underline{h}$  are each the partial derivative of the measurement  $z$  with respect to the corresponding navigation-error state variable.

The  $\underline{b}$  vector expressed in east-north-up geocentric coordinates at the vehicle (not at the transponder) may be calculated in terms of the indicated vehicle position ( $\lambda$ ,  $L$ ,  $h$ ) and the transponder position ( $\lambda_1$ ,  $L_1$ ,  $h_1$ ) as

$$\begin{aligned} b_{1e} &= \frac{1}{r_1} \rho_1 \cos L_1 \sin(\lambda - \lambda_1) \\ b_{1n} &= \frac{1}{r_1} \rho_1 [\sin(L - L_1) - 2 \sin L \cos L_1 \sin^2 \frac{\lambda - \lambda_1}{2}] \\ b_{1z} &= \frac{1}{r_1} [\rho - \rho_1 + 2\rho_1 \sin^2 \frac{\theta_1}{2}] \end{aligned} \quad (3-96)$$

As discussed in Section 2.1, the largest range measurement errors are contributed by the uncertainty in the radio

propagation velocity in the atmosphere, possible random errors, and equipment bias. The range-difference-measurement error  $v_r$  contributed by these effects is

$$v_r = -e_{b_1} - r_1 e_p f(h) - e_m - e_r \quad (3-97)$$

where  $e_{b_1}$  is the bias in the 1-th transponder,  $r_1$  is the range from the vehicle to the 1-th transponder,  $e_p$  is the propagation error at sea level (expressed as a fraction of range),  $e_m$  is the multipath random error, and  $e_r$  is other random error. The function  $f(h)$  expresses the decrease in propagation error at increasing altitude  $h$ .

$$f(h) = (1 - e^{-h/h_s}) / (h/h_s) \quad (3-98)$$

Note, in the limit as  $h$  goes to zero,  $f(h)$  goes to its maximum value unity.

The mean value of the error  $v_r$  is zero, because  $e_b$ ,  $e_p$ ,  $e_m$ , and  $e_r$  each have zero mean (over the ensemble of transponders and weather conditions).

$$E[v_r] = 0 \quad (3-99)$$

The variance  $r_r$  of the error  $v_r$  is

$$r_r = \sigma_b^2 + r_1^2 \sigma_p^2 f^2(h) + \sigma_m^2 \cos^2 \epsilon + \sigma_r^2 \quad (3-100)$$

where  $\sigma_b$ ,  $\sigma_p$ ,  $\sigma_m \cos \epsilon$ , and  $\sigma_r$  are the 1-sigma values of the transponder bias, propagation error, multipath random errors and other random error. The cosine dependence of multipath error upon the elevation angle  $\epsilon$  (of the vehicle above the horizon as seen from the transponder) indicates reduced multipath error at high elevation angles.

A summary of the range-difference-measurement equations is presented in Table 3-5. Given the calculated values of  $z_r$ ,  $h_r$ , and  $r_r$ , the Kalman filter incorporates the measurement according to Eqs. (3-13), (3-14), and (3-15).

A problem in filter performance can arise if the transponder bias or propagation effect are the dominant error sources, rather than the random error. The underlying statistical assumptions, under which the Kalman filter is an optimal estimator, include Eq. (3-10) which states (among other things) that

Difference measurement

$$z_r = r_{\text{calc}} - r_{\text{meas}}$$

Measurement gradient vector (non-zero elements)

$$h_{r_1} = b_e$$

$$h_{r_2} = b_n$$

$$h_{r_3} = b_z$$

Assumed measurement-error variance

$$r_r = \sigma_b^2 + r^2 \sigma_p^2 f^2(h) + \sigma_m^2 \cos^2 \epsilon + \sigma_r^2$$

$$f(h) = (1 - e^{-h/h_s}) / (h/h_s)$$

$$\cos^2 \epsilon = [1 - b_z^2]^{1/2}$$

Data

$\sigma_b$  transponder bias                      0.3 m

$\sigma_p$  propagation error                       $50 \times 10^{-6}$

$\sigma_m$  multipath random error              0.9 m

$\sigma_r$  other random error                    0.2 m

$h_s$  scale height                              6900 m

TABLE 3-5 RANGE-DIFFERENCE MEASUREMENT SUMMARY



$$E[v(t_i)v(t_j)] = 0 \quad \text{for } i \neq j \quad (3-101)$$

That is, the measurement error is uncorrelated with the error in every other measurement. Transponder bias and propagation error clearly introduce correlation into the measurements. The formal mathematical solution to this problem is to introduce additional state variables associated with the correlations. However, one wishes to keep the dimension of the state space as small as possible, to minimize the onboard computation and the memory required. Additional state variables should be added only if a problem is discovered through simulation and if such problem cannot be handled in a less costly manner.

Successful Kalman filter performance (utilizing the range-difference measurement equations summarized in Table 3-5 in conjunction with the standard measurement-incorporation equations (3-13), (3-14), and (3-15)) depends on the linearizing assumption that the error in indicated position is small compared with the actual range to the transponder. If this underlying assumption is violated, nonlinear effects become important and the filter performance deteriorates.

We have designed compensation for the nonlinear elongation of the measured range. A discussion of the nonlinear problem and a derivation of the compensation is presented in Appendix C. The addition of these compensation equations increases significantly the domain of convergence of the navigation filter. A summary of the compensation equations is presented in Table 3-6. The on-board-computed covariance is assumed to match satisfactorily the actual level of navigation position error. The mean elongation of the measured range, due to position uncertainty, is computed and is subtracted from the measured range. The variance assumed for the range-difference measurement is increased to account for the addition of error by the nonlinear elongation. The so-modified range-difference measurement  $z_r'$  and assumed measurement error variance  $r_r'$  are then utilized in the standard measurement-incorporation equations (3-13), (3-14), and (3-15).

Estimated line-of-sight coordinates

$$\underline{u}_a = \text{unit } (\underline{b}_E \times \underline{r}_{VE})$$

$$\underline{u}_b = \underline{u}_a \times \underline{b}_E$$

Position covariance normal to estimated line-of-sight

$$P_{aa} = \underline{u}_a^T P_{rr} \underline{u}_a$$

$$P_{ab} = \underline{u}_a^T P_{rr} \underline{u}_b$$

$$P_{bb} = \underline{u}_b^T P_{rr} \underline{u}_b$$

Eigenvariances of normal covariance

$$\sigma_2^2, \sigma_3^2 = (P_{aa} + P_{bb} \pm [(P_{aa} - P_{bb})^2 + 4 P_{ab}^2]^{1/2})/2$$

Modified range difference measurement

$$z_r' = z_r + (\sigma_2^2 + \sigma_3^2)/2r_C$$

Modified assumed measurement error variance

$$r_r' = r_r + (\sigma_2^4 + \sigma_3^4)/2r_C^2$$

Table 3-6 COMPENSATION FOR NONLINEAR ELONGATION OF MEASURED RANGE

3.3.2 Delta-Range-Difference Measurement. The delta-range circuits of the DME measure the change in range  $\Delta r_M$  to the  $i$ -th transponder. The interval  $\Delta t$ , during which the change in range is measured, is under computer control. Counting of the doppler cycles begins upon computer command at  $t_1$  and stops upon computer command at  $t_2$ . The end of the counting interval also is the time at which the associated range measurement is taken.

At both the beginning  $t_1$  and end  $t_2$  of the counting interval, the computer must sample and hold the vehicle position  $(\lambda, L, h)$  indicated by the inertial navigation equations. The calculated ranges  $r_C(t_1)$  and  $r_C(t_2)$  are computed by means of Eqs. (3-91) and (3-92). The calculated change in range is

$$\Delta r_C = r_C(t_2) - r_C(t_1) \quad (3-102)$$

The delta-range-difference measurement is the calculated delta-range minus the measured delta-range

$$z_{\Delta r} = \Delta r_C - \Delta r_M \quad (3-103)$$

It can be shown that for errors in indicated position small compared with the actual range, the delta-range-difference measurement is comprised of

$$z_{\Delta r} = \underline{b}^T(t_2)\underline{e}_x(t_2) - \underline{b}^T(t_1)\underline{e}_x(t_1) + v_{\Delta r} \quad (3-104)$$

where  $\underline{b}$  is the unit vector from the transponder to the vehicle,  $\underline{e}_x$  is the vector error in the inertial-indicated vehicle position, and  $v_{\Delta r}$  is the negative of the error in the measured delta range. The error in position at  $t_1$  may be expressed in terms of the errors at  $t_2$  according to

$$\underline{e}_x(t_1) = \underline{e}_x(t_2) - \underline{e}_v(t_2) \Delta t \quad (3-105)$$

where  $\underline{e}_v$  is the vector error in the inertial-indicated vehicle velocity. The small acceleration error (due to platform tilts, accelerometer biases, scale factor errors misalignments, etc.) has been neglected. The small rotation of the local-vertical coordinates has also been neglected. Substituting Eq. (3-105) into Eq. (3-104) yields

$$z_{\Delta r} = \Delta \underline{b}^T \underline{e}_x(t_2) + \underline{b}^T(t_1) \underline{e}_v(t_2) \Delta t + v_{\Delta r} \quad (3-106)$$

where

$$\Delta \underline{b} = \underline{b}(t_2) - \underline{b}(t_1) \quad (3-107)$$

From the point of view of the Kalman filter, the delta-range-difference measurement is considered to take place at  $t_2$ , at which time the measurement is

$$z_{\Delta r} = \underline{h}_{\Delta r}^T \underline{x} + v_{\Delta r} \quad (3-108)$$

where the measurement gradient vector is all zeros except for

$$\begin{aligned} h_{\Delta r_1} &= \Delta b_e \\ h_{\Delta r_2} &= \Delta b_n \\ h_{\Delta r_3} &= \Delta b_z \\ h_{\Delta r_4} &= b_e(t_1) \Delta t \\ h_{\Delta r_5} &= b_n(t_1) \Delta t \\ h_{\Delta r_6} &= b_z(t_1) \Delta t \end{aligned} \quad (3-109)$$

The measurement error  $v_{\Delta r}$  contributed by propagation error and random error is

$$v_{\Delta r} = -\Delta r_1 e_p f(h) - e_{\Delta r} \quad (3-110)$$

where  $\Delta r$  is the change in range and  $e_{\Delta r}$  is the random error. Note transponder bias drops out of a delta-range measurement. The mean measurement error is zero

$$E[v_{\Delta r}] = 0 \quad (3-111)$$

The variance  $r_{\Delta r}$  of the measurement error is

$$r_{\Delta r} = (\Delta r_1)^2 \sigma_p^2 f^2(h) + \sigma_{\Delta r}^2 \quad (3-112)$$

A summary of the delta-range-difference-measurement equations is presented in Table 3-7. Given the calculated values of  $z_{\Delta r}$ ,  $h_{\Delta r}$ , and  $r_{\Delta r}$ , the Kalman filter incorporates the measurement according to Eqs. (3-13), (3-14), and (3-15).

A point, not often emphasized, is that a delta-range measurement is not a simple "range-rate" measurement. Eq. (3-106) showed that the difference measurement is a function of both vehicle velocity error and vehicle position error. While flying over a transponder at low altitude (such as on final approach), the shift  $\Delta b$  in the transponder-to-vehicle-direction vector can be substantial. Consider a speed of 150 m/sec, an altitude of 1000 meters and a measurement interval of 1.0 sec. The shift  $\Delta b$  (if the vehicle is over the transponder) is .15, directed forward. If estimated position is in error by 2 meters, forward, then according to Eq. (3-106) the position error contributes .30 meters to the delta-range difference measurement. If position error were ignored in the formulation and the data were treated as "range-rate" data, the .3 meter measurement-difference (accumulated in the 1.0 sec interval) would be interpreted erroneously as a .3 meter/sec altitude rate error. This might be intolerable, because the touchdown altitude-rate navigation accuracy specification is 0.05 m/s.

The relative contribution of position error and velocity error to the difference measurement is not changed by choosing a different interval size  $\Delta t$ , because (assuming constant  $b$

Difference measurement

$$z_{\Delta r} = \Delta r_{\text{calc}} - \Delta r_{\text{meas}}$$

Measurement gradient vector (non-zero elements)

$$h_{\Delta r_1} = \Delta b_e$$

$$h_{\Delta r_2} = \Delta b_n$$

$$h_{\Delta r_3} = \Delta b_z$$

$$h_{\Delta r_4} = b_e(t_1)\Delta t$$

$$h_{\Delta r_5} = b_n(t_1)\Delta t$$

$$h_{\Delta r_6} = b_z(t_1)\Delta t$$

Assumed measurement-error variance

$$r_{\Delta r} = (\Delta r)^2 \sigma_p^2 f^2(h) + \sigma_{\Delta r}^2$$

Data

$\sigma_{\Delta r}$ random error	0.1 m
$\sigma_p$ propagation error	$50 \times 10^{-6}$

TABLE 3-7 DELTA-RANGE-DIFFERENCE MEASUREMENT SUMMARY

during the interval) the coefficients weighting position error and velocity error in Eq. (3-106) are both proportional to  $\Delta t$ . Hence, making  $\Delta t$  small still does not permit treating the data as a simple "range-rate" measurement. A disadvantage of making  $\Delta t$  small is that the contribution of position and velocity error to the difference measurement (the "signal") becomes small compared with the assumed 0.1 meter random error (the "noise").

Using the formulation proposed here<sup>†</sup> the measurement interval  $\Delta t$  may be made as large as desired to increase the measurement "signal-to-noise ratio". Vehicle maneuvering during the interval introduces no error, because data at the middle of the interval is not used to represent the entire interval. Rather the exact indicated positions at the beginning and end of the interval are used. These indicated positions include, without approximation, the effect of vehicle acceleration, and ranges calculated based on these indicated positions include, without approximation, the effect of non-uniform range rate. A limit to increasing the "signal-to-noise-ratio" is reached when the propagation error dominates the added measurement error. At a velocity of 200 m/sec with propagation error of  $50 \times 10^{-6}$ , if  $\Delta t$  is 10 sec the error introduced is .1 meter - which is comparable to the assumed random error. For larger  $\Delta t$  the vehicle position error, the vehicle velocity error, and the propagation error all have the same relative contribution to the difference measurement.

To take advantage of the "signal-to-noise" improvement associated with a larger delta-range measurement interval  $\Delta t$ , in the present Kalman filter design we have selected the maximum interval  $\Delta t$  that is compatible with the sequential-measurement organization of the CR-100 DME subsystem. That is, upon completion of a range and delta-range measurement to one transponder, the computer immediately initiates the interrogation of a second transponder. As soon as the carrier-loop lockup is established, the computer commands the start of the delta-range measurement. A maximum of 0.2 sec is required from the end of the measurements with the first transponder to the start of the delta-range measurement with the second transponder. The entire remaining

---

<sup>†</sup>An alternate formulation (whereby delta-range is treated as a range-rate measurement) is discussed in Appendix B.

interval (up to the time desired for the range measurement to the second transponder) is utilized to accumulate the delta-range measurement. That is, if range measurements occur every 10 sec, then the delta-range-measurement interval  $\Delta t$  is about 9.8 sec.

3.3.3 Altitude-Difference Measurement. If an independent source of altitude information is found necessary, a possible source is the barometric altitude derived from the air-data. The altitude-difference measurement is the altitude indicated by the inertial navigation equations minus the altitude derived from the air data

$$z_h = h_{INS} - h_{AD} \quad (3-113)$$

In terms of the navigation-error state-vector elements, the difference measurement is

$$z_h = \underline{h}_h^T \underline{x} + v_h \quad (3-114)$$

where  $v_h$  is the short correlation measurement error. The measurement gradient vector  $\underline{h}_h$  is all zeros except for

$$h_{h_3} = 1 \quad (3-115)$$

$$h_{h_{11}} = -1$$

The measurement error is assumed to have zero mean.

$$E[v_h] = 0 \quad (3-116)$$

The maximum tolerable variance  $r_h$  of the measurement error is a parameter to be determined (if independent altitude is required to meet the landing navigation accuracy specification).

A summary of the altitude-difference measurement is presented in Table 3-8.



Difference measurement

$$z_h = h_{\text{INS}} - h_{\text{Air Data}}$$

Measurement gradient vector (non-zero elements)

$$h_{h_3} = 1$$

$$h_{h_{11}} = -1$$

Maximum tolerable measurement-error variance

$$r_h \text{ to be determined}$$

Table 3-8 Altitude-Difference Measurement  
Summary

3.3.4 Rectification of Inertial Navigation Errors. The indications of vehicle position and velocity are maintained by the inertial navigation equations at a higher frequency than the Kalman-cycle frequency. The inertial-navigation-equation variables therefore are chosen as the navigation variables with which to drive the guidance and control equations. To maintain these variables as best estimates of the vehicle position and velocity, it is necessary to introduce corrections in the variables as computed by the Kalman filter.

In general, the Kalman filter lags behind the inertial navigation equations, which are processing the accelerometer data nearly continuously. At a Kalman measurement time, the  $\Delta v$ 's and  $\Delta \theta$ 's from the inertial navigation equations are incorporated into the transition matrix and noise equations, the covariance matrix is brought-up to the measurement time, the measurement data (that was taken and stored at the correct measurement instant) is incorporated. All these computations require time, so the estimate of the navigation errors (based on all the data including the present measurement) becomes available some delay after the measurement time.

Since the navigation errors are all slowly varying, very little loss in navigation and guidance accuracy will result if the correction of the estimated navigation errors is delayed by a full Kalman cycle  $T$ . Let  $\Delta \underline{x}$  be the vector of navigation variable corrections to be implemented at the next Kalman measurement instant. In the Kalman filter during the next computation cycle Eq. (3-11) is modified to be

$$\hat{\underline{x}}_1 = \Phi_{1-1} \hat{\underline{x}}_{1-1} + \Delta \underline{x} \quad (3-117)$$

Note, the corrections are the negative of estimated navigation errors, so the rectification process represented by Eq. (3-117) drives the estimated errors toward zero.

### 3.4 Landing Navigation Initialization

3.4.1 Concept. During hypersonic entry, the estimate of vehicle position and velocity is maintained by the inertial navigation equations, processing the measured specific force from the inertial measurement unit. Satisfactory estimates of horizontal position and velocity can be maintained throughout entry. Typical horizontal position errors at the end of entry might be of the order of 10 km.

The estimates of altitude and altitude rate will diverge, if pure inertial navigation equations are used. The vertical instability can be bounded, however, if one derives altitude from the measured specific force, using suitable stored data for the vehicle aerodynamics, vehicle weight, and atmospheric density-altitude relationship. In this manner, the altitude error can be bounded to the order of 3 km.

After coming-out of the communications black-out (if any), and when the transponders located at the terminal area appear over the radio horizon, the updating of the onboard navigation can begin. In principle, range measurements can be incorporated immediately, utilizing the Kalman filter measurement-incorporation equations. However, problems can arise due to measurement nonlinearities associated with the relatively large position uncertainty. The compensation for the nonlinear elongation of the measured range, derived in Appendix C, extends the domain of convergence of the navigation filter to the order of a 4 km position error at 200 km range. (This observation is based on a very limited number of simulations.) To be confronted with a 10 km initial position error creates more severe nonlinearities. And if the vehicle is so fortunate as to have the terminal area at the center of the remaining footprint (rather than at the far edge), the ranges to the transponders are reduced, further amplifying the error-to-range ratio and increasing nonlinearities.

Fortunately, a relatively simple start-up algorithm exists, which can fix the initial vehicle position utilizing the DME data alone. The position as indicated by the inertial navigation is not used at all. Hence, a large inertial-navigation-position error (relative to the vehicle/transponder range) is no problem. In addition, an initial covariance of the position errors can be computed as an explicit function of the position-fix geometry and of the assumed radio-range-measurement errors. This initial covariance is a good match for the actual level of errors.

Following the initial position fix and covariance initialization, additional range and delta-range measurements are

incorporated using the Kalman filter. In this manner the velocity estimates quickly become updated, completing the initial capture of the navigation state-vector errors. A functional flow diagram of the landing navigation initialization logic is presented in Fig. 3-1.

**3.4.2 Position-Fix Logic.** In rapid succession, the range and delta-range to three of the terminal area transponders are measured. The transponders having the widest geographic separation should be utilized to minimize the geometric dilution of the ranging accuracy. The measured range-changes associated with the first and third range measurements are used to estimate the ranges that would have been measured had simultaneous ranging at  $t_2$  been possible

$$r_1(t_2) = r_1(t_1) + \Delta r_1(t_2 - t_1)/\Delta t$$

$$r_2(t_2) = r_2(t_2) \quad (3-118)$$

$$r_3(t_2) = r_3(t_3) + \Delta r_3(t_2 - t_3)/\Delta t$$

Figure 3-2 illustrates the start-up geometry. Typical timing might be 0.4 sec between  $t_1$  and  $t_2$  and between  $t_2$  and  $t_3$ . The delta-range-accumulation interval  $\Delta t$  could be 0.2 sec. Delta-range divided by  $\Delta t$  is an estimate of the range rate at the center of the measurement interval. To use this range rate (to estimate the range at a different time) neglects the range acceleration. Suppose the range acceleration (due to vehicle maneuvering or geometry shift) were a maximum of 10 m/sec<sup>2</sup> (1 G). The error in extrapolating  $r_1(t_1)$  to time  $t_2$  would be a maximum of

$$\frac{1}{2}a(t_2 - t_1 + \Delta t/2)^2 = 1.2 \text{ meter} \quad (3-119)$$

The error in extrapolating  $r_3(t_3)$  back to the time  $t_2$  would be smaller

$$\frac{1}{2}a(t_3 - t_2 - \Delta t/2)^2 = 0.5 \text{ meter} \quad (3-120)$$

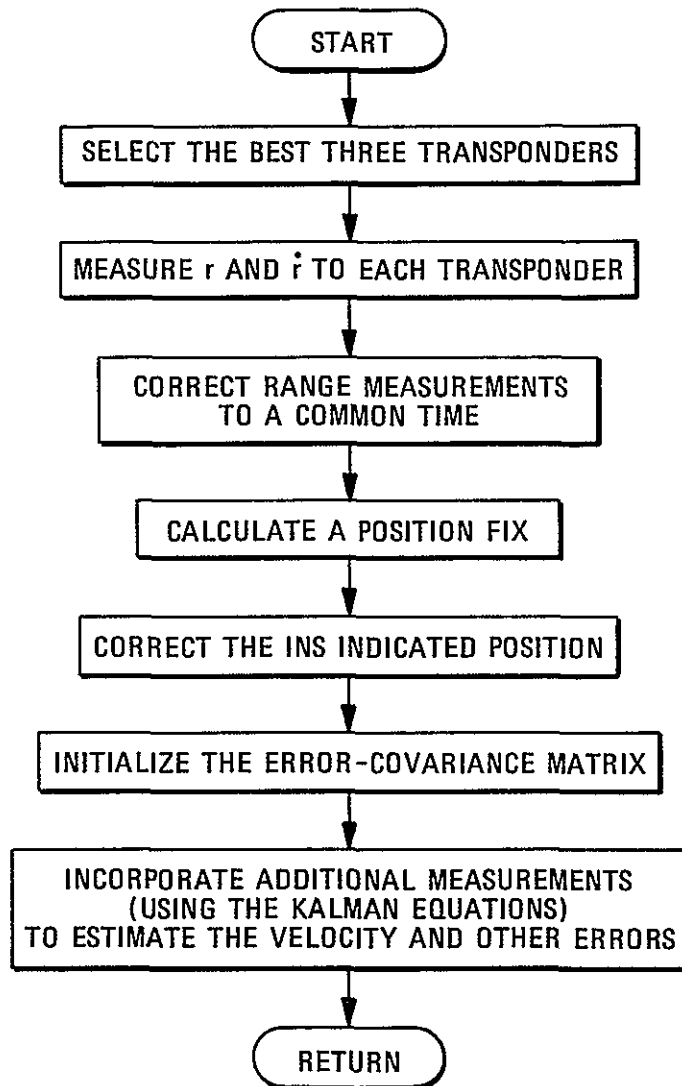


Fig. 3-1 Landing Navigation Initialization Logic

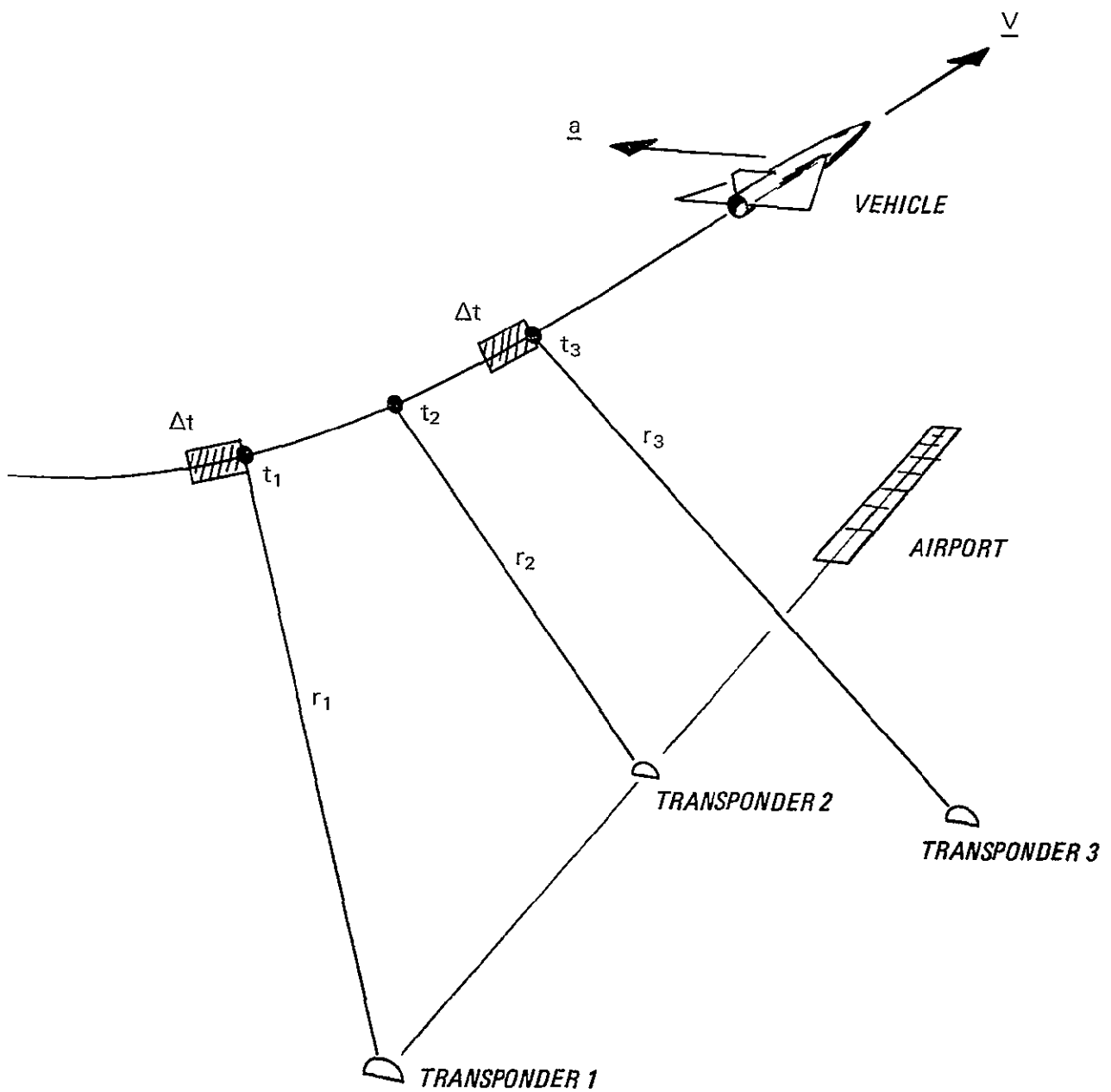


Fig. 3-2 Geometry of Flight Path and Transponder Locations

The range acceleration is likely to be smaller than the 10 m/sec<sup>2</sup> assumed here, so the extrapolation errors should be smaller. The timing intervals assumed are based on a maximum of 0.2 sec required to establish carrier lock and start a delta-range measurement. The typical acquisition time is less. A shorter typical acquisition time would further reduce the extrapolation errors shown in Eqs. (3-119) and (3-120).

Given the estimated simultaneous ranges  $r_1$ ,  $r_2$ , and  $r_3$ , a navigation fix giving vehicle position at  $t_2$  can be obtained. It is convenient to convert the transponder-location data into earth-centered Greenwich cartesian position vectors. That is, the position vector for transponder 1 is

$$\begin{aligned} p_{1x} &= \rho_1 \cos L_1 \cos \lambda_1 \\ p_{1y} &= \rho_1 \cos L_1 \sin \lambda_1 \\ p_{1z} &= \rho_1 \sin L_1 \end{aligned} \quad (3-121)$$

where  $\rho_1$  is earth radius plus transponder altitude,  $L_1$  is transponder geocentric latitude, and  $\lambda_1$  is transponder longitude. The three-simultaneous-range-measurement position fix equations suggested by Carlson in Ref. [3-8] can now be used. A transponder-plane coordinate system is established with transponder 1 the origin. Direction  $\underline{u}_1$  is chosen perpendicular to the plane containing the three transponders. Direction  $\underline{u}_2$  is along the line from transponders 1 to 2. Direction  $\underline{u}_3$  completes the orthogonal triad.

$$\Delta \underline{p}_2 = \underline{p}_2 - \underline{p}_1; \quad \Delta p_2 = |\Delta \underline{p}_2| \quad (3-122)$$

$$\Delta \underline{p}_3 = \underline{p}_3 - \underline{p}_1; \quad \Delta p_3 = |\Delta \underline{p}_3| \quad (3-123)$$

$$\underline{s} = \Delta \underline{p}_2 \times \Delta \underline{p}_3; \quad s = |\underline{s}| \quad (3-124)$$

$$\underline{u}_1 = \text{unit } [\underline{s}] \quad (3-125)$$

$$\underline{u}_2 = \text{unit } [\Delta \underline{p}_2] \quad (3-126)$$

$$\underline{u}_3 = \underline{u}_1 \times \underline{u}_2 \quad (3-127)$$

The sine and cosine of the (positive) angle between the direction from transponder 1 to 2 and the direction from transponder 1 to 3 are

$$s_{23} = s / \Delta p_2 \Delta p_3 \quad (3-128)$$

$$c_{23} = \Delta p_2 \cdot \Delta p_3 / \Delta p_2 \Delta p_3 \quad (3-129)$$

The estimated vehicle position  $p_{VE}$  is then determined according to

$$d_2 = (r_1^2 - r_2^2) / 2\Delta p_2 + \Delta p_2 / 2 \quad (3-130)$$

$$q_3 = (r_1^2 - r_3^2) / 2\Delta p_3 + \Delta p_3 / 2 \quad (3-131)$$

$$d_3 = (q_3 - d_2 c_{23}) / s_{23} \quad (3-132)$$

$$d_1 = (r_1^2 - d_2^2 - d_3^2)^{1/2} \quad (3-133)$$

$$p_{VE} = \pm d_1 \underline{u}_1 + d_2 \underline{u}_2 + d_3 \underline{u}_3 + p_1 \quad (3-134)$$

In general, two positions exist having the same ranges  $r_1, r_2, r_3$ . One position is above the plane of the transponders, the other position is the mirror image below the plane of the transponders. This solution ambiguity is indicated by the plus and minus sign for the term  $d_1 \underline{u}_1$ . The sign of the term should be chosen to place the estimated vehicle position above the plane of the transponders. A comparison of the magnitudes of the two possible geocentric position vectors determines which solution is farther from the center of the earth.

A derivation by Carlson of the equations for the position fix is presented in Ref. [3-10].

Having determined the estimated vehicle geocentric position vector  $p_{VE}$ , the corresponding altitude, geocentric latitude, and longitude may be extracted.

$$h = p_{VE} - r_E \quad (3-135)$$



$$L = \sin^{-1}(p_{VE_z}/p_{VE}) \quad (3-136)$$

$$\lambda = \tan^{-1}(p_{VE_y}/p_{VE_x}) \quad (3-137)$$

The two-argument version of the arctan routine is used to obtain the proper quadrant.

These values for latitude, longitude, and altitude are appropriate for the time  $t_2$  at which the "simultaneous" range measurements were made available. At the same instant  $t_2$  the position of the vehicle indicated by the inertial navigation equations was noted. The difference between the INS position at  $t_2$  and the DME-fix position at  $t_2$  is used to correct the running INS position indication, as soon as the result of the position fix calculation becomes available.

**3.4.3 Initial Error-Covariance Matrix.** Given the result of the position fix, the estimated directions  $\underline{b}_1$ ,  $\underline{b}_2$ ,  $\underline{b}_3$  from the three transponders to the vehicle are calculated using Eq. (3-96). Define a 3x3 B matrix whose rows are the b vectors.

$$B = \begin{bmatrix} \underline{b}_1^T \\ \underline{b}_2^T \\ \underline{b}_3^T \end{bmatrix} \quad (3-138)$$

Let the errors in the three range measurements form a range-error vector  $\underline{e}_r$

$$\underline{e}_r = \begin{bmatrix} e_{r_1} \\ e_{r_2} \\ e_{r_3} \end{bmatrix} \quad (3-139)$$

Let the east, north, and altitude position errors be the components of the vehicle position error vector  $\underline{e}_x$

$$\underline{e}_x = \begin{bmatrix} e_e \\ e_n \\ e_z \end{bmatrix} \quad (3-140)$$

It can be shown that, for the vehicle position errors small compared with the ranges to the three transponders, the range errors are related to the resulting position fix errors according to

$$\underline{e}_r = B \underline{e}_x \quad (3-141)$$

If the three  $b$  vectors span the three-dimensional vector space (that is, if the three  $b$  vectors do not all lie in a single plane), the  $B$  matrix can be inverted.

$$\underline{e}_x = B^{-1} \underline{e}_r \quad (3-142)$$

Assume the range errors have zero mean, in which case the position-fix errors also have zero mean. The  $3 \times 3$  range-error covariance matrix  $R$  and the  $3 \times 3$  position-fix error covariance matrix  $P_{3 \times 3}$  are by definition

$$R = E[\underline{e}_r \underline{e}_r^T] \quad (3-143)$$

$$P_{3 \times 3} = E[\underline{e}_x \underline{e}_x^T] \quad (3-144)$$

The covariance matrix  $P_{3 \times 3}$  can be calculated in terms of the range-error covariance matrix  $R$  according to

$$P_{3 \times 3} = B^{-1} R B^{-1T} \quad (3-145)$$

The error  $e_{r_1}$  in the  $1^{\text{th}}$  range measurement is as was given in Eq. (3-97)

$$e_{r_1} = r_1 e_p f(h) + e_{b_1} + e_{m_1} + e_{r_1} \quad (3-146)$$

where  $e_p$  is the sea-level propagation error (expressed as a fraction of range),  $e_{b_1}$  is the bias in the  $1^{\text{th}}$  transponder,  $e_{m_1}$  is the multipath random error, and  $e_{r_1}$  is other random error.<sup>1</sup> The a priori variance assumed for the  $1^{\text{th}}$  range measurement error is, as was given in Eq. (3-100)

$$R_{11} = r_1^2 \sigma_p^2 f^2(h) + \sigma_b^2 + \sigma_m^2 \cos^2 \epsilon + \sigma_r^2 \quad (3-147)$$

The cross-correlation (covariance) of the range-measurement errors to two different transponders is

$$R_{1j} = r_1 r_j \sigma_p^2 f^2(h) \quad i \neq j \quad (3-148)$$

Note it has been assumed that the same propagation error  $e_p$  exists throughout the terminal area, such that the range errors are correlated.

To summarize the initial position error covariance matrix  $P_{3 \times 3}$  (associated with the position fix utilizing the three "simultaneous" range measurements) is computed from Eqs. (3-138), (3-147), (3-148), and (3-145).

The matrix  $P_{3 \times 3}$  is used to initialize the upper-left  $3 \times 3$  partition of the full Kalman filter covariance matrix  $P$ .  $P_{44}$ ,  $P_{55}$ , and  $P_{66}$  are initialized with appropriate values for the variances of the east, north, and up velocity errors after entry.  $P_{77}$ ,  $P_{88}$ , and  $P_{99}$  are initialized with appropriate values for the variances of the east, north, and azimuth platform misalignment after entry.  $P_{10,10}$  is initialized with the variance of the magnitude-of-gravity and vertical-accelerometer error. If the barometric altimeter were to be used,  $P_{11,11}$  would be initialized with the variance of the altimeter error. Values for these initial diagonal elements of the covariance matrix, used in this study are

$$P_{44} = P_{55} = P_{66} = (10 \text{ m/sec})^2 \quad (3-149)$$

$$P_{77} = P_{88} = P_{99} = (1.5 \text{ milliradian})^2 \quad (3-150)$$

$$P_{10,10} = \sigma_{gz}^2 + \sigma_{ABIAS}^2 + \sigma_{ASF}^2 g^2 \quad (3-151)$$

$$P_{11,11} = \sigma_{alt}^2 + \sigma_{temp}^2 h_s^2 + \sigma_{sp}^2 v_s^4 \quad (3-152)$$

The data required for Eq. (3-151) and (3-152) was presented in Table 3-4.

No attempt has been made to compute the cross-correlation of the initial errors in state variables 4 through 11. Therefore, the corresponding off-diagonal elements of the covariance matrix have been set to zero.

A summary of the covariance matrix initialization is presented in Table 3-9.

Following the initial position fix and covariance matrix initialization, additional range and delta-range measurements are incorporated using the normal navigation filter equations. In this manner the velocity estimates quickly become updated, completing the initial capture of the navigation position and velocity errors.

Geometry Matrix

$$B = \begin{bmatrix} \underline{b}_1^T \\ \underline{b}_2^T \\ \underline{b}_3^T \end{bmatrix}$$

Assumed range error-covariance matrix

$$R_{1j} = r_1 \ r_j \ \sigma_p^2 \ f^2(h) \\ + \delta_{1j} (\sigma_b^2 + \sigma_m^2 \cos^2 \epsilon + \sigma_r^2)$$

Position-fix error-covariance matrix

$$P_{3 \times 3} = B^{-1} R B^{-1T}$$

Complete state error-covariance matrix

$$P = \begin{bmatrix} P_{3 \times 3} & 0 \\ 0 & D \end{bmatrix}$$

Table 3-9 Covariance Matrix Initialization Summary

## CHAPTER 4

### TOTAL SYSTEM DESIGN AND PERFORMANCE

In Chapter 3 we have presented the on-board approach and landing navigation equations design, including: a Kalman filter algorithm, the choice of state variables, the modeling in the filter of the various sources of navigation error, the measurement incorporation equations, and the landing navigation initialization logic.

In this chapter we address broader system design questions such as: How many transponders are required? Where should the transponders be located? Is an independent source of altitude information required to meet the landing navigation accuracy specification? Do the on-board equations deliver the desired performance? Does the approach trajectory affect the performance results? What is the effect of measurement rate on performance? What DME accuracy is required? What is the effect of earlier transponder drop-out just before touchdown? What is the effect of degraded IMU performance?

The principal tool, used through this chapter, to help obtain answers to these design questions, is a detailed digital simulation of the on-board navigation equations, the vehicle approach and landing trajectory, the inertial measurement unit, the distance measuring equipment, and other sources of landing navigation error.

#### 4.1 Baseline System Performance

4.1.1 Landing Trajectory. The landing trajectory utilized in the baseline simulation is shown in Fig. 4-1 and 4-2. This landing pattern is typical of the approach and landing trajectories commanded by the Morth approach guidance (Reference [4-1]).

The simulation begins in the terminal area at an altitude of 6100 meters. The speed is 170 m/sec. The vehicle performs a

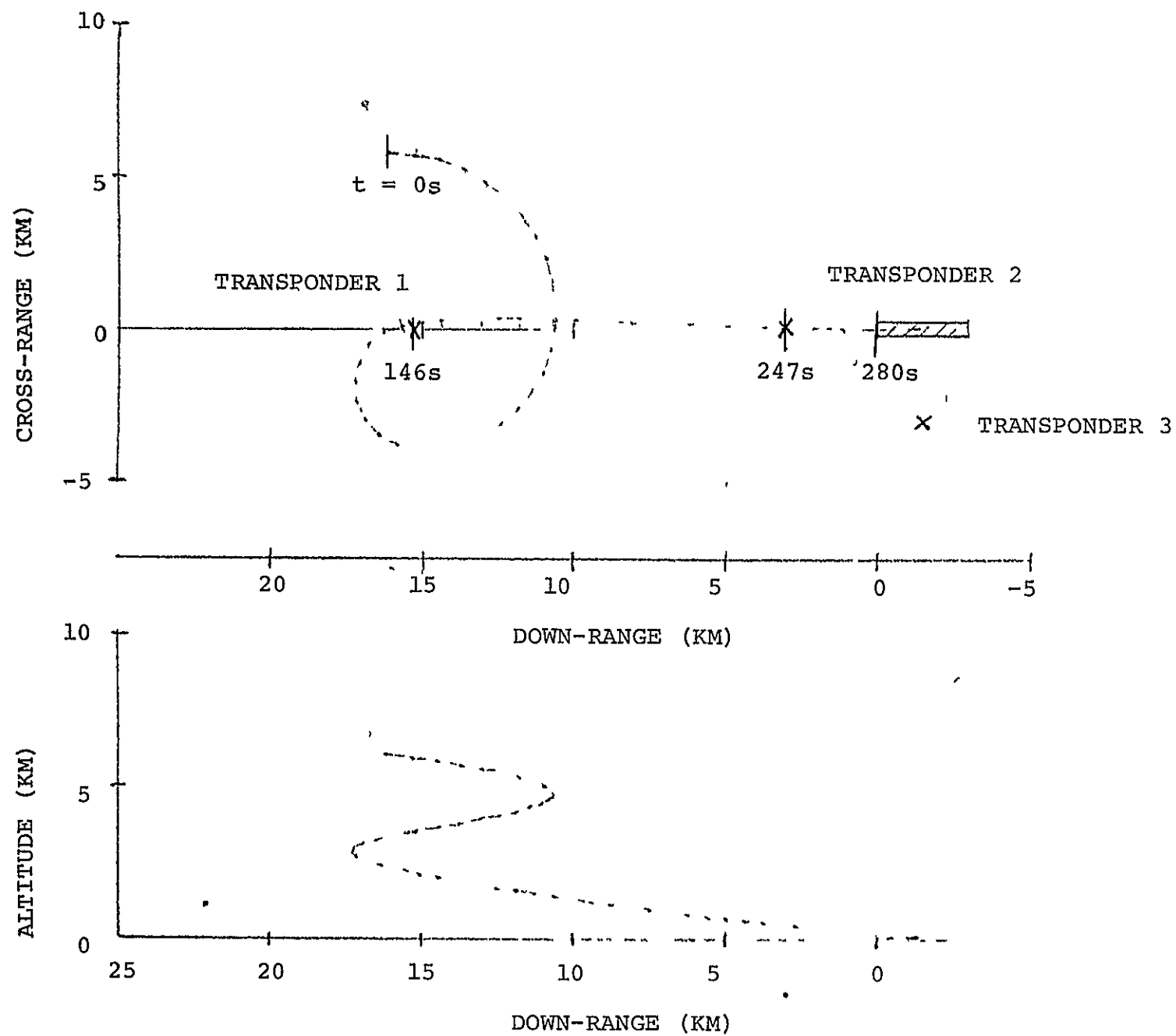


Fig. 4-1 BASELINE LANDING TRAJECTORY

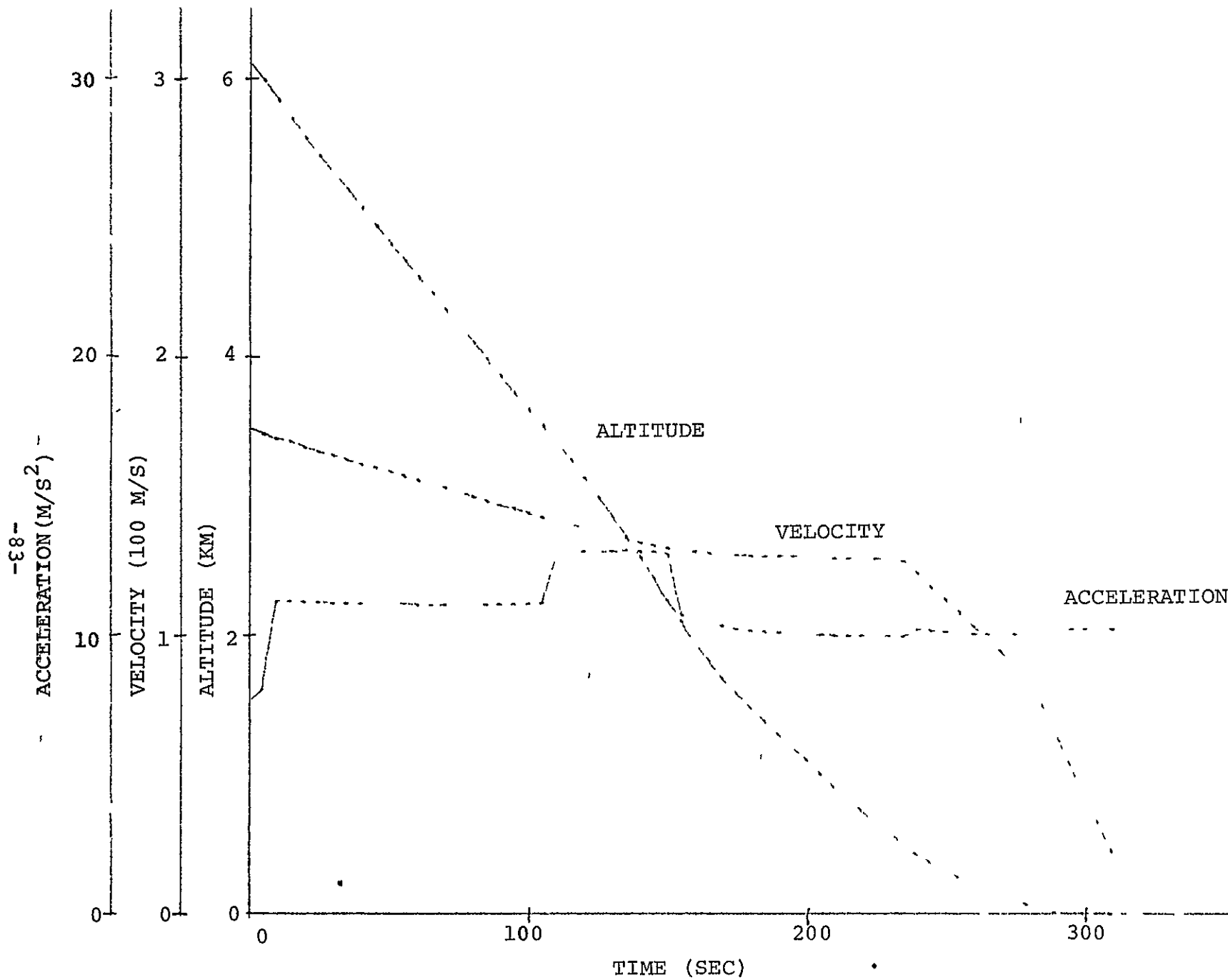


Fig. 4-2 BASELINE LANDING TRAJECTORY TIME HISTORIES



right turn circle arriving on final approach 15 km from the end of the runway. Before the flare, the vehicle speed has gradually decreased to 130 m/sec. During the prolonged flare maneuver the vehicle decelerates, arriving over the runway threshold at a speed of 90 m/sec. After touchdown, the vehicle decelerates at 0.2 g. The simulation ends after the vehicle has almost rolled to a stop.

4.1.2 Transponder Locations. Three transponders are utilized in the baseline simulation. Their locations are also shown in Fig. 4-1. Two transponders are placed under the final approach path, transponder 1 being 15 km from the runway threshold and transponder 2 being 3 km from the runway threshold. The third transponder is located 3 km to the side of the middle of the 3 km runway. The rationale for this transponder deployment is discussed in Section 4.3.

4.1.3 Measurement Sequence. The first three range measurements are used to calculate the initial position fix at  $t=0$ . Following the position fix and error-covariance-matrix initialization, the Kalman filter equations are activated. At  $t=2$  sec, range and delta-range measurements with transponder 1 are incorporated. At  $t=4$  sec, range and delta-range measurements with transponder 2 are incorporated. At  $t=6$  sec range and delta-range measurements with transponder 3 are incorporated. This completes the landing navigation initialization sequence.

Following initialization, the measurement-incorporation rate is reduced to one pair of range and delta-range measurements every 10 sec. The transponder sequence is simply 1, 2, 3, 1, 2, 3, etc. The effect of other measurement rates on performance is presented in Section 4.5.

Clearly, the measurements with transponder 2 during the final approach have a critical effect on the altitude and altitude-rate navigation accuracy obtained for touchdown. To ensure obtaining the best altitude geometry, as transponder 2 is approached the normal measurement cycle is interrupted. Several pairs (usually three) of range and delta-range measurements are obtained with transponder 2. The overflight logic includes a computation of estimated time-to-go to the point-of-closest-approach. Thus, one of the measurement pairs is timed to occur as close as possible to the point directly over the transponder.

Following the overflight of transponder 2, the measurement selection logic, attempts to resume the normal cycle. The simulation of the DME performance assumes that range and delta-range

measurements cannot be obtained (or cannot be trusted) if the vehicle elevation angle (as seen from the transponder) drops below  $1^\circ$ . If a measurement to the desired transponder cannot be obtained, the measurement selection logic immediately calls for a measurement with the next transponder. If none of the three transponders can be reached, the measurement selection logic allows the normal 10 sec interval to pass before again attempting to reach any transponder. As a result, with the baseline trajectory and baseline transponder locations, after the overflight of transponder 2, one finds that measurements to the most distant transponder (1) can no longer be obtained. Typically only one more measurement to transponder 3 is obtained before it also is unreachable. Finally, only two more measurements are obtained to the nearest transponder (2) before it also is unreachable. Touchdown and rollout are accomplished based on the inertial navigation alone. The effect of other values for the elevation cut-off angle is presented in Section 4.7.

4.1.4 Monte Carlo Simulation. For the baseline system performance demonstration, five landings have been conducted with independent random sources of navigation error. Errors selected independently (by a random number generator) for each of the five landings include: initial position errors (3), initial velocity errors (3), initial platform misalignments (3), transponder biases (3), propagation error (1), acceleration biases (3), accelerometer scale-factor errors (3), accelerometer input axis misalignments ( $3 \times 2$ ), gyro bias drift rates (3), gyro acceleration sensitive drift coefficients ( $3 \times 2$ ), gyro input axis misalignments ( $3 \times 2$ ), gyro torquing scale factor errors (3), and gravity deflections and anomaly biases (3). In addition, the random number generator utilized throughout the simulation (for multipath and other random measurement errors) is started at a different random number for each of the five landings. The standard deviations used in conjunction with the random number generator to select the five sets of navigation-error sources are those presented in Section 2.1 for the DME, in Section 2.2 for the IMU and gravity, and in Section 3.4 for the initial navigation errors.

The results of the five landings are summarized in Table 4-1. The root-mean-square (RMS) values (taken over the five landings) of the actual navigation errors are presented. Also shown is the square-root of the corresponding diagonal element of the on-board-computed error-covariance matrix  $P$ . Three instants of time are presented: 1) immediately after the initial position fix and covariance initialization, 2) turning onto final approach, and 3) touchdown. The changing value of the gravity anomaly (as the vehicle flies across the terrain) is not printed by the simulation, so the actual RMS value of state-variable 10 is not presented in the table.

State Variable	Units	After initial position fix t = 0 sec		Turning onto final approach t = 126 sec		At touchdown t = 280 sec	
		RMS error 5 runs	P <sup>1/2</sup> 1st run	RMS error 5 runs	P <sup>1/2</sup> 1st run	RMS error 5 runs	P <sup>1/2</sup> 1st run
1. Error in east position	meters	1.6	1.4	.67	.71	.35	.37
2. Error in north position	meters	7.3	9.6	4.8	3.8	.88	.88
3. Error in altitude	meters	7.5	8.7	5.0	4.1	.57	.82
4. Error in east velocity	cm/sec	1140	1000	3.1	2.8	1.9	1.0
5. Error in north velocity	cm/sec	1350	1000	9.6	11.1	6.7	6.5
6. Error in altitude rate	cm/sec	1140	1000	2.8	6.7	2.6	3.4
7. Platform tip about east	milli-radian	.96	1.50	.36	.26	.14	.26
8. Platform tip about north	milli-radian	.78	1.50	.18	.27	.11	.15
9. Platform azimuth error	milli-radian	1.23	1.50	.19	.74	.36	1.4
10. Magnitude of gravity and accel. error	cm/sec <sup>2</sup>	-	.12	-	.082	-	.037

Table 4-1 Baseline System Performance Results

The time histories of the position and velocity errors for each of the five landings are plotted in Figures 4-3 through 4-8. In addition, the on-board computed position and velocity  $1\sigma$  uncertainties (square root of the corresponding covariance-matrix element) are shown. The onboard-computed uncertainty is taken from the first of the five Monte-Carlo runs. (The computed uncertainties from the other runs are equal to within two or three significant figures.) The cross-hatched area is the band between plus and minus the onboard-computed  $1\sigma$  uncertainty. The plot program was told to skip the first 50 sec of data to avoid problems with the frequently off-scale early navigation errors and uncertainties.

The onboard-computed  $1\sigma$  uncertainties are plotted by themselves in Fig. 4-9 and 4-10. This is for clarity and is also for comparison with the similarly-presented results of the subsequent parametric studies. Each plot-point is the computed uncertainty after incorporating one measurement. The vertical discontinuities show the uncertainty reduction associated with the second measurement of the measurement pair (the delta range measurement).

4.1.5 Interpretation of Results. The performance of the initial position fix logic (shown in Table 4-1) is excellent. Independent of the initial inertial navigation position error (30 km east, 30 km north, 3 km altitude  $1\sigma$  in this Monte-Carlo simulation), all components of position error have been reduced to less than 10 meters RMS. Of course, this very excellent performance is related to the good initial measurement geometry of this simulation, which starts at  $t=0$  already in the terminal area. The performance of the initial-position-fix logic starting much farther from the terminal area is presented in Section 4.4. The initial position  $1\sigma$  uncertainties (computed by the onboard equations as a function of the position-fix results) are seen to be in excellent agreement with the RMS errors.

The majority of the individual Monte-Carlo position and velocity error time-histories (Figs. 4-3 through 4-8) are seen to be within the onboard-computed  $1\sigma$  uncertainty band. Similarly, the RMS results, calculated at three instants, (Table 4-1), are generally close to the onboard-computed  $1\sigma$  uncertainty. This is evidence that the on-board navigation equations have been designed satisfactorily. The choice of state variables is satisfactory. The statistical models, used to account for the sources of navigation error, maintain the computed uncertainties at appropriate levels. We are pleased that no adjustment of the statistical models used by the filter (as presented in Chapter 3) was necessary to obtain these performance results. The filter has not been "tuned" to the baseline simulation.

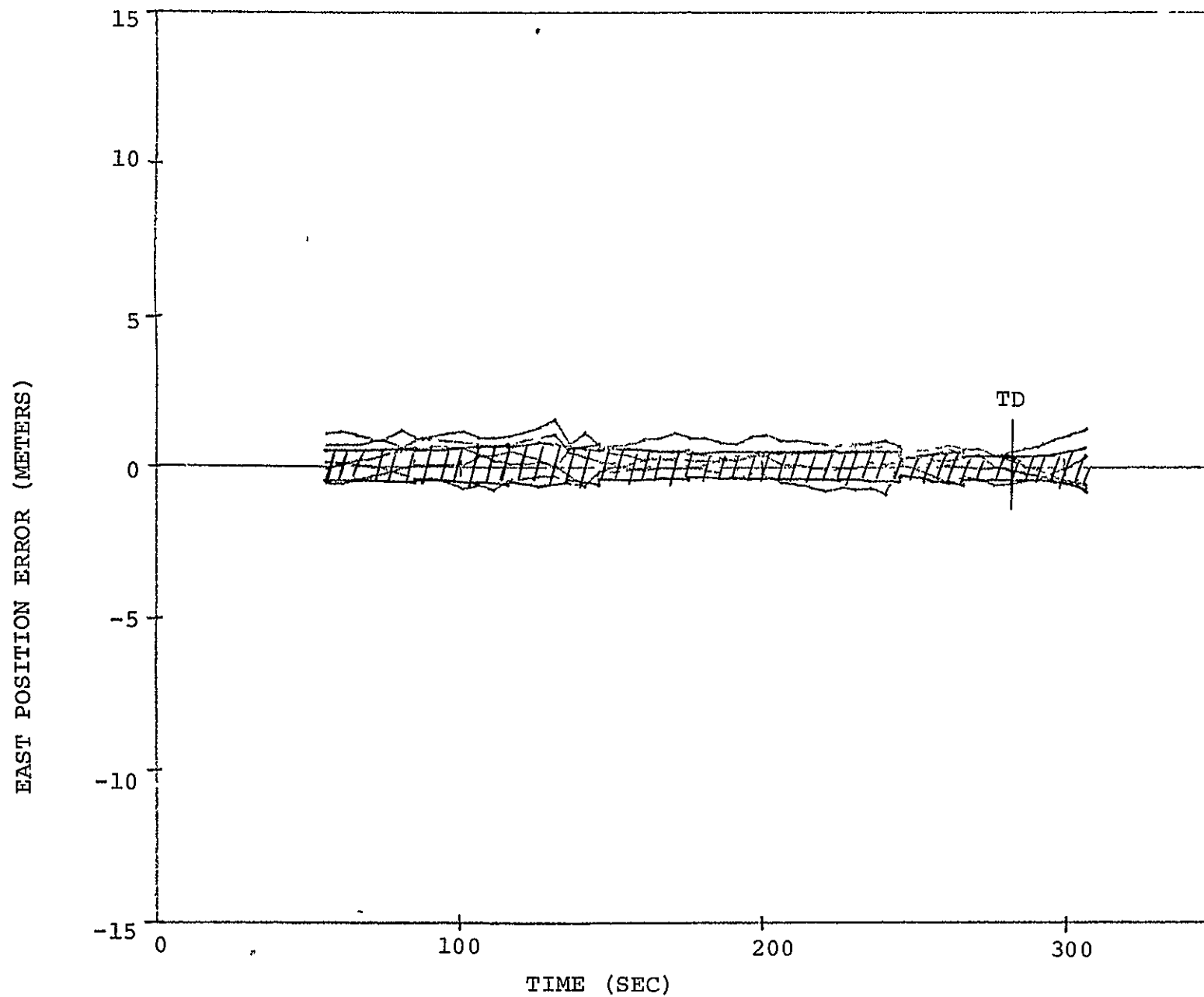


Fig. 4-3 EAST POSITION ERROR MONTE-CARLO RESULTS

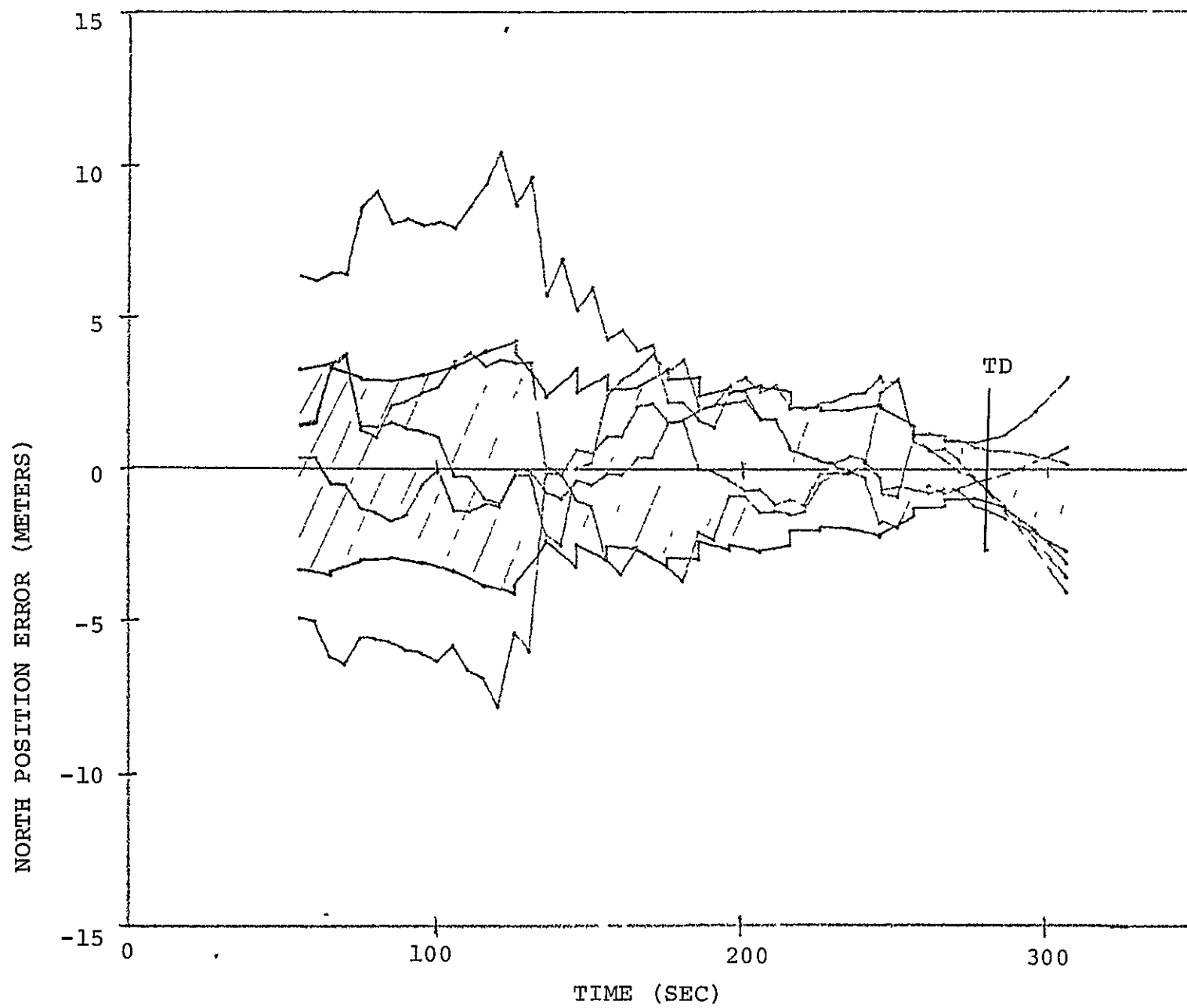


Fig. 4-4 NORTH POSITION ERROR MONTE-CARLO RESULTS

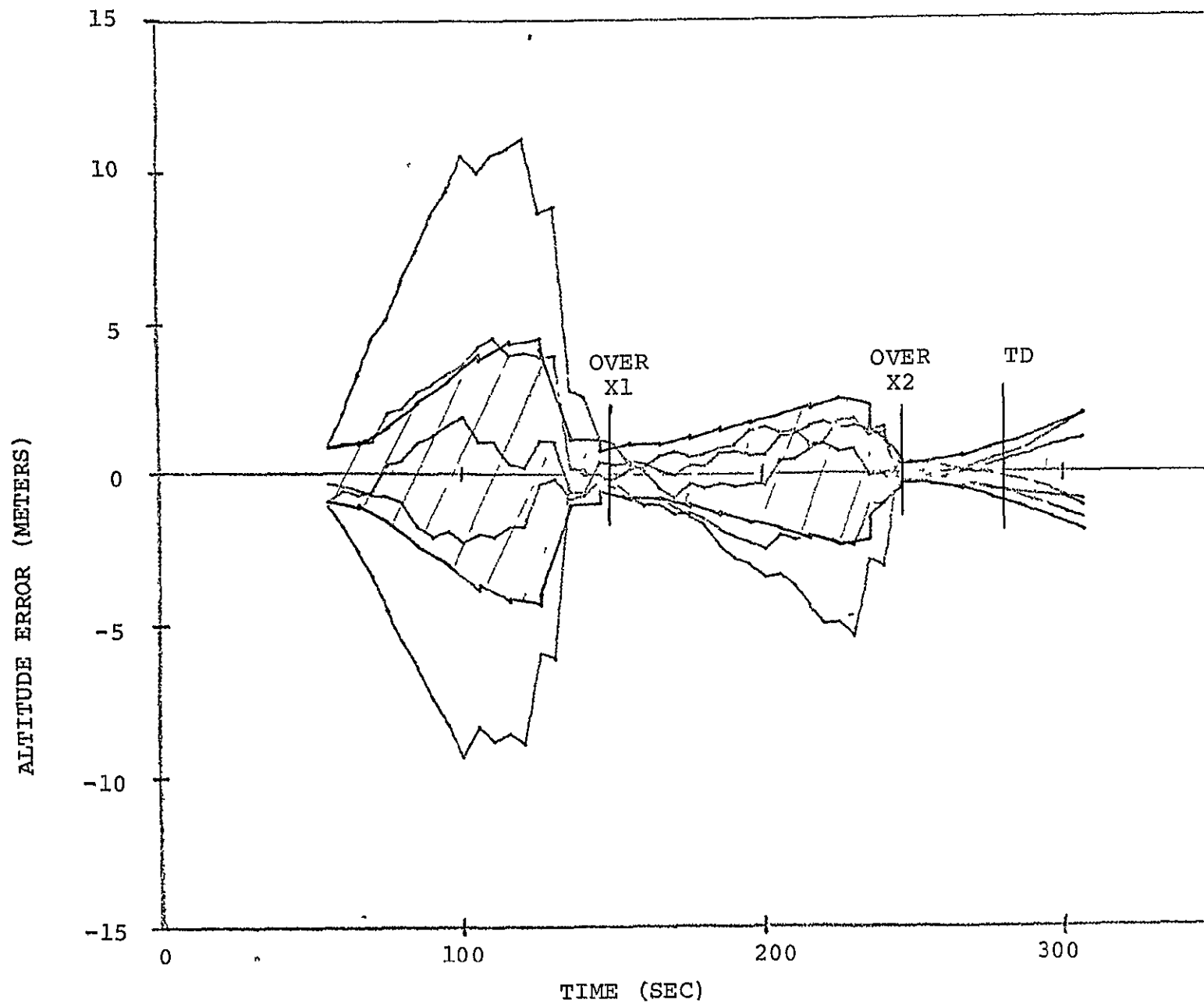


Fig. 4-5 ALTITUDE ERROR MONTE-CARLO RESULTS

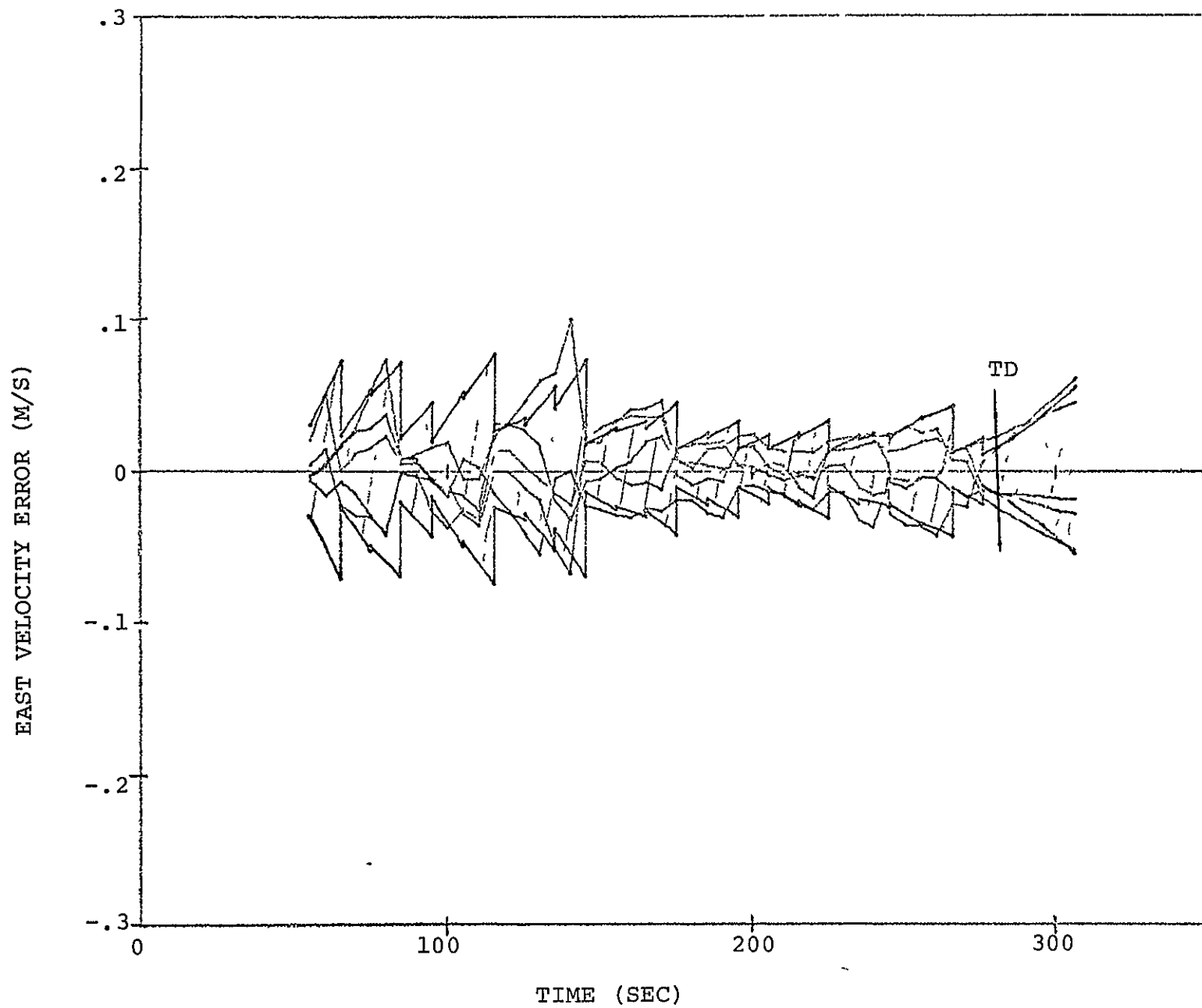


Fig. 4-6 EAST VELOCITY ERROR MONTE-CARLO RESULTS



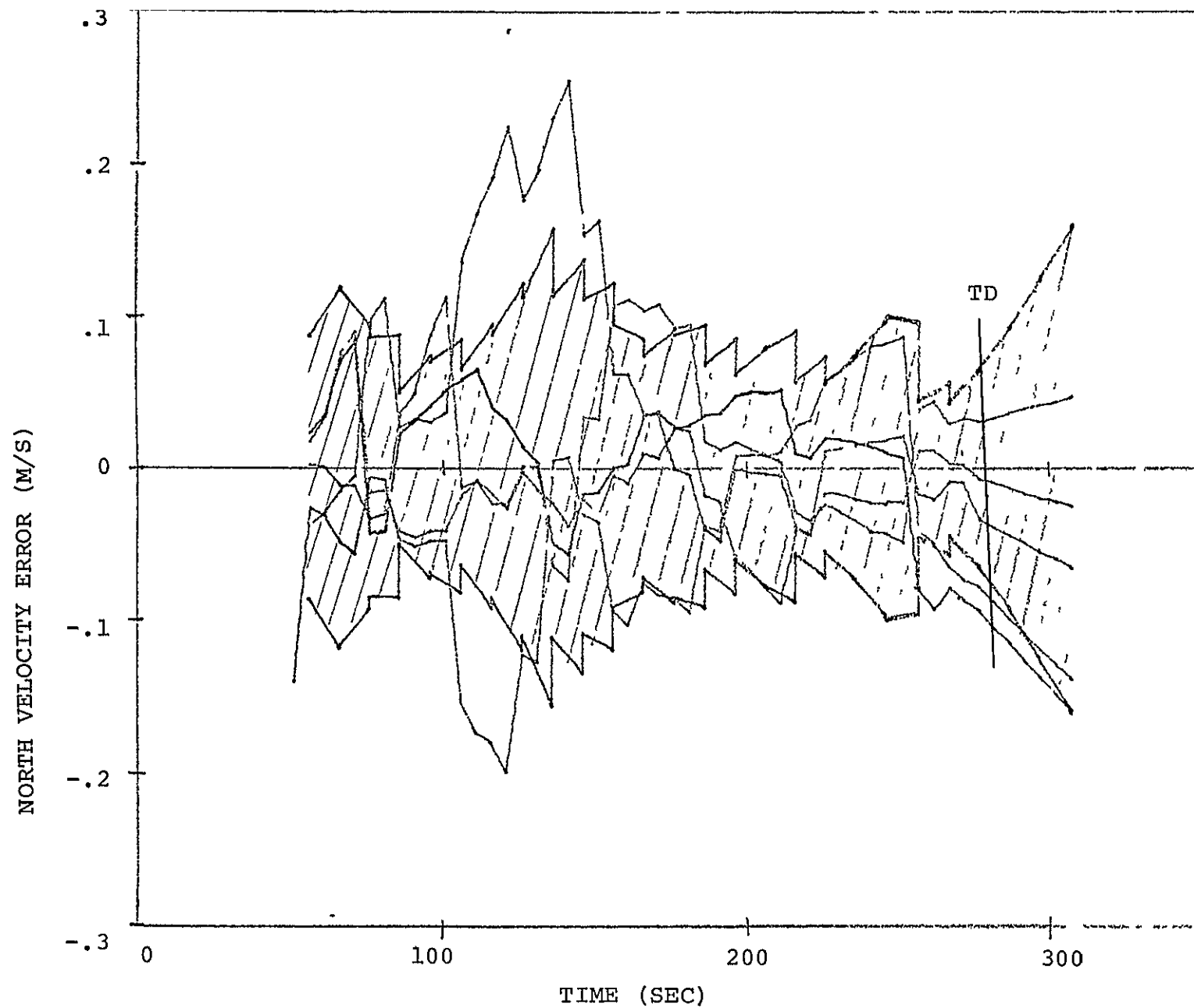


Fig. 4-7 NORTH VELOCITY ERROR MONTE-CARLO. RESULTS

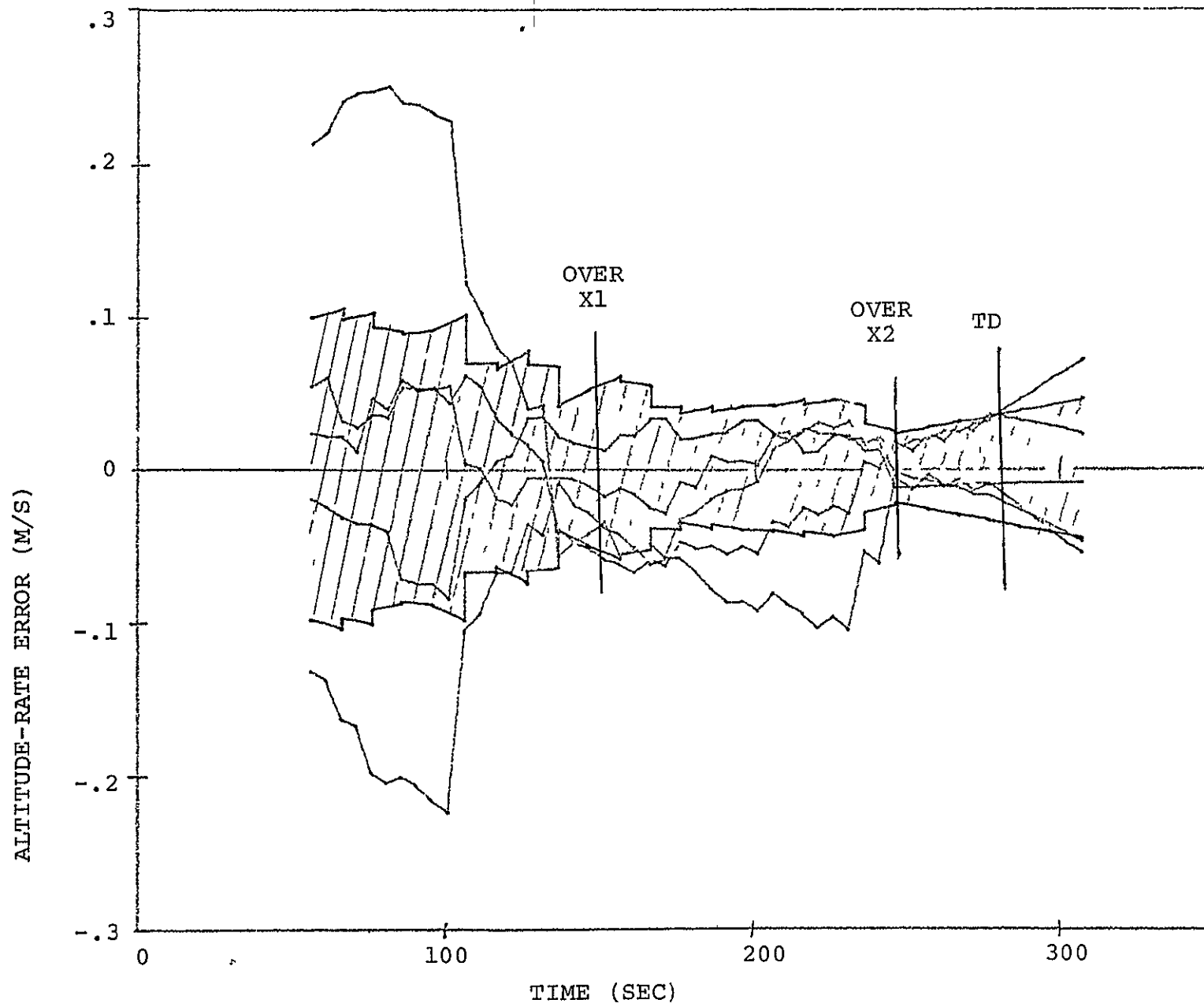


Fig. 4-8 ALTITUDE-RATE ERROR MONTE-CARLO RESULTS

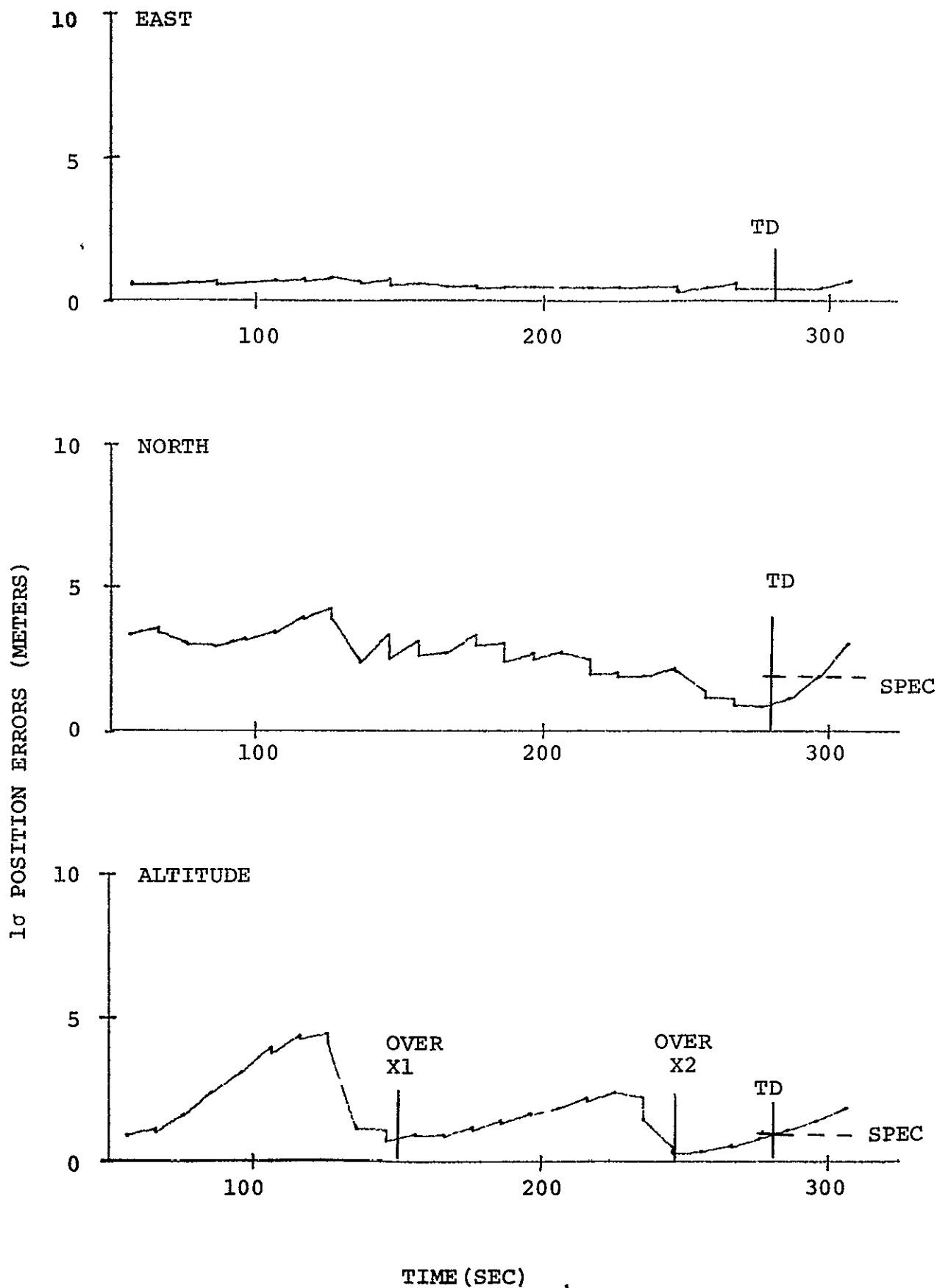


Fig. 4-9 BASELINE SYSTEM POSITION UNCERTAINTY

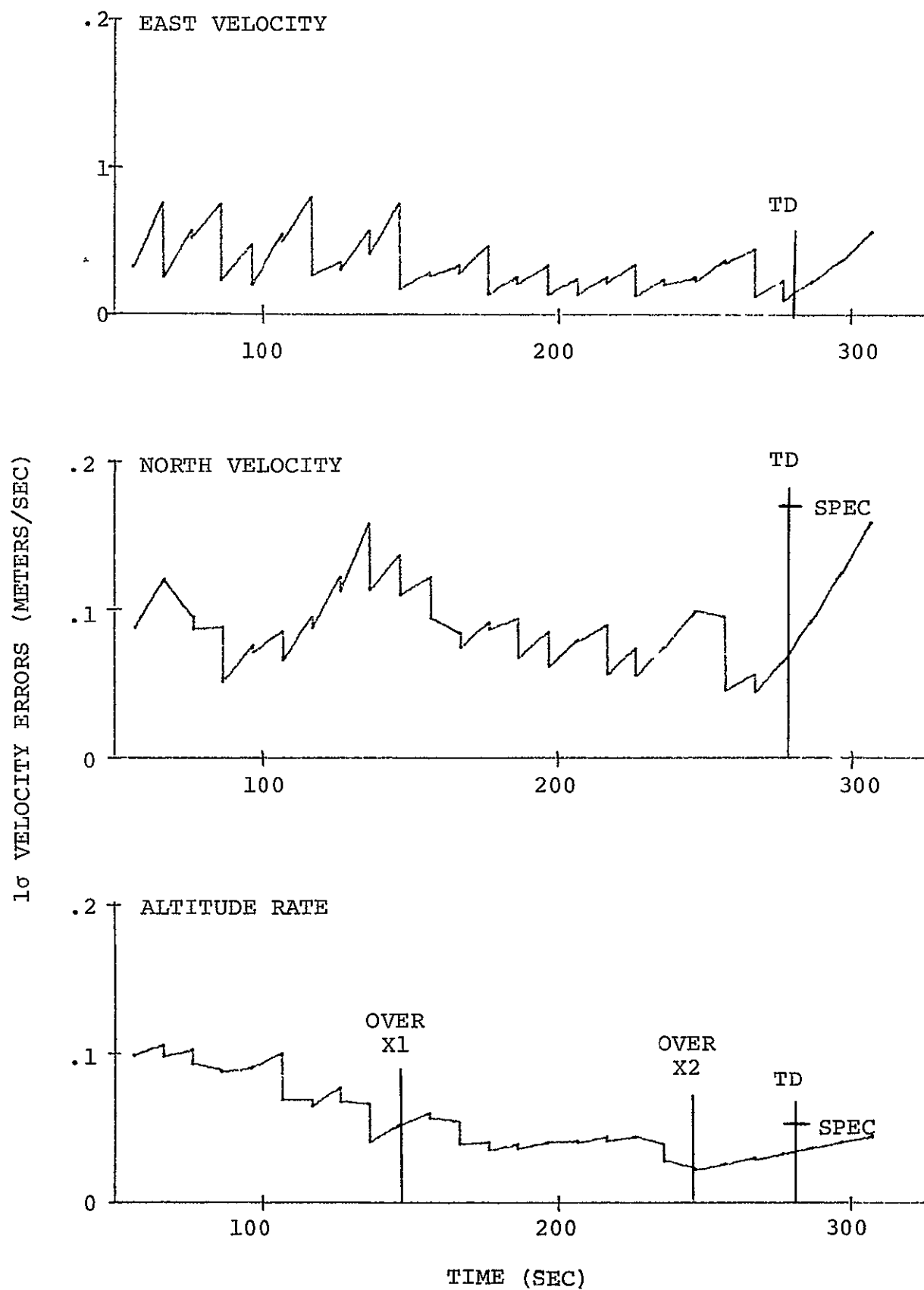


Fig. 4-10 BASELINE SYSTEM VELOCITY UNCERTAINTY

In this and all subsequent simulations, the runway is oriented east-west. Thus, easterly navigation errors are errors directed parallel to the runway. This is the direction having the most relaxed accuracy specifications. The northerly navigation errors are errors directed across the runway. Moderately tight accuracy specifications apply to this direction to ensure that the vehicle will not let its landing gear slip off the side of the runway. The altitude direction has the most stringent accuracy requirements. The RMS position and velocity errors at touchdown are again presented in Table 4-2. Also presented are the navigation accuracy specifications (1 $\sigma$ ) for each component of position and velocity. The RMS errors in every case show better performance than the accuracy specification. A  $\chi^2$  test of the statistical significance of the five-run Monte-Carlo results gives confidence that the baseline system indeed meets the accuracy specification. The confidence that an individual component of position or velocity meets its specification is presented in the last column of Table 4-2.

The figures and tabulated data show that accurate navigation is achieved throughout final approach, touchdown, and rollout. After touchdown, the divergence of the altitude and altitude-rate can be ignored. The north position error also diverges, but cannot be ignored if this is a Category III-C landing (cannot see to control rollout or taxiing). If measurements to transponder 3 could be guaranteed while on the runway (0° elevation angle) then the growth of cross-runway position error would be eliminated.

The effect of flying over transponders 1 and 2 on final approach is clearly seen in Fig. 4-5. The excellent altitude-measurement geometry reduces the altitude error to near zero.

Note the excellent performance of the in-flight alignment capability. Table 4-1 shows that near the end of the turn onto final approach ( $t = 126$  sec), the IMU misalignment has been reduced noticeably about all axes including the azimuth axis. The excellent azimuth performance in this simulation is due to the prolonged-turn acceleration. A straight-in approach trajectory would not have the necessary horizontal  $\Delta V$  to improve the azimuth misalignment significantly. On final approach, the steady 1g vertical specific force permits the in-flight alignment capability to reduce further the tips about the east and north axes. The absence of strong horizontal  $\Delta V$  permits the azimuth gyro drift to degrade the azimuth alignment. However, the accuracy at touchdown is still noticeably better than at the beginning of the simulation. Note the driving noise that models azimuth-gyro-drift rate is conservatively large, the onboard-computed 1 $\sigma$  uncertainty in azimuth alignment at touchdown being four times the actual RMS misalignment.

Navigation Error	Units	RMS error 5 runs	1 $\sigma$ Spec	Confidence nav. system meets spec.
Error in east position (along runway)	meters	.35	10	.99
Error in north position (across runway)	meters	.88	1.7	.92
Error in altitude	meters	.57	1	.90
Error in east velocity (along runway)	cm/sec	1.9	100	.99
Error in north velocity (across runway)	cm/sec	6.7	17	.98
Error in altitude rate	cm/sec	2.6	5	.92

Table 4-2 System Performance and Accuracy Specification

The most significant conclusion that follows from the baseline system performance demonstration is that the DME-aided-inertial system meets the shuttle landing navigation accuracy specification. An independent source of altitude information is not required.

A five-run Monte-Carlo simulation requires five times as much computer time to generate its results as is required for a single run. Having established with confidence the basic performance capability of the landing navigation system, we will no longer exercise the Monte-Carlo simulation. For the parametric results presented in the following sections, we shall quote the onboard-computed 1 $\sigma$  navigation uncertainties from single runs. The baseline Monte-Carlo results have shown that there is excellent agreement between these uncertainties and the actual RMS navigation errors.

#### 4.2 Does the Approach Pattern Affect the Results?

One might reasonably ask: does the excellent performance, demonstrated in the previous section, depend on the approach trajectory? Two additional landings have been simulated to answer this question.

4.2.1 Landing With Airport Overflight. The approach pattern shown in Figs. 4-11 and 4-12 has been simulated. This approach pattern is typical of the two-turn energy management guidance of Moore (Reference [4-2]). This particular trajectory is quite favorable for the navigation because it flies directly over the airport at high altitude, thereby giving excellent geometry for the initialization.

The resulting navigation performance is shown in Figs. 4-13 and 4-14. (The baseline system performance was shown in Figs. 4-9 and 4-10.) As expected, there is some improvement in the initial performance, especially in the velocity errors. After turning on to final approach, there is very little difference between this and the baseline simulation. After touchdown, the easterly (down runway) position and velocity errors are larger. This is because the flare trajectory was somewhat lower in this simulation causing a loss of data from all transponders earlier before touchdown. The level of error, however, is still extremely small compared with the down-runway tolerable errors.

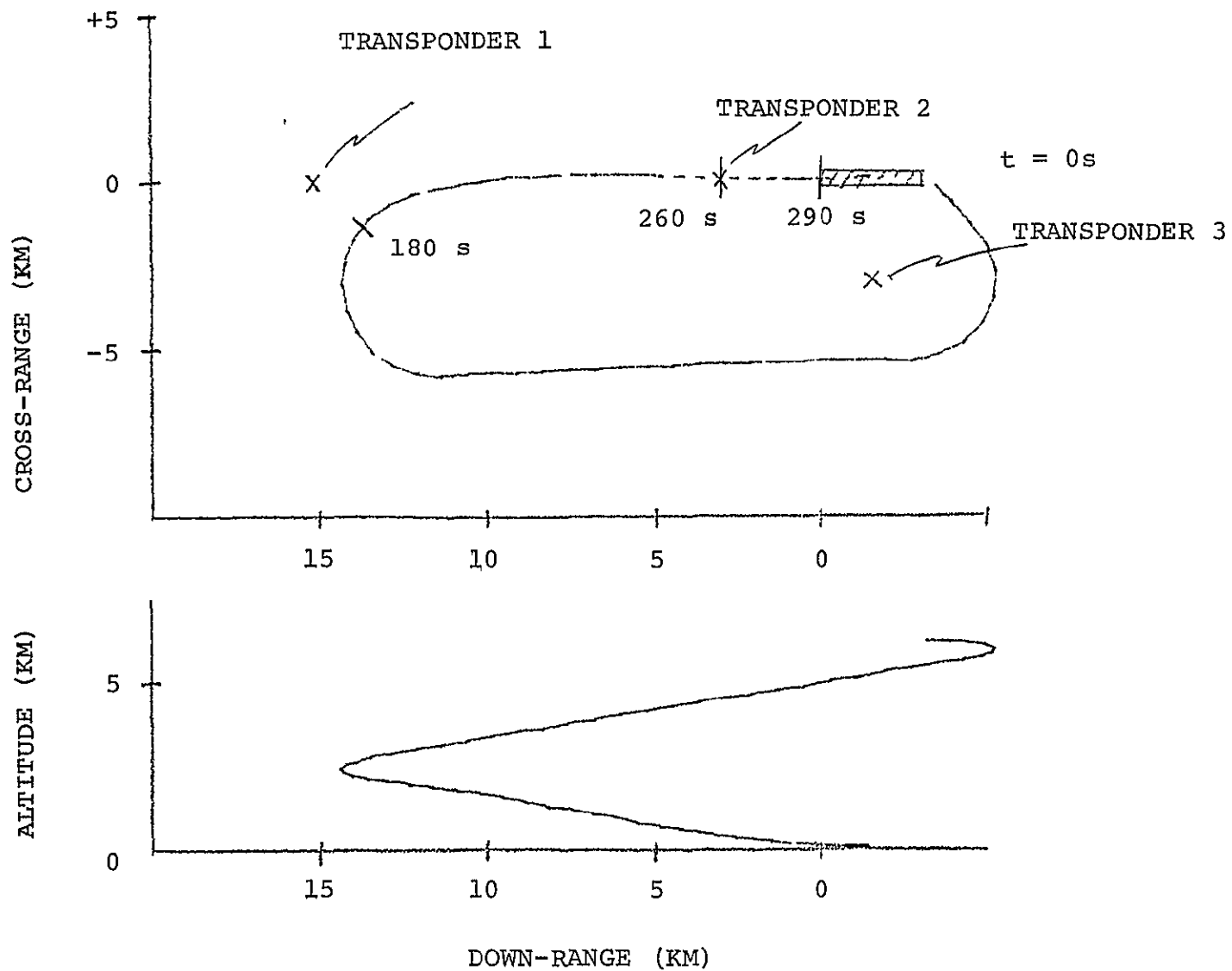


Fig. 4-11 LANDING TRAJECTORY WITH AIRPORT OVERFLIGHT



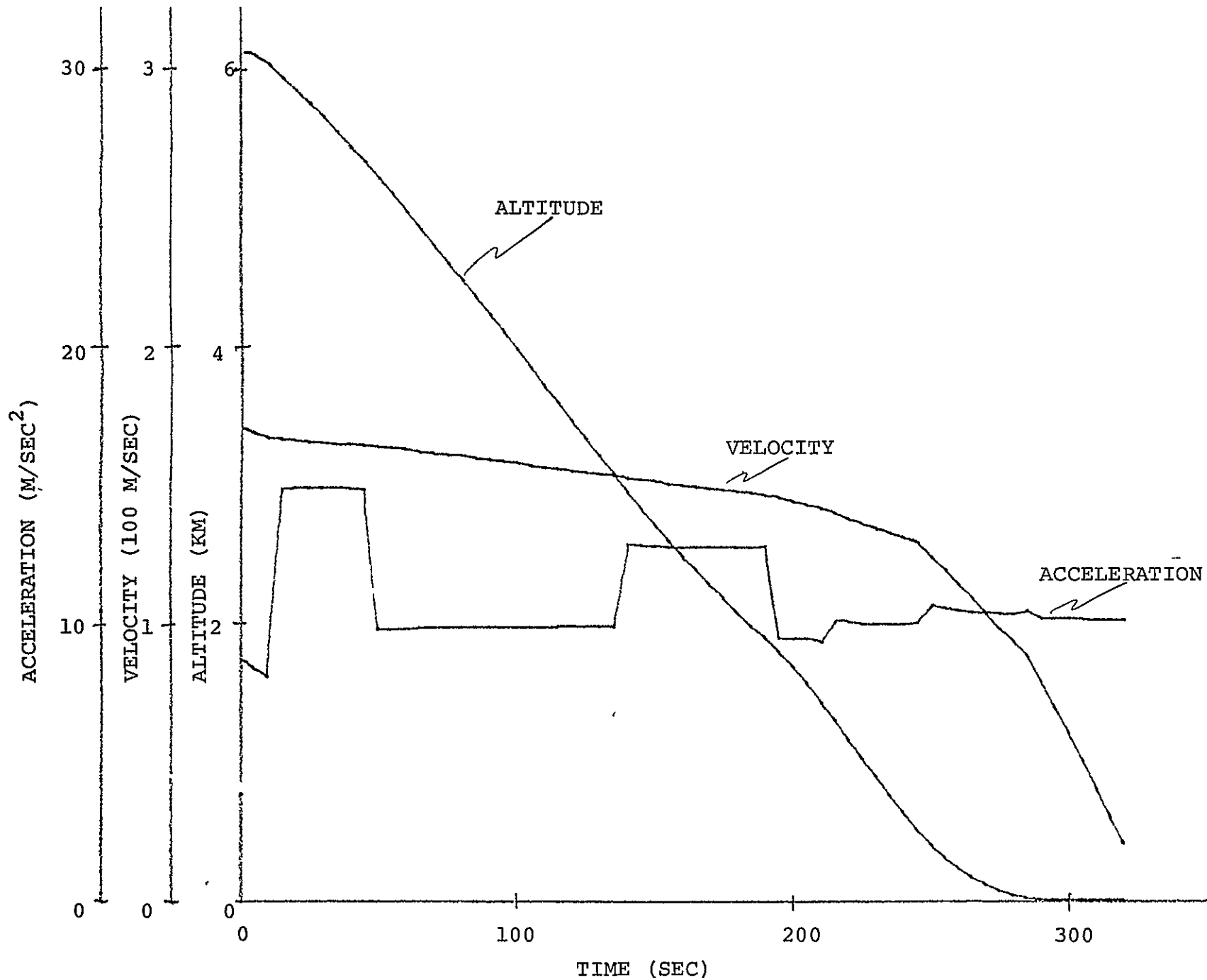


Fig. 4-12 OVERFLIGHT TRAJECTORY TIME HISTORIES

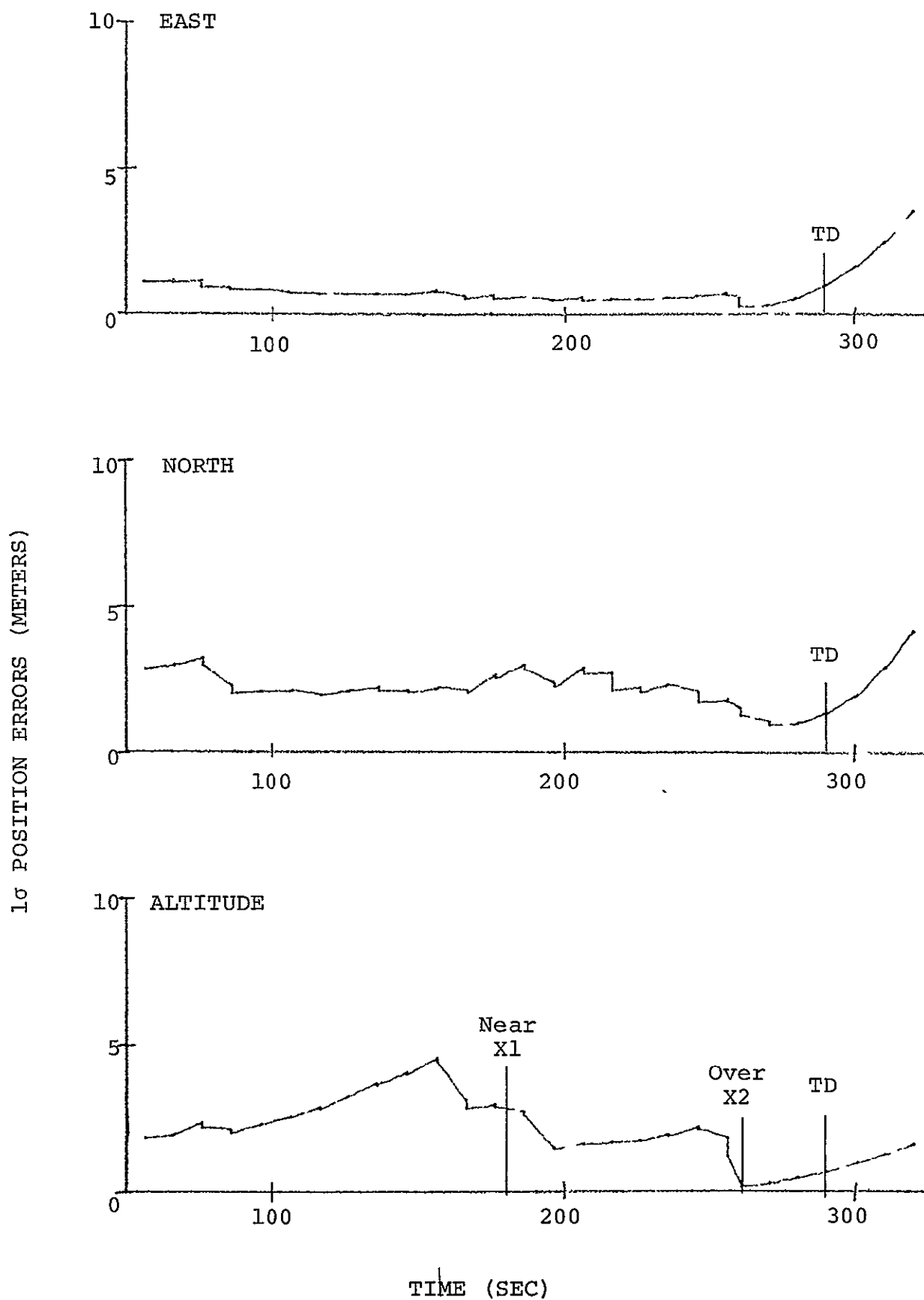


Fig. 4-13 OVERFLIGHT POSITION UNCERTAINTY

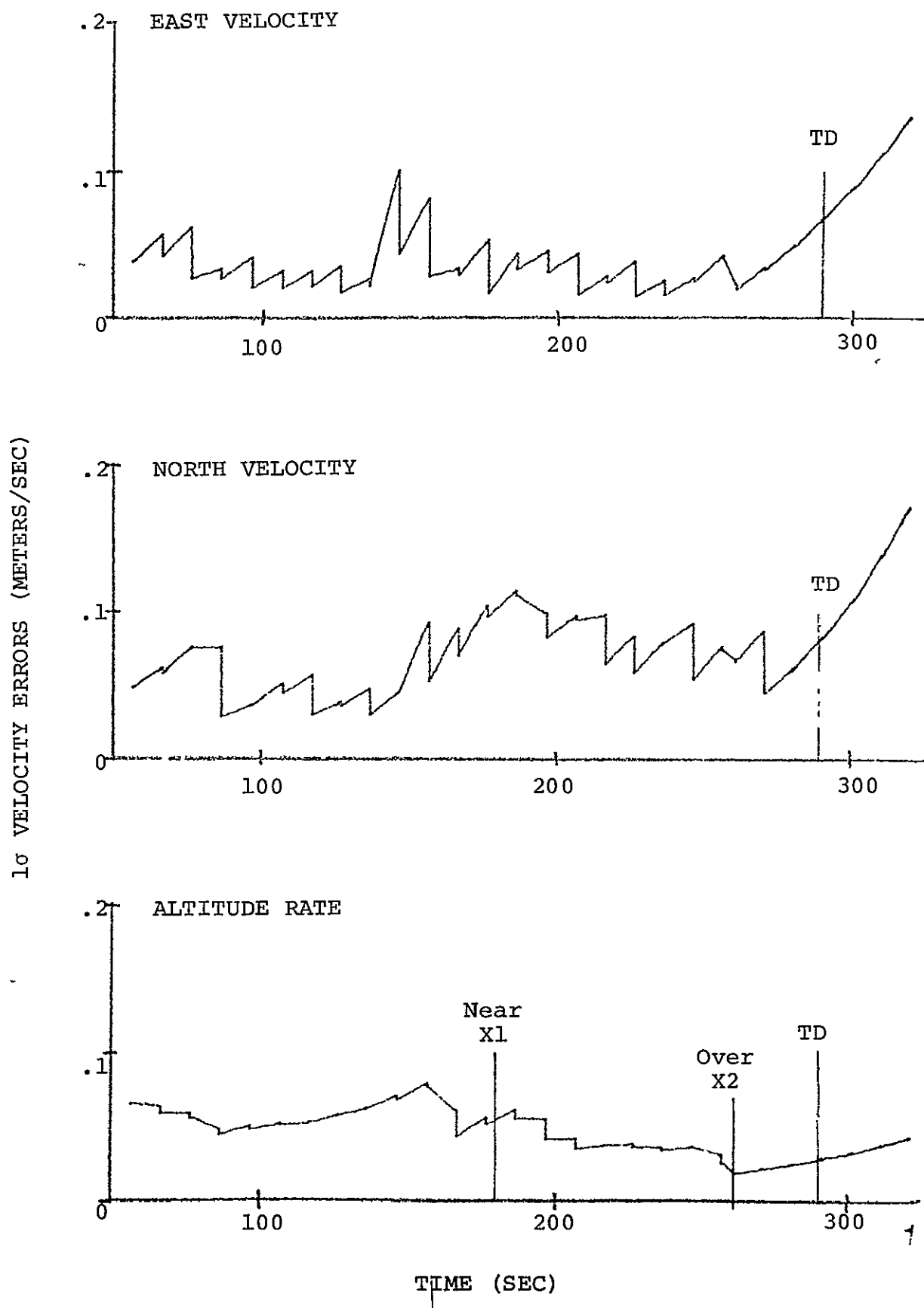


Fig. 4-14 OVERFLIGHT VELOCITY UNCERTAINTY

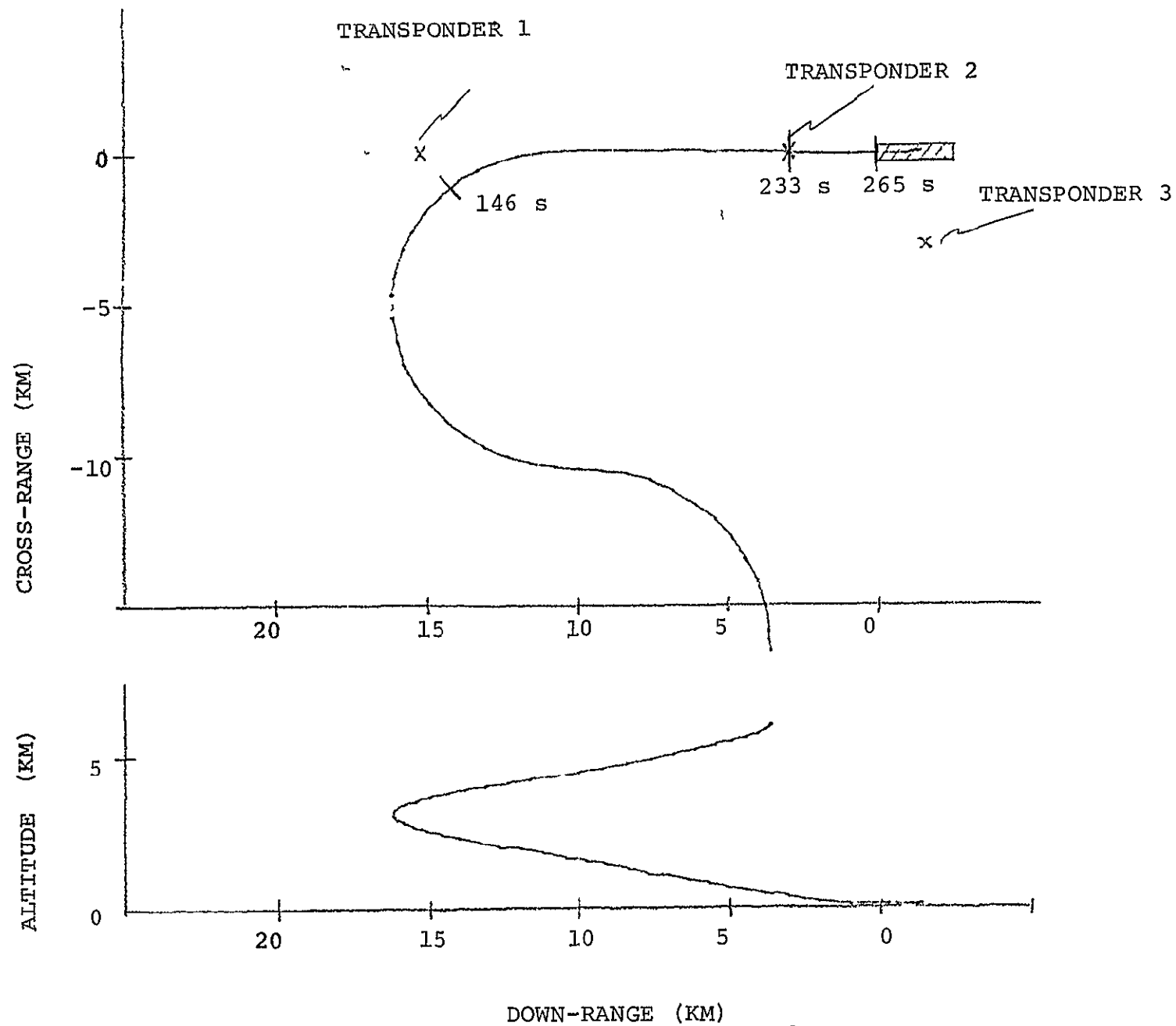


Fig. 4-15 LANDING TRAJECTORY WITH APPROACH FROM SIDE

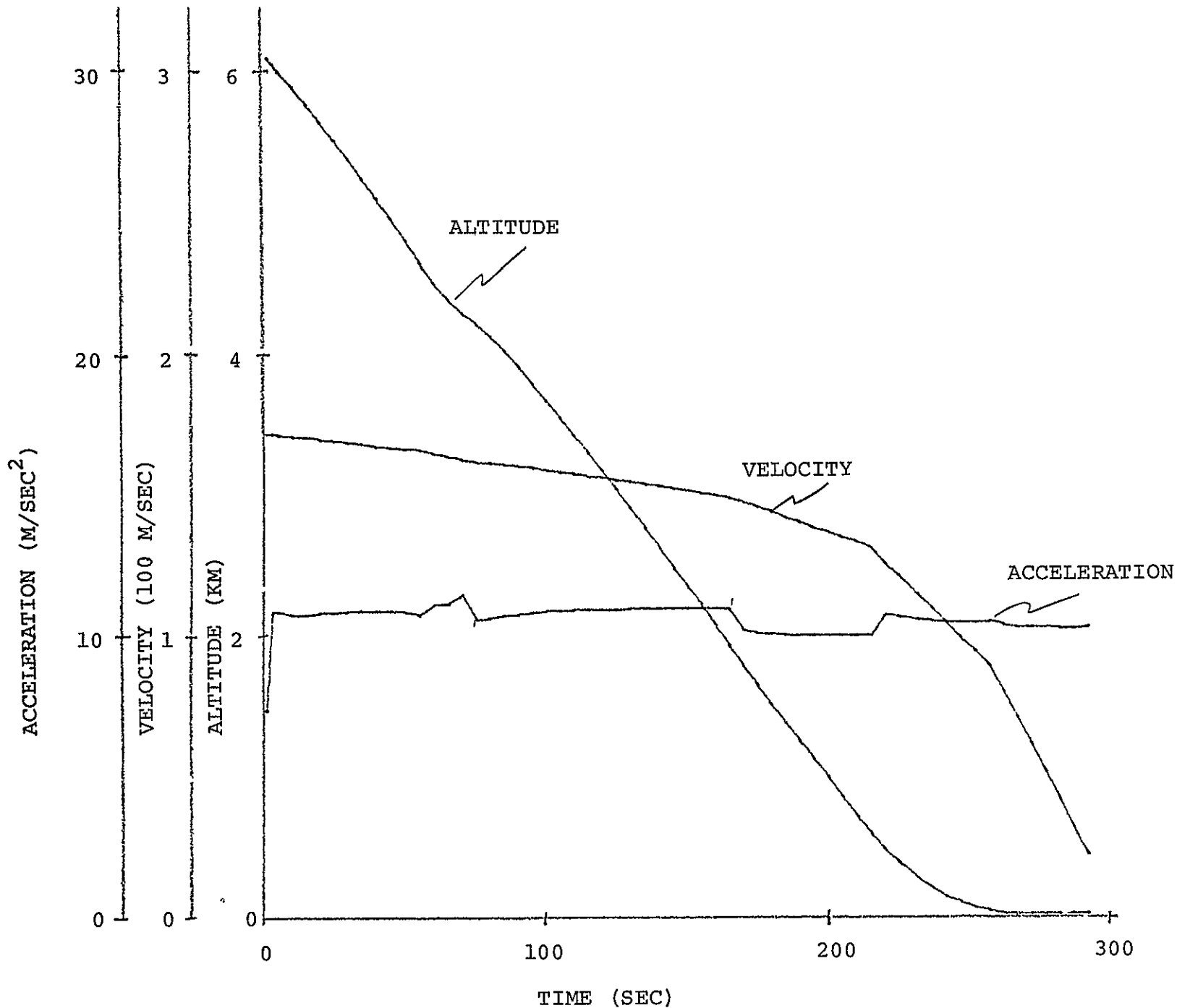


Fig. 4-16 SIDE-APPROACH TRAJECTORY TIME HISTORIES

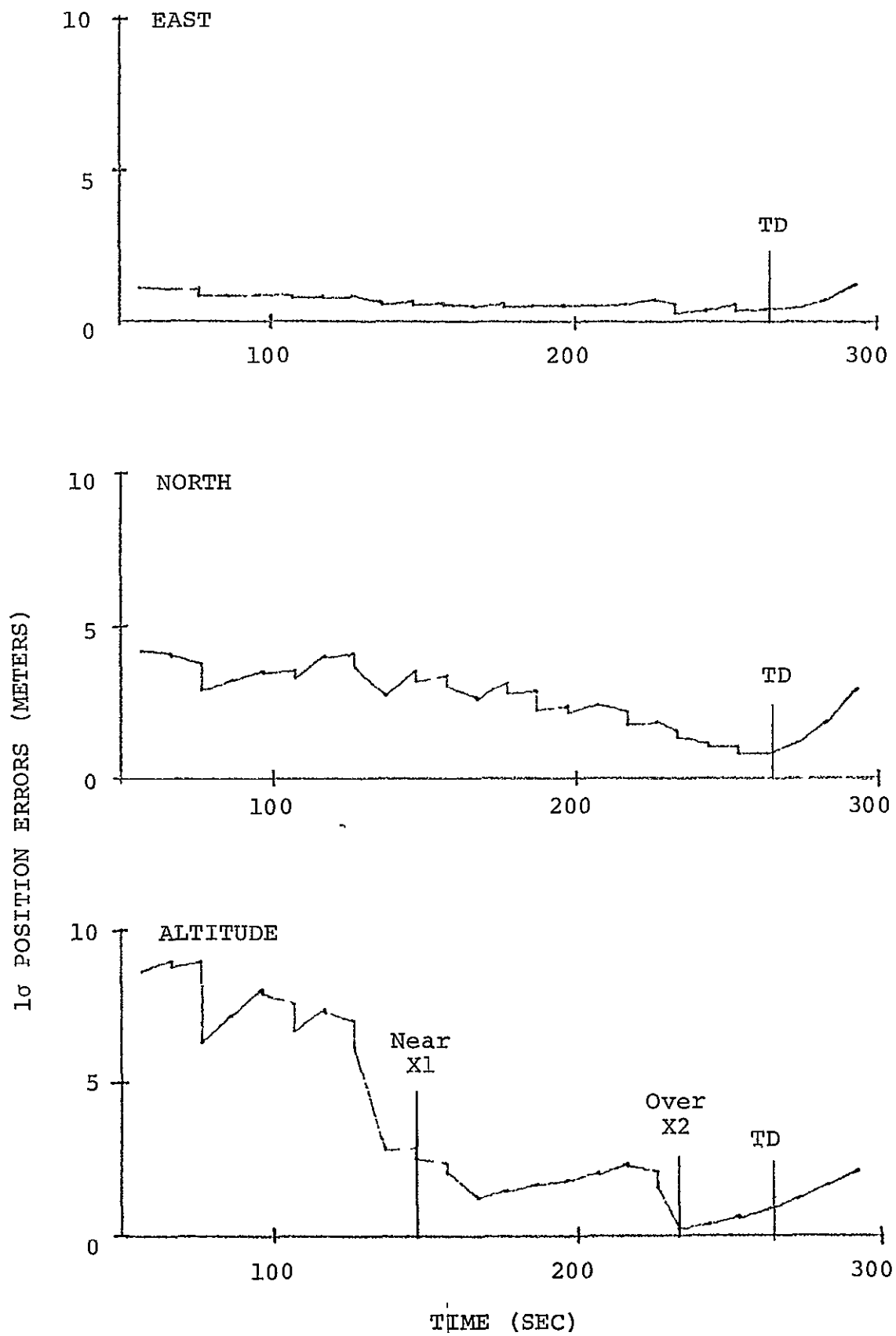


Fig. 4-17 SIDE-APPROACH POSITION UNCERTAINTY

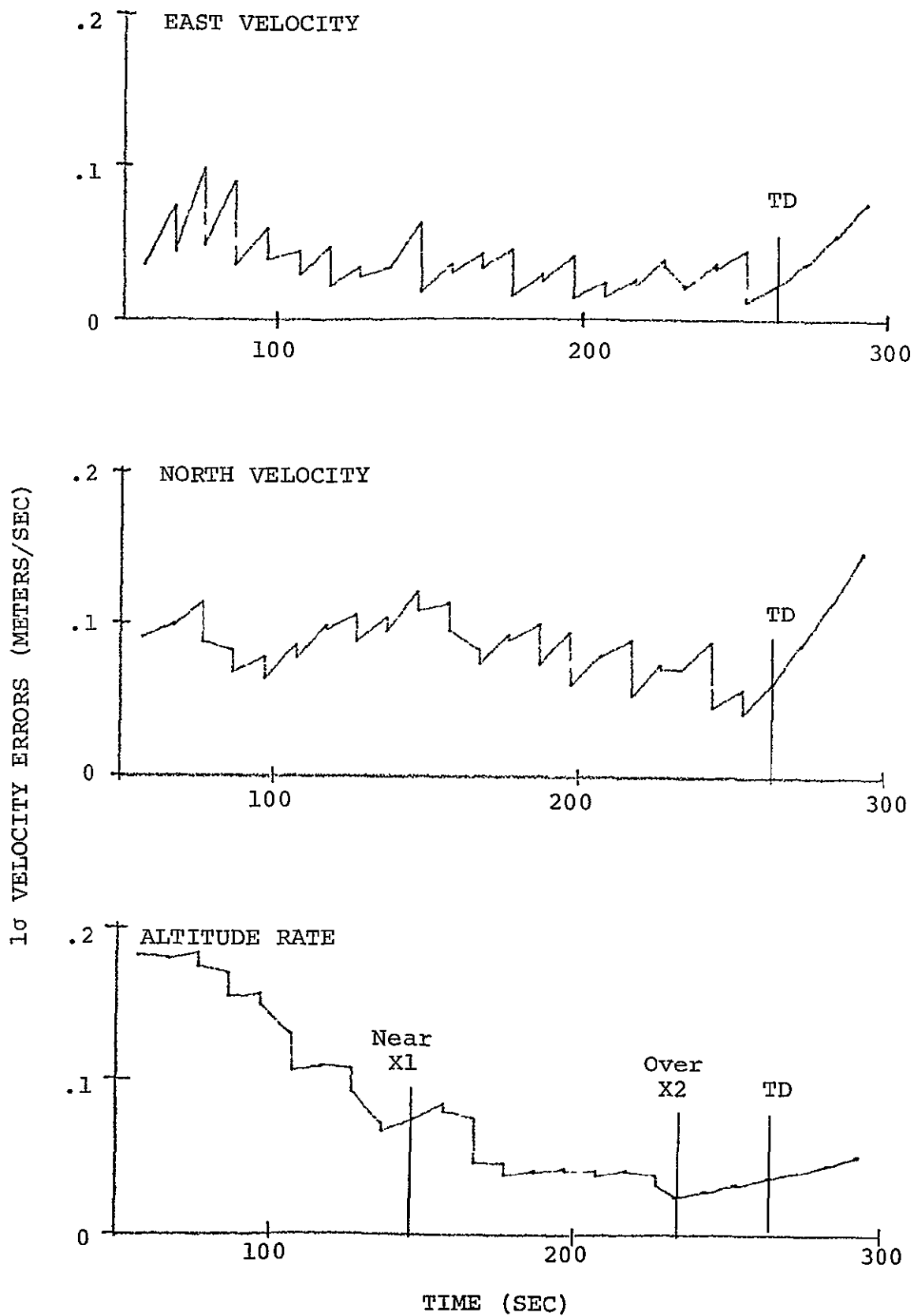


Fig. 4-18 SIDE-APPROACH VELOCITY UNCERTAINTY

4.2.2 Landing With Approach From Side. A less favorable approach pattern is shown in Figs. 4-15 and 4-16. Here the vehicle approaches the terminal area from the side and does not overfly the airport before turning onto final approach.

The resulting navigation performance is shown in Figs. 4-17 and 4-18. As expected, the errors after initialization are somewhat larger. Most noticeable are the increased altitude and altitude-rate errors. However, after turning onto final approach, there is very little difference between this and the previous simulations.

We conclude that with adequate transponder geometry the approach pattern has very little influence on the navigation accuracy at touchdown.

#### 4.3 How Many Transponders Are Required and Where?

The baseline system simulation results presented in Section 4.1 showed that there exists at least one configuration with three transponders that permits the landing navigation system to meet the accuracy specification. Are there better locations for the three transponders? Is it possible to land with only two transponders? How many additional transponders must be deployed to ensure satisfactory failure tolerance? These and other questions concerning transponder deployment are discussed in this section. A recommended deployment is presented.

4.3.1 Geometric Considerations. The transponder configuration utilized in the baseline simulation was shown in Fig. 4-1. Two transponders are placed under the final approach path: the outer transponder 15 km from touchdown, the inner transponder 3 km from touchdown. A third transponder is located 3 km to the side of the middle of the runway. The placement of two transponders under the final approach path has been suggested by McGee and his associates [4-3] at NASA/ARC and by Price [4-4] at NASA/MSD. We have placed the third transponder to the side of the middle of the runway so that it will be equally effective for a final approach from either direction. This helps minimize the total transponders to be required.

Price [4-3] analyzed the geometric dilution factors associated with alternate locations for three transponders. Some of his conclusions are: the down-runway and altitude accuracy is depen-



dent only on the outer and inner transponder placement. The cross-runway accuracy is dependent only on the lateral transponder placement. All in-plane transponder placements give satisfactory down-runway accuracy. The lateral transponder when placed farther from the runway generally gives better cross-runway accuracy. But if the vehicle pattern has a blind zone to the side, for the farther lateral locations the signal is lost earlier. The outer approach transponder if placed at a greater distance from the runway gives better altitude accuracy earlier. If placed closer to the runway, it gives better altitude accuracy between it and the inner transponder. The placement of the inner transponder is a trade-off between the desire to minimize the duration of the pure-inertial-navigation period versus the desire to have sufficient time to obtain multiple measurements over the inner transponder with good altitude geometry.

4.3.2 Inner-Approach-Transponder Placement. Two simulations have been run, one with shorter and one with longer inner-transponder distances from the runway. The outer and lateral transponders have been held at their baseline locations. The baseline landing trajectory (Figs. 4-1 and 4-2) has been used. The results with the inner transponder only 1.5 km from touchdown are shown in Figs. 4-19 and 4-20. (The results with the inner transponder at the baseline distance of 3 km were shown in Figs. 4-9 and 4-10.) Comparing the 1.5-km and 3.0-km results, the performance is nearly identical from initialization through the turn onto final approach over the outer transponder. On final approach the altitude errors build in a similar fashion. The peak altitude error (before reaching the inner transponder) is slightly larger for the 1.5-km case because of the additional 15 sec to reach the inner transponder. Conversely, the altitude error at touchdown is smaller in the 1.5 km case because the pure-inertial flight time has been shortened from about 30 sec to about 15 sec. The touchdown navigation-accuracy specifications are met in both cases.

The results with the inner transponder moved out to 6 km from touchdown are shown in Figs. 4-21 and 4-22. Again the performance is unchanged from initialization through the turn onto final approach. On final approach the altitude error is held to less than two meters, because of the consistently good geometry between the outer and inner transponders. This excellent performance early on final approach is achieved at the expense of the touchdown accuracy. The duration between the time the vehicle is directly over the inner transponder and the touchdown time is 58 sec. During this interval the normal measurement sequence is resumed. The measurement pairs incorporated during this interval are with transponder 3,1,2,3,3 (in that

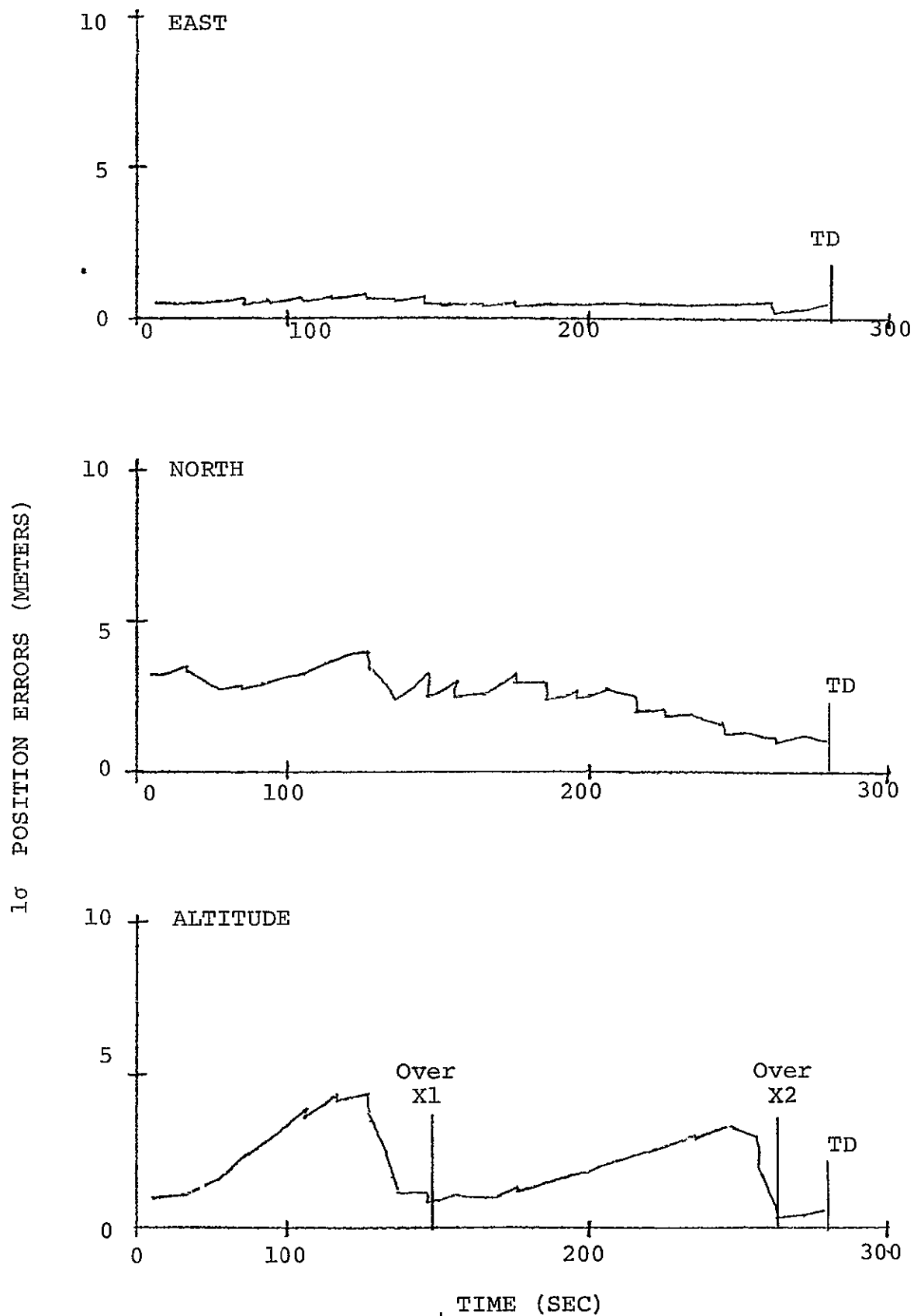


Fig. 4-19 POSITION UNCERTAINTY WITH INNER TRANSPONDER  
AT 1.5 KM

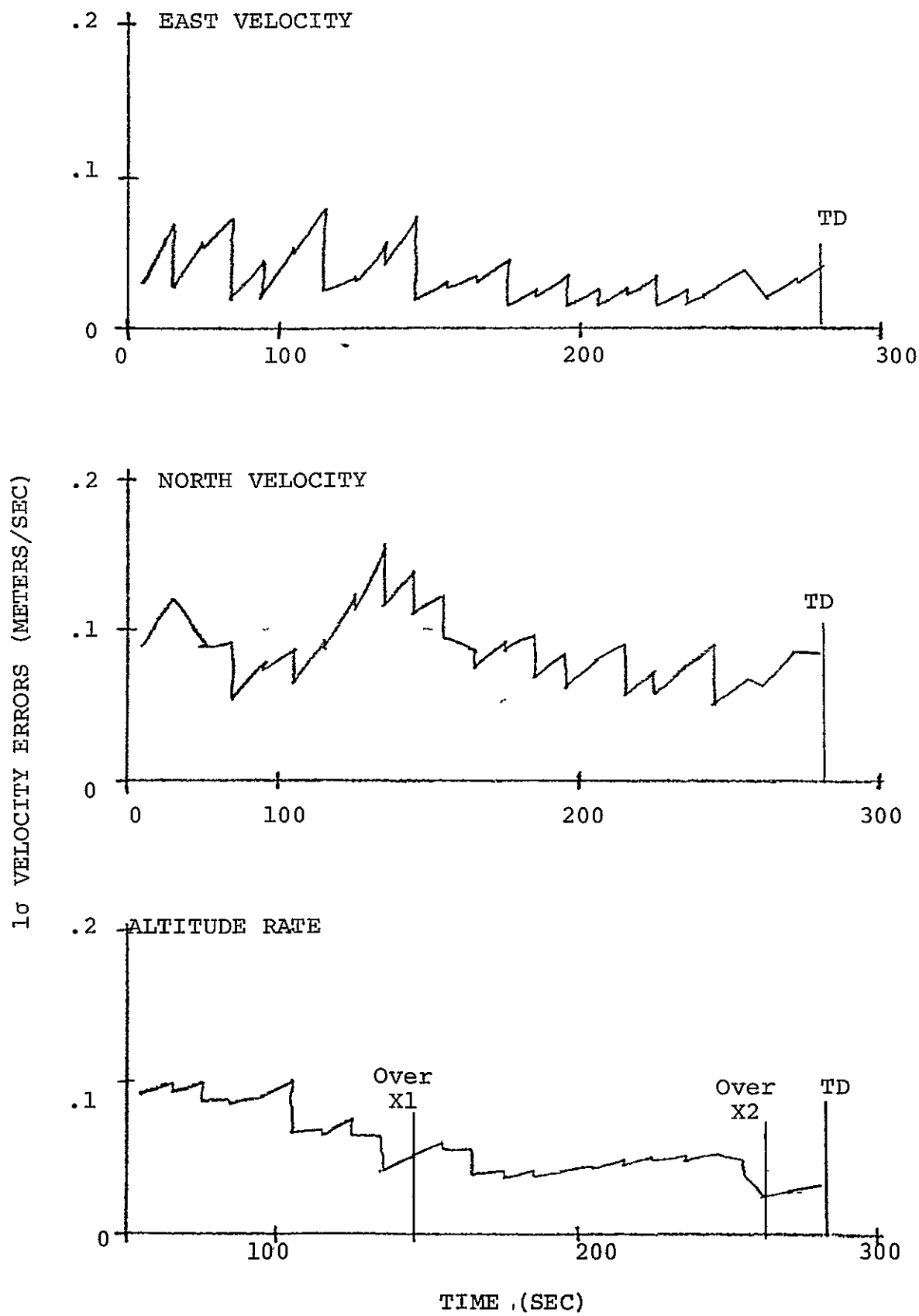


Fig. 4-20 VELOCITY UNCERTAINTY WITH INNER TRANSPONDER AT 1.5 KM

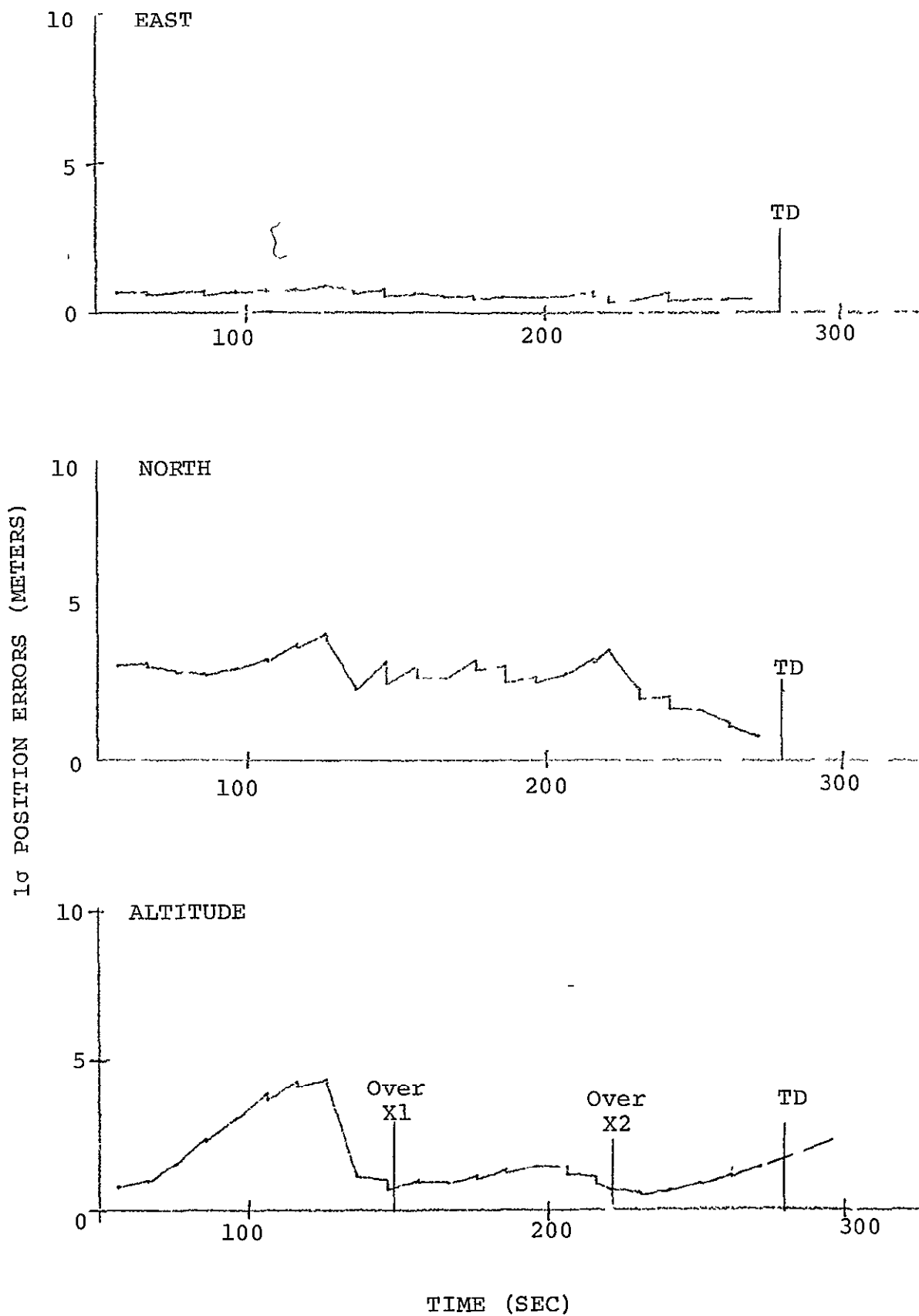


Fig. 4-21 POSITION UNCERTAINTY WITH INNER  
TRANSPONDER AT 6 KM

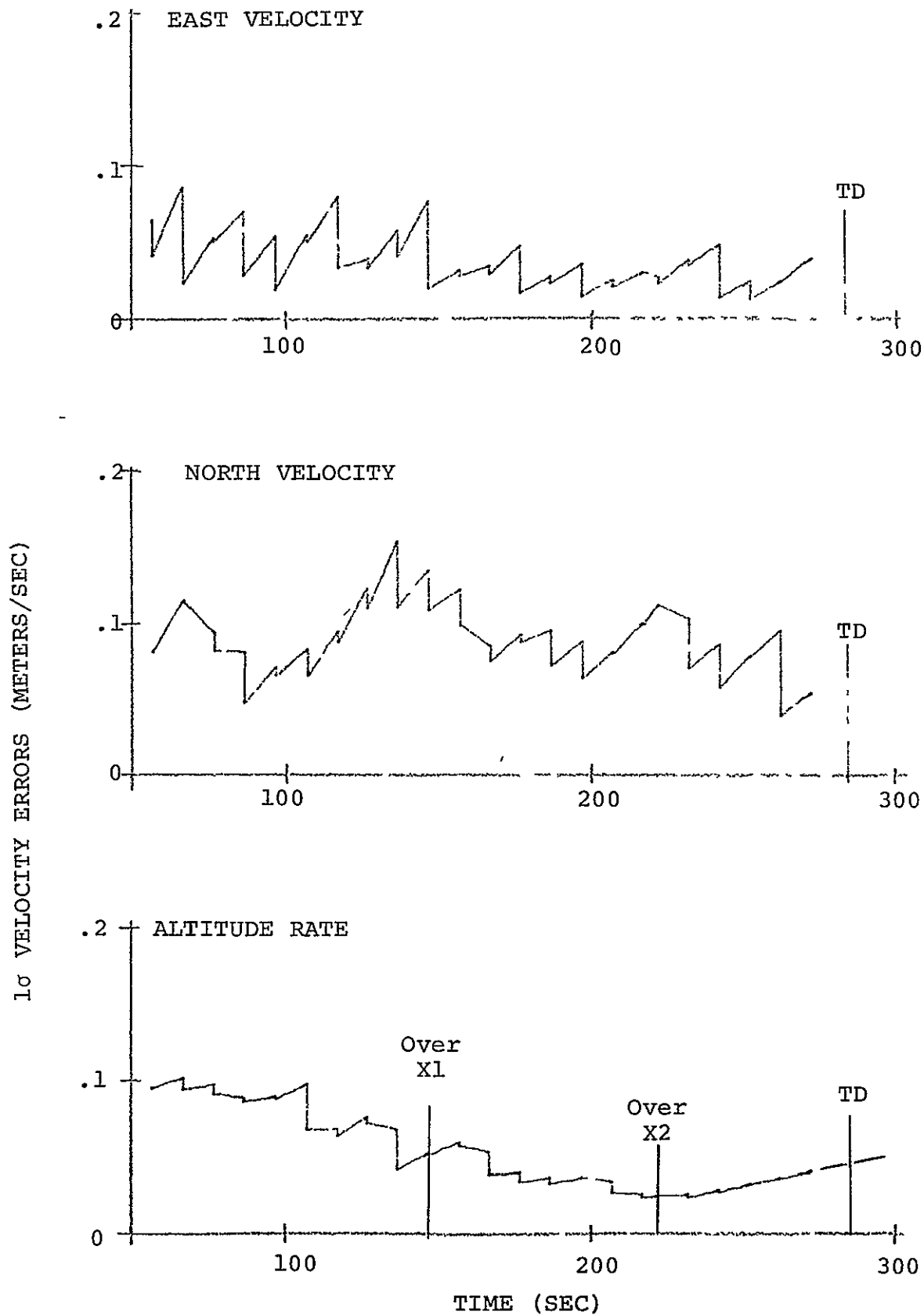


Fig. 4-22 VELOCITY UNCERTAINTY WITH INNER  
TRANSPONDER AT 6 KM

order) each pair 10 sec apart, after which no additional measurements can be obtained because of the  $1^\circ$  elevation-angle cut-off. The 58 sec interval with extremely poor vertical geometry permits the altitude error to grow to about 1.7 meters and the altitude-rate error to grow to about 5 cm/sec at touchdown. (The exact values at touchdown were not printed or plotted by the simulation; so these values are estimates obtained by extrapolating the available data.) The onboard-computed altitude uncertainty of 1.7 meters  $\geq$  exceeds the navigation system specification of 1 meter  $\leq$ . The altitude-rate uncertainty is exactly at the specification level. The 6-km inner transponder deployment is unacceptable.

The factors influencing the choice of inner-transponder distance are summarized in Fig. 4-23. The transponder may be placed no more than 4 km from the nominal touchdown point, or the altitude navigation accuracy will not meet the 1 meter  $\leq$  specification at touchdown.

On the other hand, the closer-in locations yield a larger peak altitude error on final approach. This peak error occurs just before reaching the inner transponder. A 3.2 meter  $\leq$  altitude error exists approaching the transponder at 1.5 km. There is only 15 sec from measuring this error (over the inner transponder) to touchdown -- 15 sec in which to incorporate the measurement into the navigation, to compute new guidance commands, and to obtain vehicle control response. The response requirement imposed upon the navigation, guidance, and control by the 1.5-km inner-transponder placement seems unacceptable.

An additional factor, working against a close-in placement, is the required measurement rate to obtain redundant measurements. Assume that three measurement pairs are desired with the inner transponder during the period of excellent altitude geometry. (The need for three measurements is established by considering the effect of not obtaining at least one good altitude measurement. Three measurements permits data voting to eliminate a bad measurement.) The region of excellent geometry extends about plus and minus  $20^\circ$  elevation angle away from zenith. The closer the transponder is placed to touchdown, the lower will be the altitude of the vehicle, the shorter will be the duration of the favorable update period, the higher will be the required measurement rate. Assuming measurement pairs can be timed to occur at the beginning of, at the middle of, and at the end of the traversal of the  $40^\circ$  cone, then the required rate for measurement pairs is as plotted in Fig. 4-23. At the 1.5 km distance, the required measurement rate is 1.9 pairs per sec. Price [4-4] has considered an even lower trajectory ( $3^\circ$  flight path angle before touchdown), which results in a higher required measurement rate.

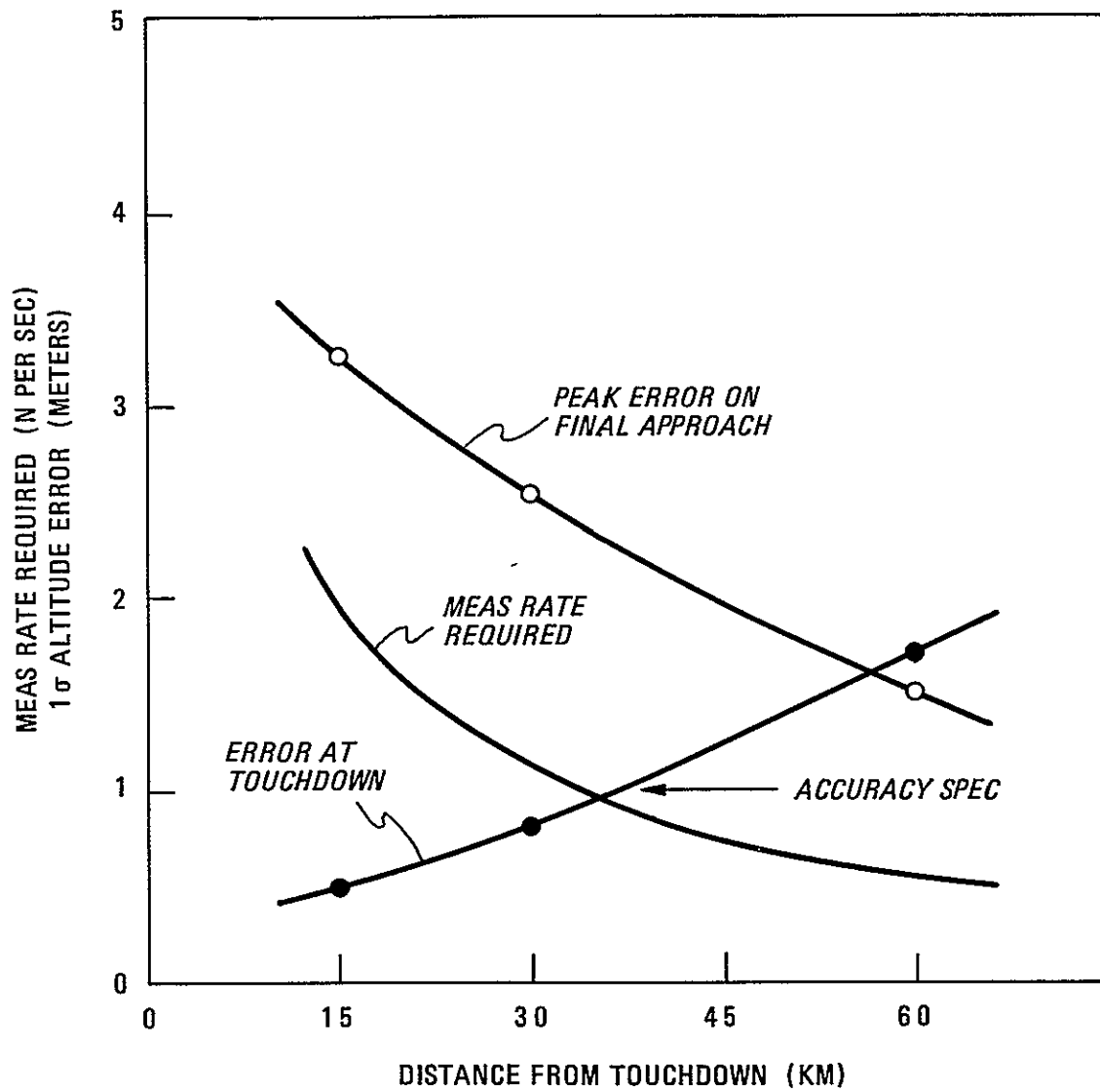


Fig. 4-23 FACTORS INFLUENCING CHOICE OF INNER-TRANSPONDER DISTANCE

Based on the above considerations we recommend that an inner-transponder placement between 2 km and 4 km (from the nominal touchdown location) be used. The baseline 3 km location is entirely satisfactory.

4.3.3 Lateral-Transponder Placement. The lateral transponder placement governs the cross runway position and velocity errors. The baseline lateral-transponder location is half-way down the 3-km (10,000-ft.) runway and 3-km to the side. The placement half-way down the runway was selected so that the lateral transponder is equally effective for approaches from either direction. The 3-km distance-to-the-side is the typical maximum distance-to-the-side still permitting an unobstructed line-of-sight from vehicle to transponder during flare and touchdown. (Such would be the case at a typical "square" airport having a second major runway and cleared ground crossing the primary runway.)

Lateral-transponder distances closer to the runway may be considered. Figs 4-24 and 4-25 present the results of a simulation with the lateral transponder at the middle of the runway only 1.5 km to the side. In comparing with the baseline system results (Figs. 4-9 and 4-10) it is seen that the navigation accuracy at touchdown is about the same. The cross-runway (north) velocity error at touchdown is slightly lower in the 1.5-km case because one more lateral measurement could be obtained before the 1°-elevation cut-off. Both systems meet the touchdown accuracy specification.

However, the cross-runway position error on final approach is noticeably higher in the 1.5 km case, due to the more severely-diluted lateral geometry. This error is not reduced until after the altitude has been updated over the inner-approach transponder. This is a dangerously-late time to make any substantial correction to the lateral vehicle position. Large bank angles must be inhibited to reduce the probability of a wing-ground contact. The wider-lateral-transponder placement is therefore judged to give superior system performance.

An additional reason to prefer a wide lateral placement is that it also provides better transponder geometry at initialization. Initialization results are presented in Section 4.4.

We recommend that the lateral transponder be placed at the middle of the runway and at the maximum distance to the side that is free of line-of-sight restrictions for either approach direction. The baseline distance of 3 km gives satisfactory system performance. An elevation-angle cut-off larger than the 1° cut-off can alter this recommendation (see Sect. 4.7).



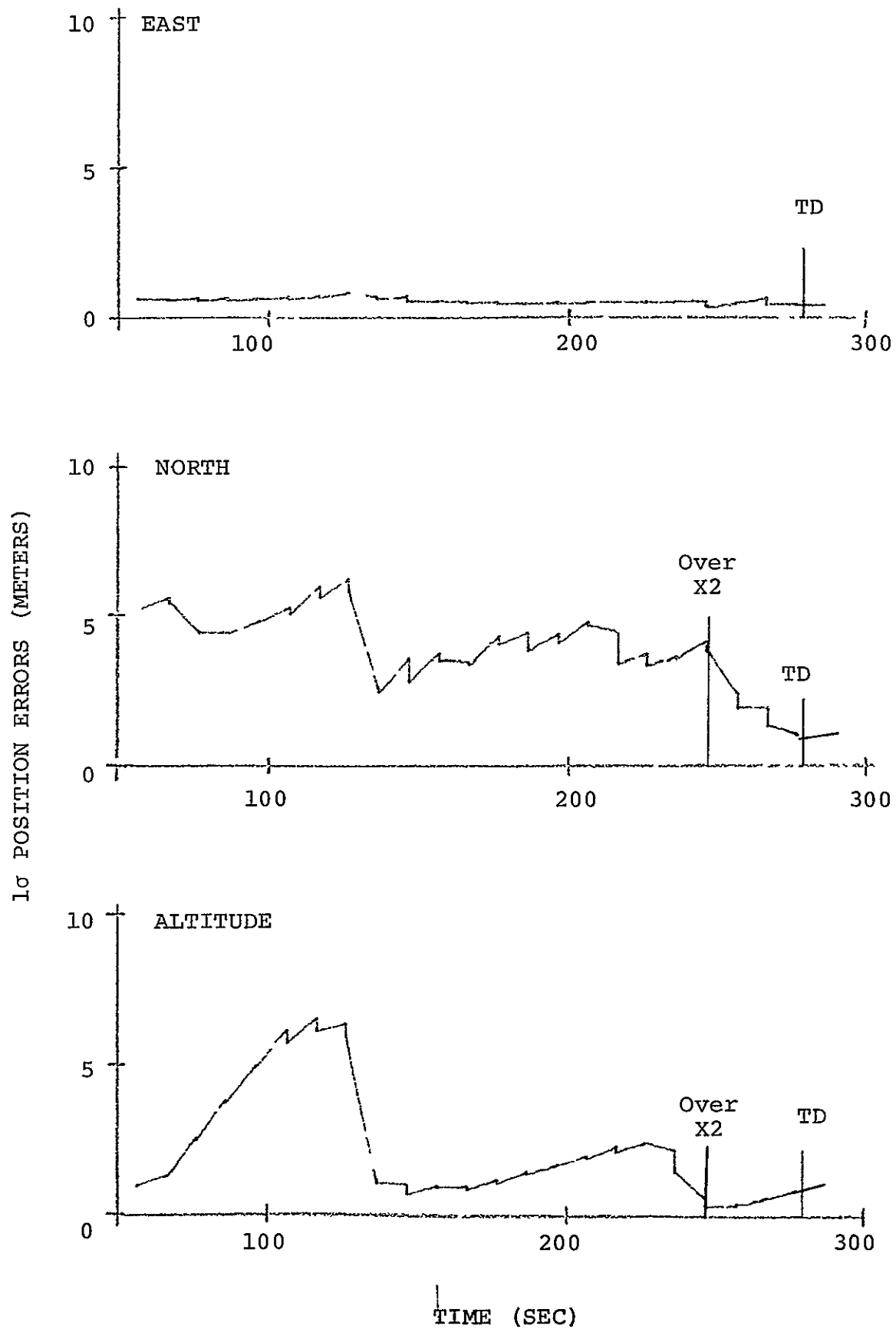


Fig. 4-24 POSITION UNCERTAINTY WITH LATERAL TRANSPONDER AT 1.5 KM

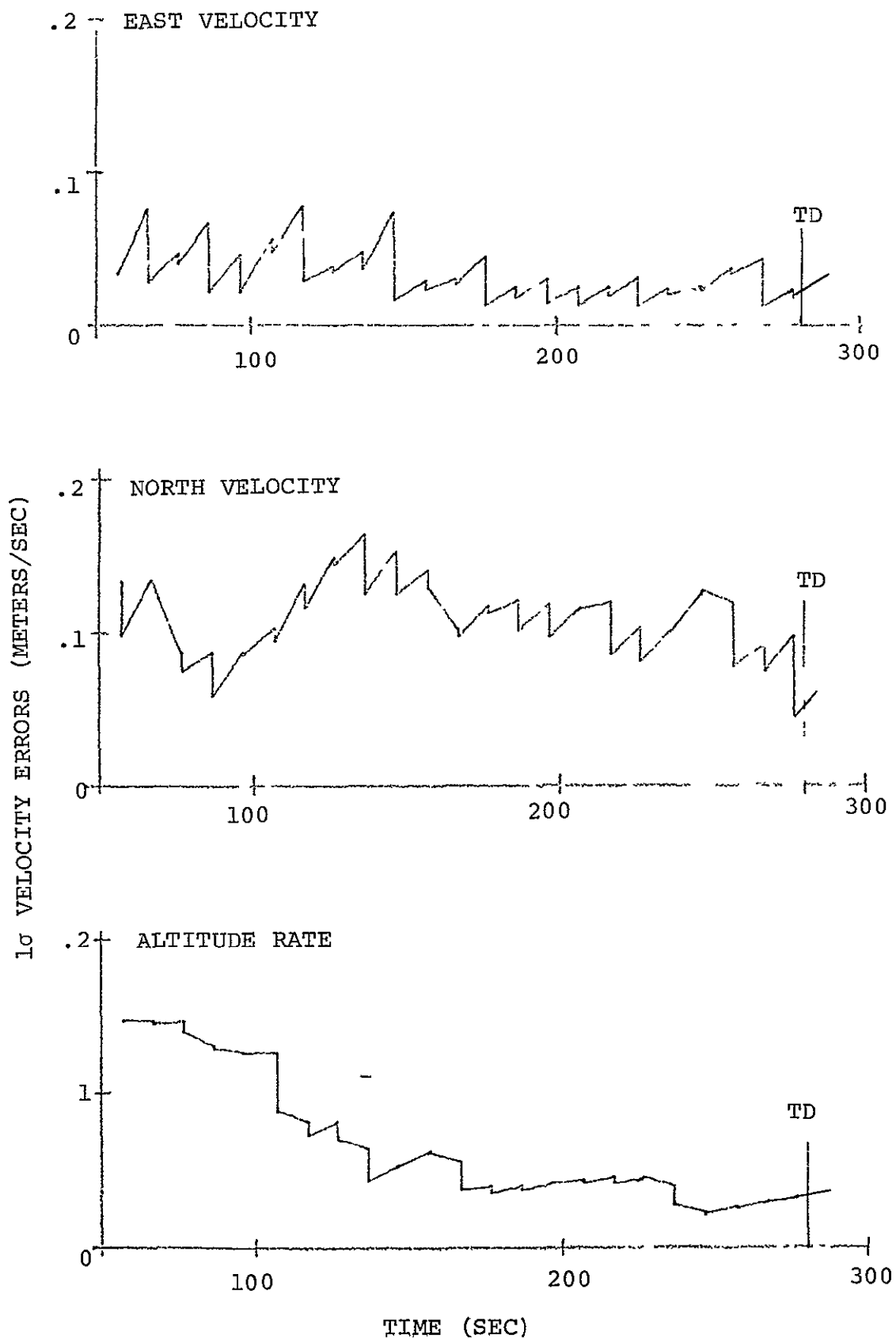


Fig. 4-25 VELOCITY UNCERTAINTY WITH LATERAL TRANSPONDER AT 1.5 KM

4.3.4 Outer-Transponder Placement. To assure good altitude geometry, the outer-approach transponder should be placed under the final-approach path. A cursory review of some proposed guidance techniques (Refs. [4-1] and [4-2]) indicated that the vehicle will have turned onto final approach no later than about 15 km from touchdown. Accordingly, the baseline outer-approach transponder was placed at 15 km. At a greater distance, one cannot be certain that the vehicle will fly over the transponder.

Shorter distances may be considered. A simulation has been run with the outer-approach transponder moved from 15 km to 9 km from the runway. This reduces in half the distance between the outer transponder and the inner transponder, which is at the baseline distance of 3 km. The simulation results are presented in Figs. 4-26 and 4-27. Compared with the baseline system performance (Figs. 4-9 and 4-10), the position and velocity navigation errors at touchdown are unaffected. Both systems meet the landing specification.

The most noticeable difference in performance is in the altitude navigation accuracy on final approach. The 15-km placement gives an earlier reduction of the altitude uncertainty. The 9-km placement gives a smaller peak altitude error between the outer and inner transponder. These results are in agreement with the observations of Price [4-4] based on purely geometric considerations. In either case the altitude errors on final approach would seem acceptable, so there is little to recommend one placement as better than the other.

One simulation has been run with only one of the three transponders under the final approach path. The transponder deployment is shown in Fig. 4-28.

This deployment was tried, because if successful, the total number of transponders required to instrument both approach directions is reduced.

The simulation results are presented in Figs. 4-29 and 4-30. The easterly and northerly position and velocity performance, compared with the baseline performance, is changed very little. These components of navigation uncertainty continue to meet the landing navigation specification. But the altitude-rate uncertainty is never brought below the 5 cm/sec landing specification, even while directly over the approach transponder. The altitude uncertainty on final approach is as large as 10 meters. This is reduced to a small value over the approach transponder, but the velocity uncertainty causes the altitude uncertainty to increase such that it is larger than the 1 meter specification at touchdown.

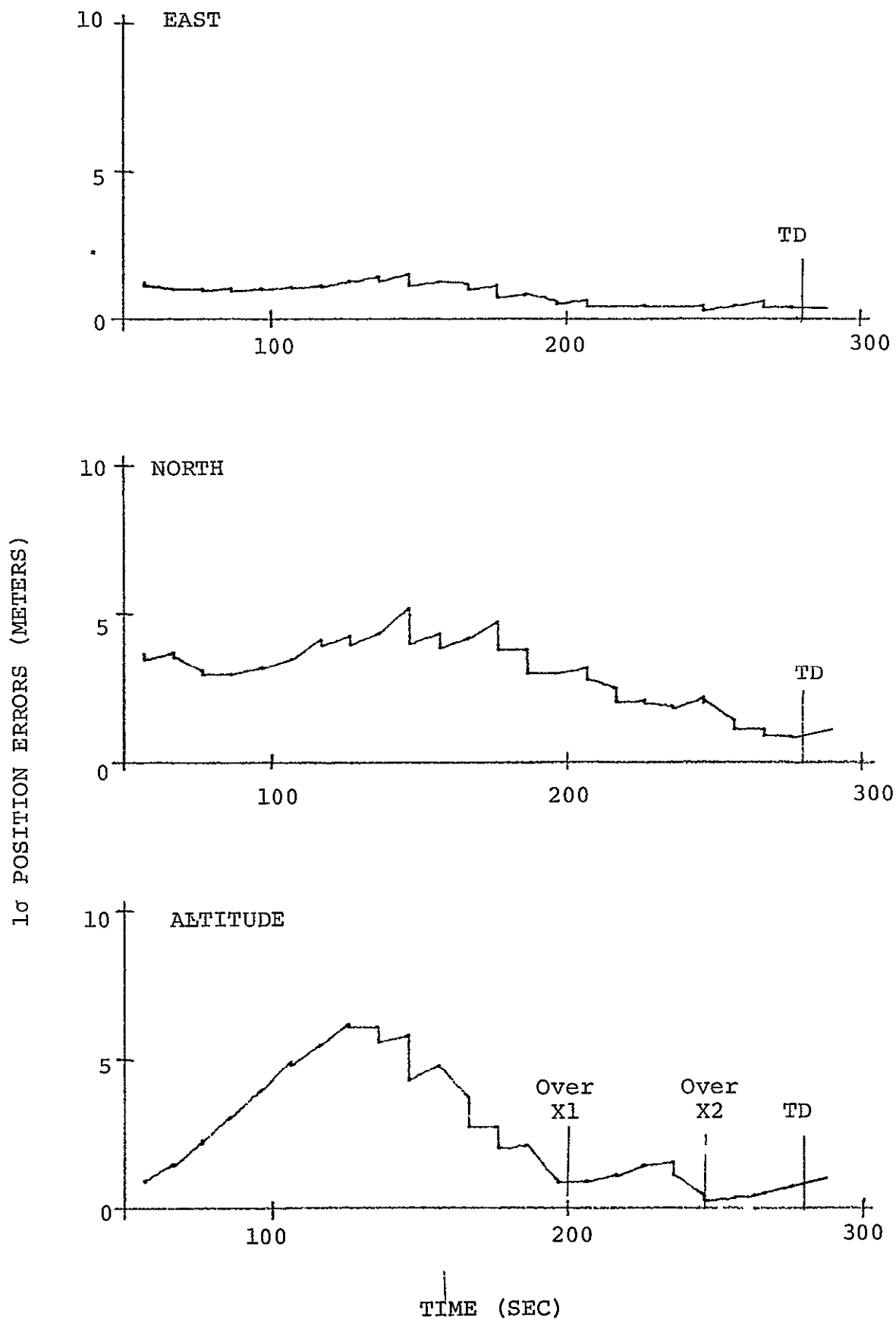


Fig. 4-26 POSITION UNCERTAINTY WITH OUTER  
TRANSPONDER AT 9 KM

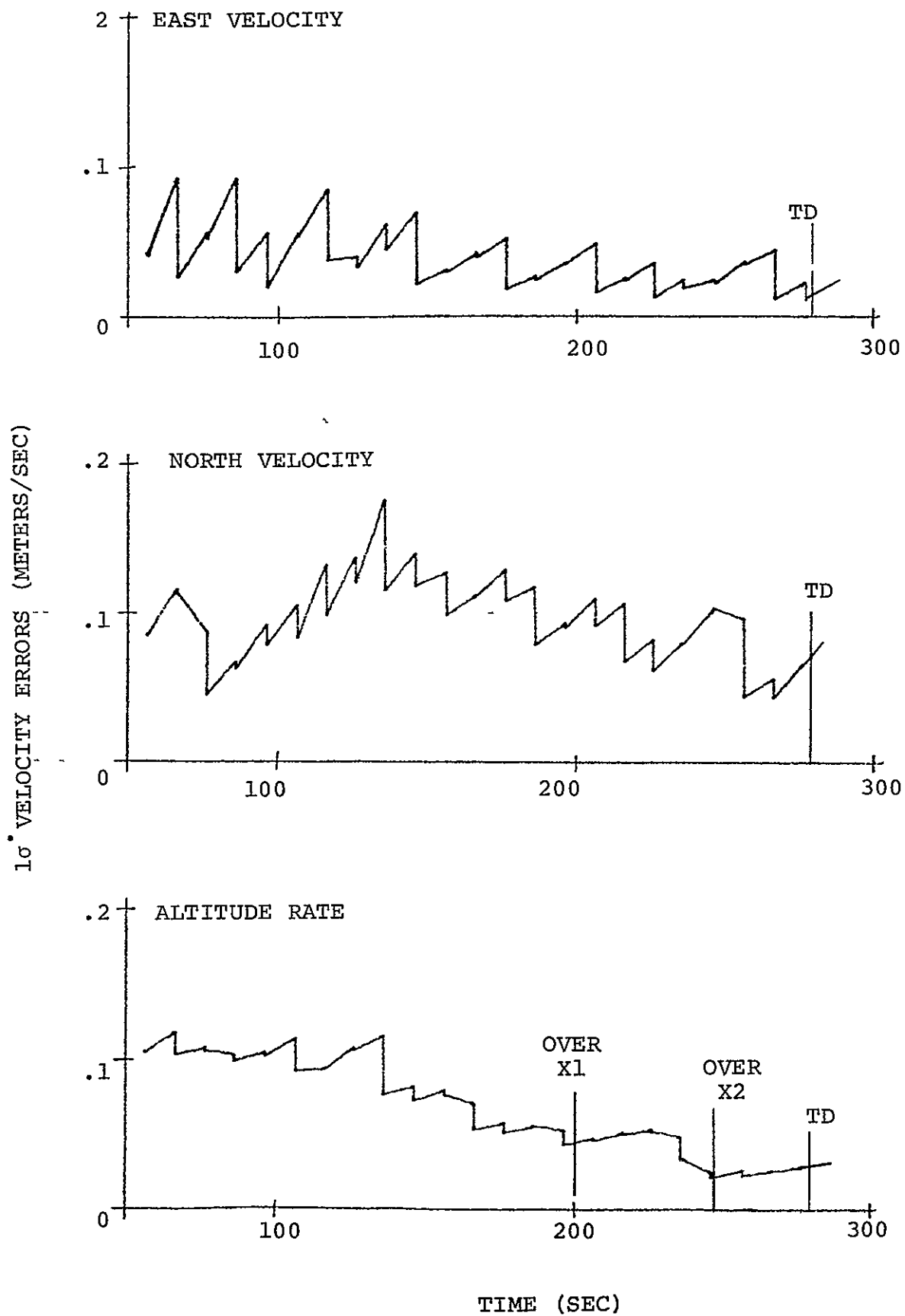


Fig. 4-27 VELOCITY UNCERTAINTY WITH OUTER  
TRANSPONDER AT 9 KM

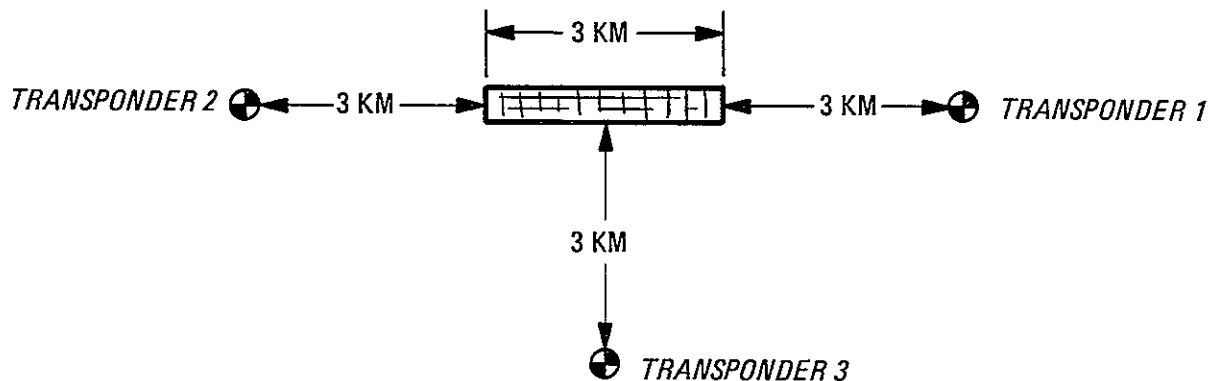


Fig. 4-28 Only One Transponder Under Final Approach

We conclude that with the very stringent Shuttle landing navigation accuracy specification (on altitude and altitude rate), two transponders are required under the final approach path. The exact placement of the outer-approach transponder is not critical. Placements from 9 km to 15 km from the runway yield satisfactory performance. Including the lateral transponder, a minimum of three working transponders are required to meet the accuracy specification.

4.3.5 Only Two Transponders. A limited number of simulations have been run to explore the navigation performance that can be achieved with only two working transponders.

The initial position fix logic as designed in Section 3.4 requires three nearly simultaneous non-coplanar range measurements. Therefore, this initialization logic cannot be used if only two transponders are working. Alternate initialization logic can be designed. For example, the altitude (as inferred from the measured acceleration) could be used in conjunction with two range measurements. The initialization logic has not been re-designed in support of the two-transponder simulations. Rather, we have assumed that a satisfactory initialization logic does exist and if used can reduce the navigation errors to 100 meters 1σ along each axis (east, north, up). It is with these 100 meter 1σ errors that we have started the two-transponder simulations in the terminal area. The trajectory of Fig. 4-1 has been used.

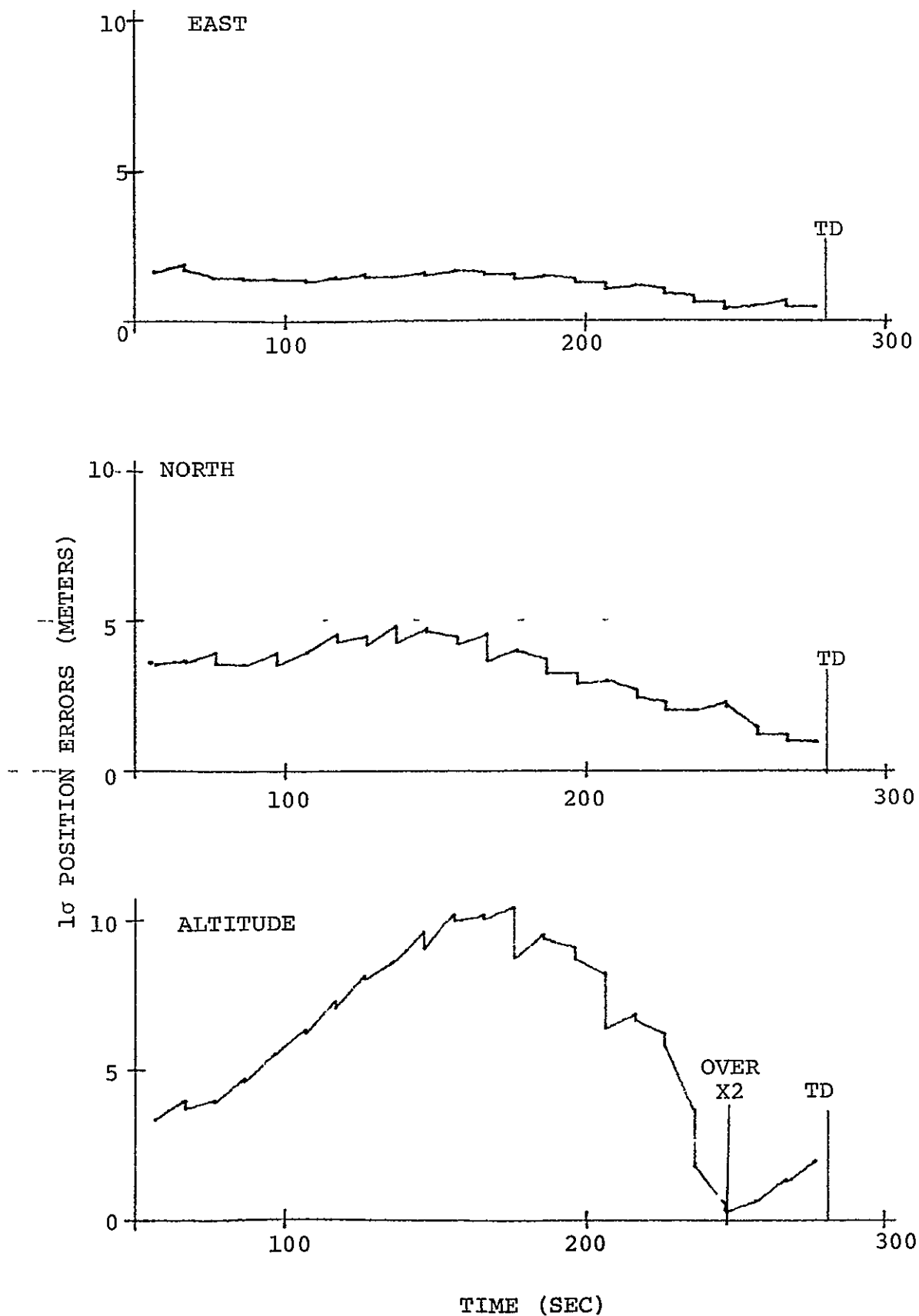


Fig. 4-29 POSITION UNCERTAINTY WITH ONLY ONE APPROACH TRANSPONDER

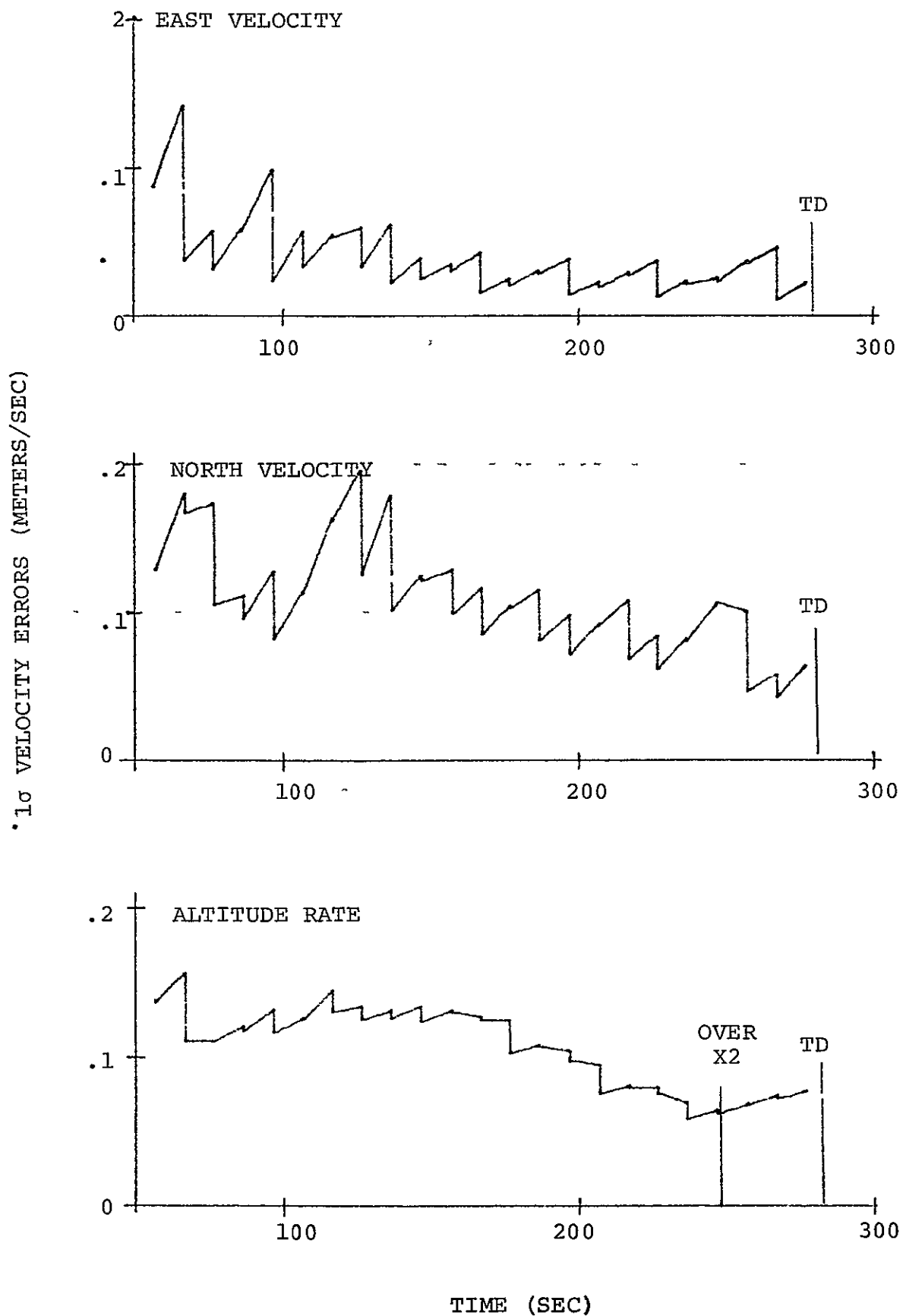


Fig. 4-30 VELOCITY UNCERTAINTY WITH ONLY ONE APPROACH TRANSPONDER



The simulation results have been disappointing. Frequently there is poor agreement between the onboard-computed 1 $\sigma$  uncertainties and the actual level of navigation error. The onboard-computed uncertainty becomes smaller as measurements are processed, however, the actual position and velocity errors decrease much more sluggishly or in some cases actually increase. Such behavior is symptomatic of nonlinear effects causing filter divergence.

Note that the range measurements have been protected against the nonlinear elongation of the measured range (subsection 3.3.1). However, we have not designed similar protection for the delta-range measurements. Suspecting that nonlinear difficulties might be entering through the delta-range measurements, the delta-range measurements were disabled in the simulation, and navigation was attempted using range measurements alone. The results were better, however, the actual-error-to-computed-uncertainty ratios still showed some divergence.

A fundamental problem with using only two transponders is that there exists a trajectory direction that is likely to yield poor navigation filter performance. If the vehicle velocity vector is parallel to the line connecting the two transponders, then the ensuing time-history of range measurements to the two transponders never yields a position fix. In other words, there exist a family of possible vehicle trajectories (having parallel velocity vectors but spread around the surface of a cylinder whose axis is the line connecting the two transponders) for which the measured ranges to the transponders evolve identically in time. This situation is illustrated in Fig. 4-31.

Such is nearly the situation in the simulations run with the baseline trajectory (Fig. 4-1) and utilizing the inner-approach transponder west of the runway and the lateral transponder south of the runway. The average vehicle velocity vector in the first 50 sec of the simulation is nearly parallel to the line connecting the two transponders.

To eliminate this unfavorable initial situation, the lateral transponder was moved to the other side of the runway (3 km north). The resulting simulation yielded the best performance of all the two-transponder simulations runs. Selected data from this simulation is presented in Table 4-3. The initial errors, IMU component errors, and other constant error coefficients generally were selected to have specific values equal to plus one-sigma (that is, the errors were not randomly selected). The initial navigation is accomplished with range measurements only. The results after the first 160 sec of range-only navigation is presented in the table. All actual navigation error components

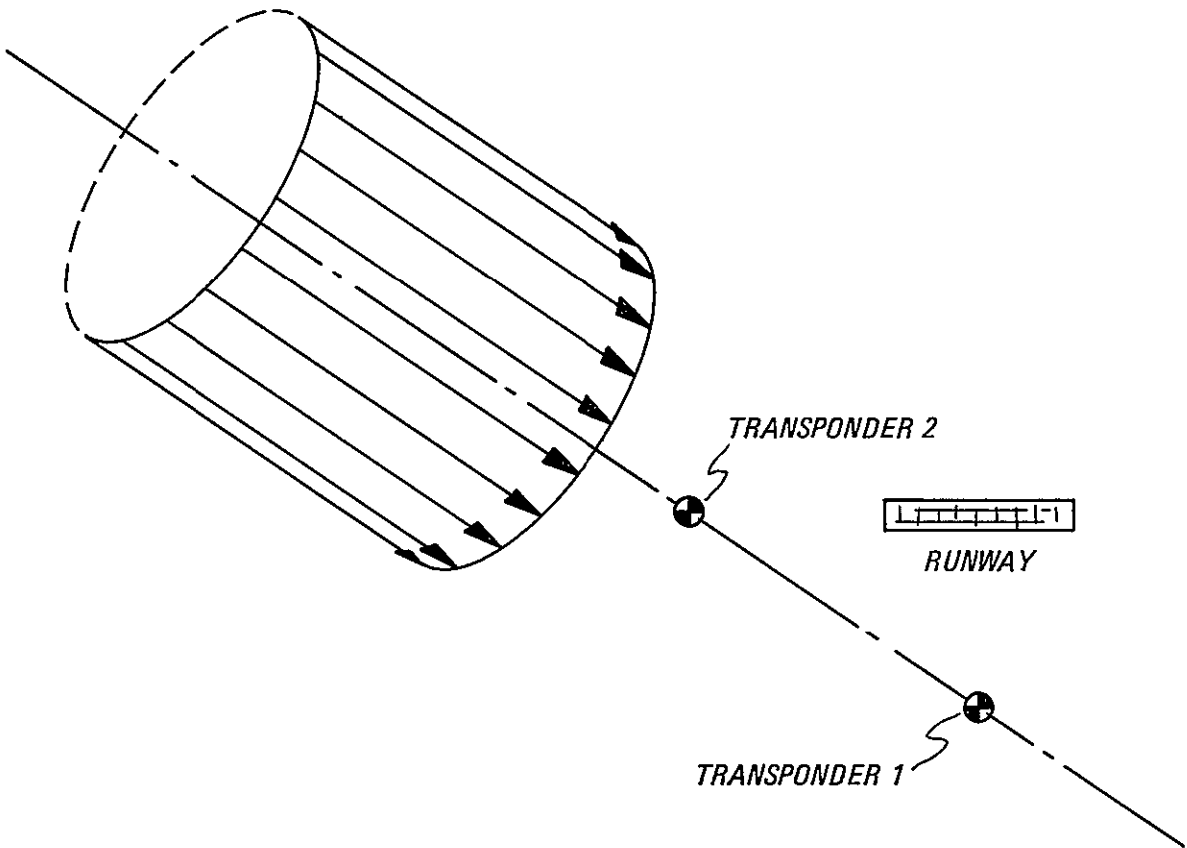


Fig. 4-31 FAMILY OF TRAJECTORIES HAVING IDENTICAL RANGE-HISTORIES TO THE TWO TRANSPONDERS

State Variable	Units	Initialization t = 0 sec		On final approach t = 160 sec		At touchdown t = 280 sec	
		Actual error	$P^{1/2}$	Actual error	$P^{1/2}$	Actual error	$P^{1/2}$
1. Error in east position	meters	100	100	-8.1	12	-.8	.3
2. Error in north position	meters	100	100	8.8	18	.4	1.3
3. Error in altitude	meters	100	100	-51	87	2.9	1.4
4. Error in east velocity	cm/sec	1000	1000	-4.4	16	-2.1	3.1
5. Error in north velocity	cm/sec	1000	1000	9.1	59	-2.7	9 2
6. Error in altitude rate	cm/sec	1000	1000	-44	86	23	14
7. Platform tip about east	milli-radian	.93	1.00	.60	.65	-.03	.28
8. Platform tip about north	milli-radian	.62	1.00	.18	.37	.05	.20
9. Platform azimuth error	milli-radian	1.00	1.00	.97	1.5	.08	1.4
10. Magnitude of gravity and accel. error	cm/sec <sup>2</sup>	-	.11	-	.10	-	.089

Table 4-3 Only Two Transponders, Performance Results

(in this single case simulation) are of comparable or smaller value than the onboard computed uncertainty. This indicates satisfactory filter performance. From  $t=210$  sec on final approach to touchdown, the delta-range measurements are also used. The vehicle flies over the approach transponder, which in this simulation was 1.4 km from touchdown. Three measurement pairs with the approach transponder are incorporated. The vehicle is at touchdown at 180 sec. The navigation accuracy at touchdown is quite good. However, the actual and onboard-computed altitude errors exceed the 1 meter 1 $\sigma$  specification, and the actual and onboard-computed altitude-rate errors exceed the 5 cm/sec specification.

With a favorable approach trajectory and transponder deployment, the accuracy specification is not quite met. With an unfavorable approach trajectory, the performance can be quite bad. This supports our previous conclusion that two transponders alone do not provide satisfactory landing navigation system performance.

4.3.6 Failure Tolerance and Recommended Deployment. A single interrogator is of the complexity that the mean time between failures (MTBF) is of the order of 2000 hours. Given that an interrogator is working before launch, the probability that it will not fail during a 200 hr. mission is approximately 0.90.

To obtain a better probability that a working interrogator is available, multiple interrogators should be installed in the vehicle. With two aboard, the probability that at least one is working after 200 hr. is .99. With three aboard, the probability that at least one is working after 200 hr. is .999, and so forth. Depending on more precise estimates of the transponder MTBF, the required operational duration, and the desired probability of mission success, one can determine whether three or four interrogators should be placed aboard each vehicle.

A transponder is less complex than an interrogator. The MTBF is of the order of 7000 hours. One or two additional transponders can be stored as spares at each landing site. When one of the deployed transponders in the terminal area is found to have failed, a spare transponder should be used to replace the failed transponder. In this manner one can insure that all transponders are working before the orbiter performs the deorbit burn committing itself to landing at the specific airport. If 70 hours elapse between the time when all transponders were last checked (and found to be working) and the time the vehicle lands, the probability that one particular transponder is working at landing is .99. If three transponders have been deployed (such as to instrument approach from a single direction), the

probability that the three are all working at touchdown is .97.

To obtain a better probability that a sufficient set of transponders is working at touchdown, additional transponders should be deployed. Assume that an additional transponder is collocated with each of the original three transponders. At each location, the probability that at least one of the two is working is .9999. The probability that at least one is working at each of the three locations is .9997. If this is not adequate to support the desired probability of mission success, then one should inspect the transponders closer to the landing time. If the time from inspection to the Shuttle landing is reduced from the order of 70 hours down to 7 hours, then the probability that at least one (of the two) is working at each of the three locations is .999997. The point is that no more than two transponders at each critical location are required.

Two transponders at the same location give no navigation performance improvement in the normal situation, where both are working. A better deployment strategy is to separate the paired transponders to increase the geometric diversity. Instead of collocating the two inner-approach transponders at 3 km from touchdown, one transponder should be placed at 2 km from touchdown and the other should be placed at 4 km from touchdown. When both are working, the navigation performance will be better than the specification. If one transponder fails, the other transponder is located such that the performance specification will still be met. Similarly, instead of collocating the two lateral transponders at the same side of the runway, one transponder should be placed on one side of the runway and the other should be placed on the opposite side (assuming both locations give good line of sight).

Similarly, the two redundant outer-approach transponders can be separated. One transponder can be placed 15 km from the runway, and the other can be placed 9 km from the runway.

The basic transponder deployment recommended is shown in Fig. 4-32. Ten transponders are deployed. This recommended deployment instruments both directions-of-approach to the longest runway, permitting upwind landing. With all transponders functioning, the landing navigation performance will be better than the specification. If any single transponder fails, the landing navigation performance will meet the specification.

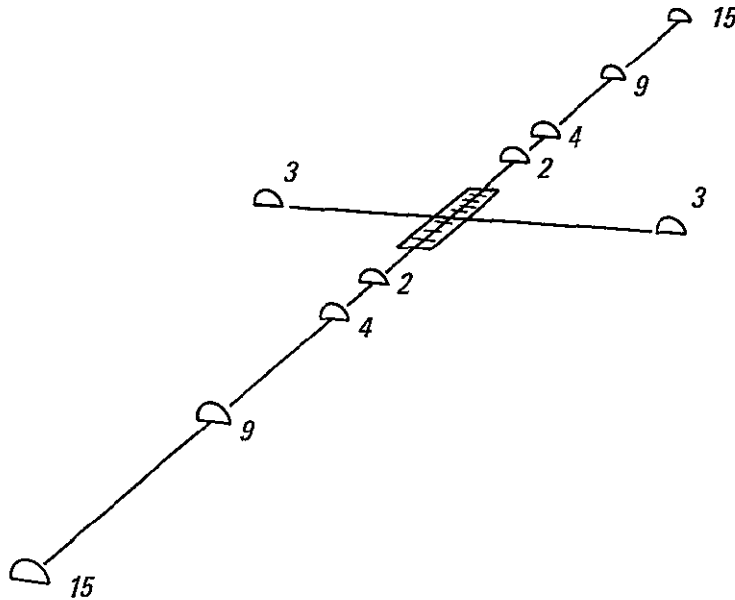


Fig. 4-32 Transponder Deployment, Tolerant of Single Failure and Instrumenting Both Approaches (distances in kilometers)

The most critical transponders are the inner-approach transponders and the lateral transponders. The outer-approach transponders are less critical. Perhaps two outer-approach transponders are not required for each approach direction. What would be the performance if only one outer-approach transponder were deployed and it failed? One three-transponder simulation was run with the two working inner-approach transponders at 2 km and 4 km from the runway and one lateral transponder 3 km to the side of the middle of the runway. The onboard-computed uncertainty almost met the touchdown specification. But the actual (single case) errors in altitude and altitude rate diverged from the onboard-computed uncertainty. At touchdown the altitude navigation error was 4.5 meters and the altitude-rate error was 17 cm/sec. Apparently, the spacing of the two inner-approach transponders (2 km) is not sufficient to guarantee good navigation performance. Perhaps if a fourth transponder (one from the opposite approach path) were added to the measurement sequence, good performance could be obtained. Such a simulation has not been run. Based on the limited simulation results, it is conservative to stay with the ten-transponder recommendation. Additional study can later indicate if the redundant outer transponders can be eliminated, reducing the required deployment to a set of eight.

#### 4.4 Are Additional Transponders Required For Distant Initialization?

4.4.1 Initialization-Range Requirement. The navigation error after hypersonic entry will be of the order of 10 km or horizontal position error. The altitude, derived from the measured acceleration, should be accurate to about 3 km or. With this quality entry navigation, early updating of the state vector is not urgent.

Consider that one waits until the vehicle has decelerated to subsonic flight. A typical altitude at which the vehicle has slowed-down to Mach 1 is 18 km. (60,000 ft.) With a maximum subsonic L/D of 8, the no-wind footprint (from 18 km altitude) is a circle of radius 150 km. The entry navigation error of 10 km or is still a small fraction of the vehicle-footprint radius. Hence, updating can wait until a 150 km distance from the airport.

Note that at Mach 1, the vehicle speed is well below the speed at which there is a blackout of S-band radio transmissions. Blackout should end at about Mach 10.

Note also that the Shuttle subsonic maximum L/D is only 8. Hence, the approach flight path angle will be no shallower than  $1/8$  radian ( $7^\circ$ ). The vehicle elevation angles as seen from the several transponders at the airport will be about the same value. Therefore, there is no problem with poor quality DME measurements associated with very low elevation angles. Also, there is reasonably good altitude-measuring geometry.

The curvature of the earth and the bending of the radio waves does not noticeably reduce the elevation angles at a distance of 150 km. Fig. 4-33 shows the elevation angle  $\theta_0$  of the radio wave at the ground as a function of the vehicle altitude and distance. This figure is based on data from Ref. [4-5]. The radio-wave paths shown assume a sea-level wave retardation of 350 parts per million. A Shuttle straight-in trajectory is the dashed line in Fig. 4-33.

Note the region of good radio-elevation angle (above  $3^\circ$ ) extends out to 600 km. Initial updating could begin as early as 600 km. Such earlier initialization would provide excellent latitude and longitude determination. The altitude measuring accuracy, however, would be degraded. An alternate initialization logic could be developed which blended the drag-derived altitude with the DME data. Such earlier initialization might be necessary if the inertial navigation errors are larger than 10 km or (such as in a once-around abort with no update since launch).

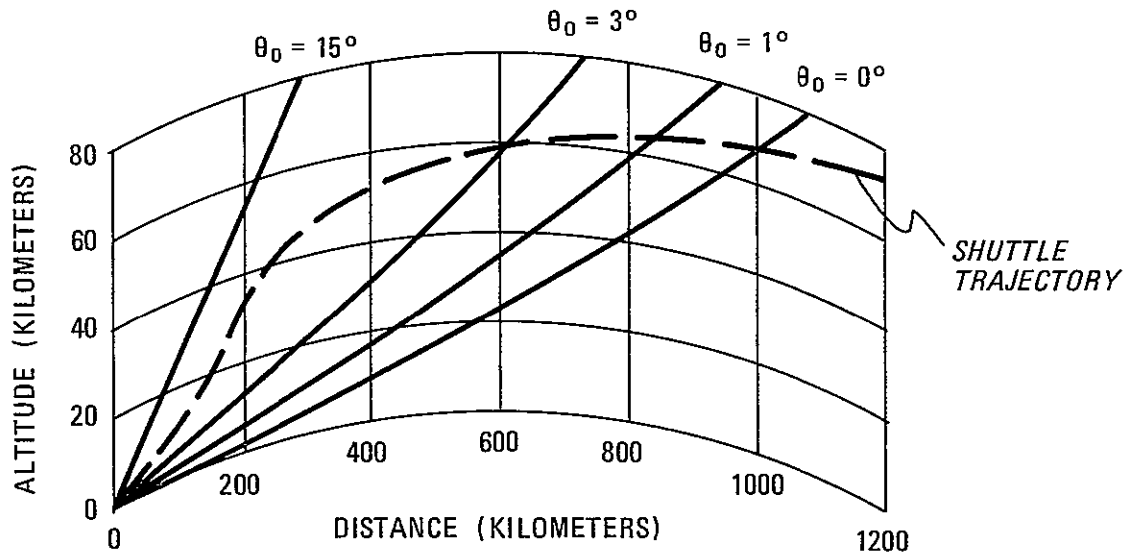


Fig 4-33 Radio Elevation Angle and Shuttle Trajectory

4.4.2 Uncertainty After Initial Fix. The initialization logic has been exercised at various locations at 150 km from the airport and at 50 km from the airport. In every case the initial altitude is 18.6 km. The three transponders utilized are located two along final approach at 15 km and 3 km from touch-down, and the third at the middle of the runway 3 km to the side. The runway and transponder locations are shown at the center of Fig. 4-34. The results of the several initializations are also shown on Fig. 4-34. The onboard-computed  $1\sigma$  uncertainties after the fix are presented near each initialization location. The most severely diluted result is the 773 meter  $1\sigma$  altitude error for the Shuttle 150 km to the north (approaching from the side of the runway). The altitude geometric dilution factor at 150 km with a northerly transponder separation of only 3 km and an elevation angle of only  $1/8$  radian is about  $8 \times 150/3 = 400$ . This factor multiplied times the accuracy of the range measurements, which are of the order of 2 meters  $1\sigma$ , makes a result of the order of 800 meters for altitude seem reasonable.



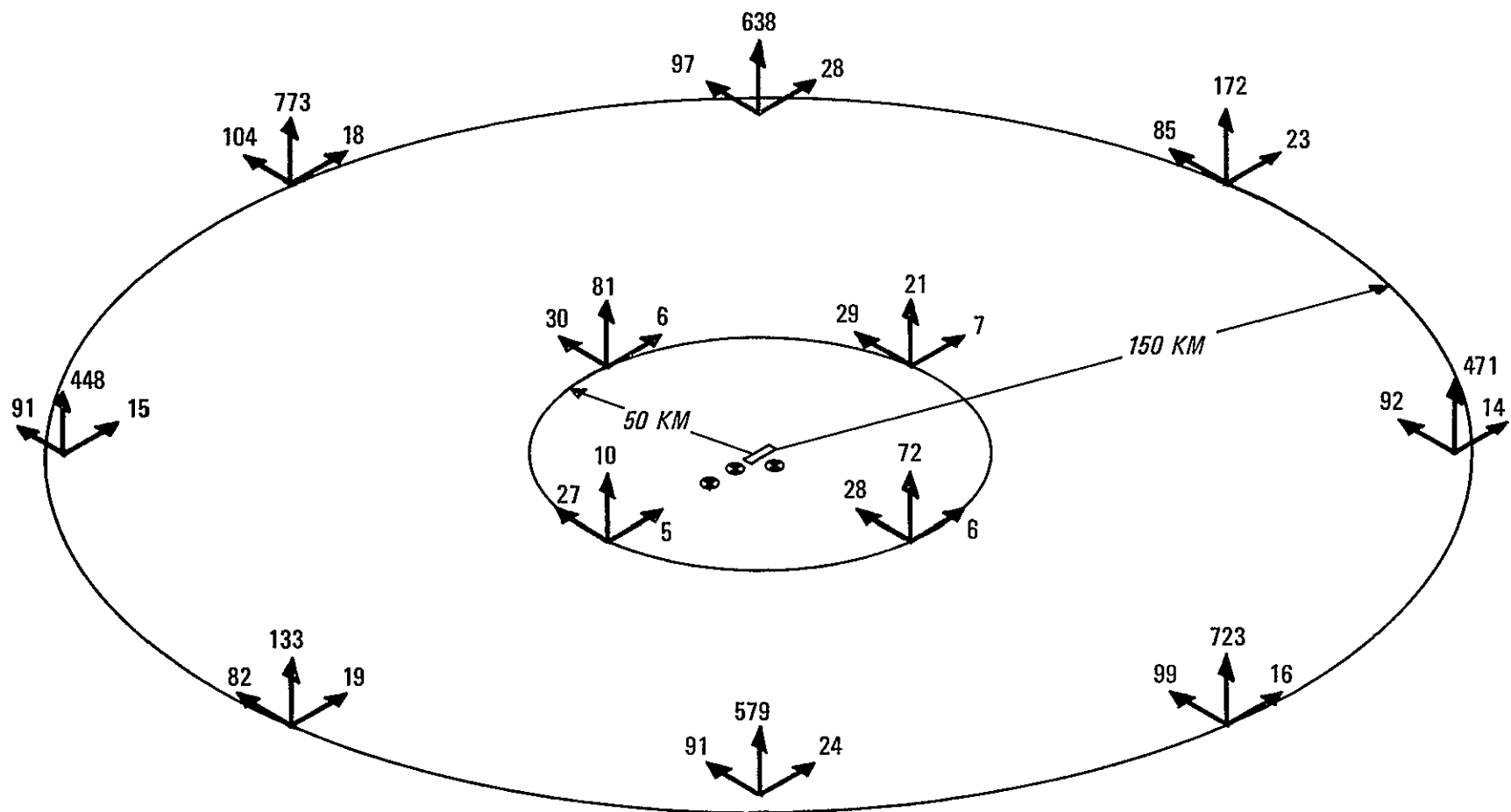


Fig. 4-34 Position Uncertainty (meters  $1\sigma$ ) After Initial Fix at 18.6 km Altitude

#### 4.4.3 Performance From Distant Initialization Through Touchdown.

Two simulations have been run all the way from initialization at 150 km to touchdown and rollout. These simulations include the three-range measurement position fix; three additional measurement pairs at  $t=2, 4$ , and  $6$  sec to update the velocity; followed by a 10 min. period with measurements taken only every 30 sec. The measurement rate is increased to one pair every 10 sec at  $t=600$ , following which the measurement selection logic is the same as in the baseline simulation. All other conditions are as in the baseline simulation.

One simulation has been started in the worst location (for the transponders being used), namely 150 km to the north. To provide a navigation test with consistently poor altitude-measuring geometry, the vehicle is not allowed to overfly the airport. Rather the vehicle glides directly to the final approach entry point and executes a left turn in, as shown in Fig. 4-35.

The onboard-computed 1 $\sigma$  navigation uncertainties are presented in Figs. 4-36 and 4-37. Note the changes in both the error scale and the time scale. After turning onto final approach and over-flying the outer transponder X1, the results are essentially the same as in the baseline simulation.

A second simulation is a straight-in approach from 150 km to the west. The straight-in approach stresses the navigation system in two ways different from the previous simulation: 1) The northerly-measuring geometry is always weak. 2) With no turn acceleration, the in-flight azimuth error is less readily controlled.

The onboard-computed 1 $\sigma$  navigation uncertainties are presented in Figs. 4-38 and 4-39. Again, after reaching the outer transponder X1, the results are essentially the same as in the baseline simulation.

The actual (single case) navigation errors in these two runs have been compared with the onboard-computed uncertainties. There is some divergence of the actual-error-to-uncertainty ratio during the long 10 min. flight from 150 km into the terminal area. At  $t=10$  min. in the north-approach simulation there is an actual north error of 45 meters with an onboard computed uncertainty of only 8.5 meters. However, on final approach such disagreement is quickly eliminated. At touchdown the actual errors are completely consistent with the onboard-computed uncertainties. Again, the onboard equations design appears quite satisfactory.

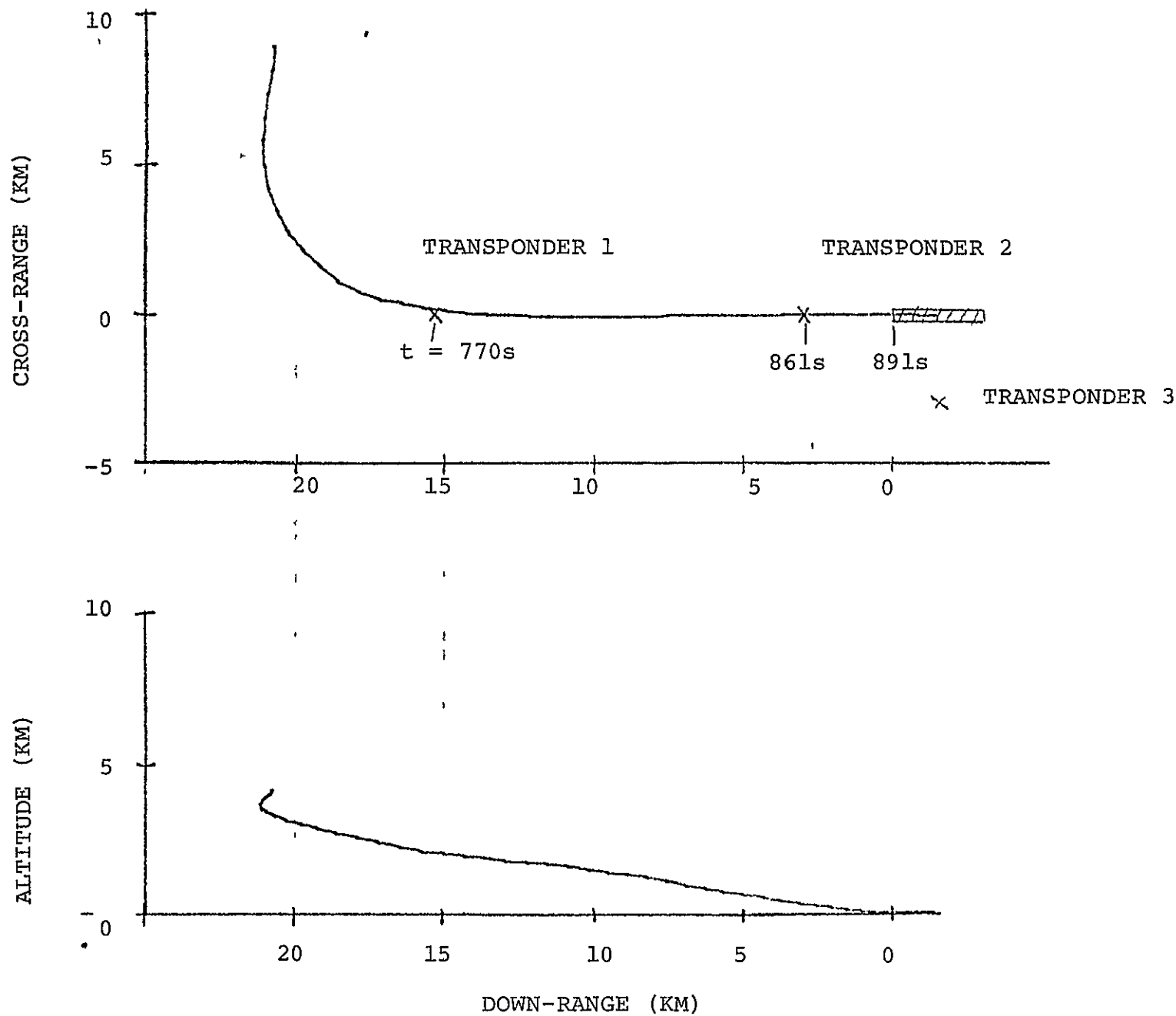


Fig. 4-35 APPROACH FROM 150 KM TO THE NORTH

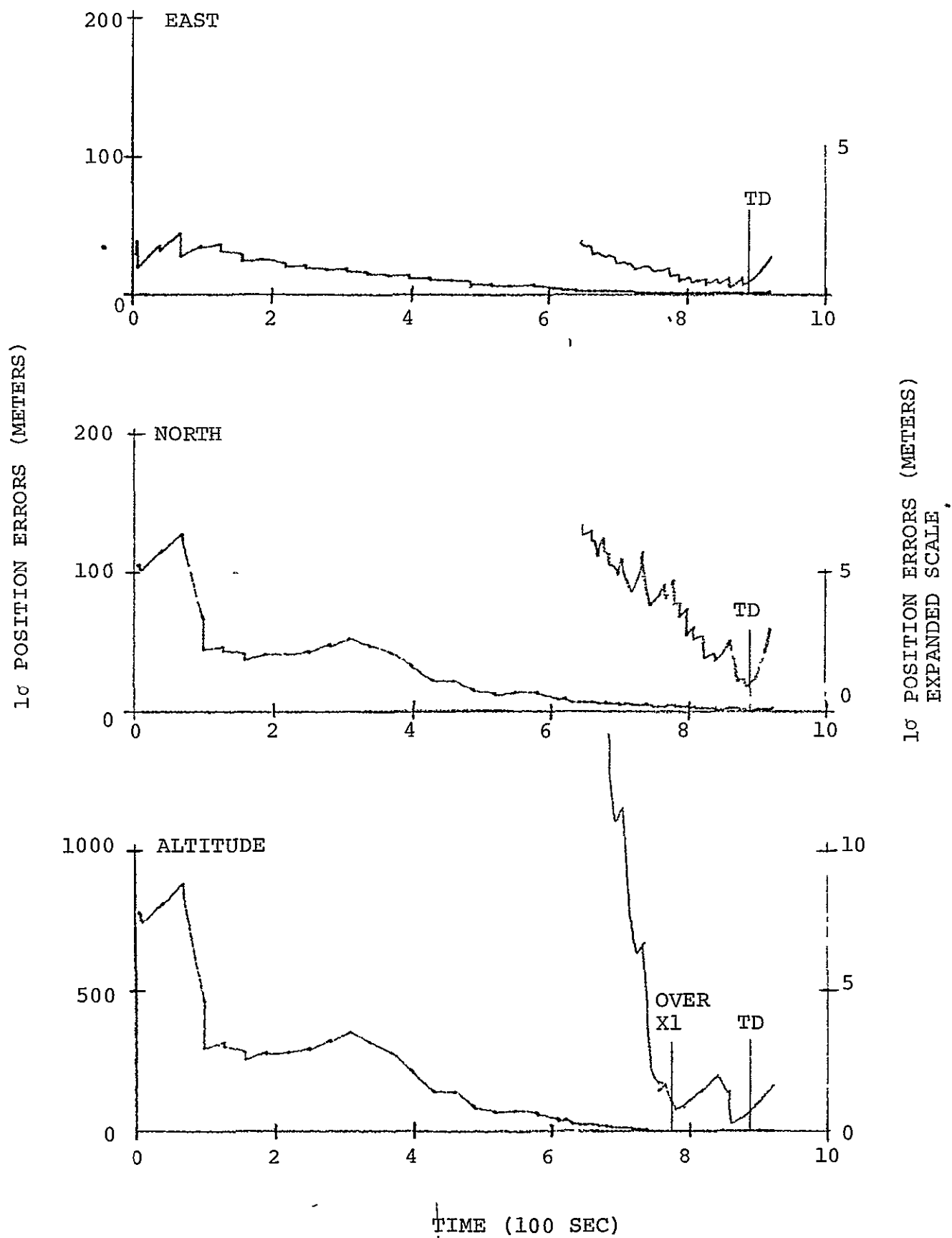


Fig. 4-36 POSITION UNCERTAINTY, APPROACH FROM 150 KM TO THE NORTH.

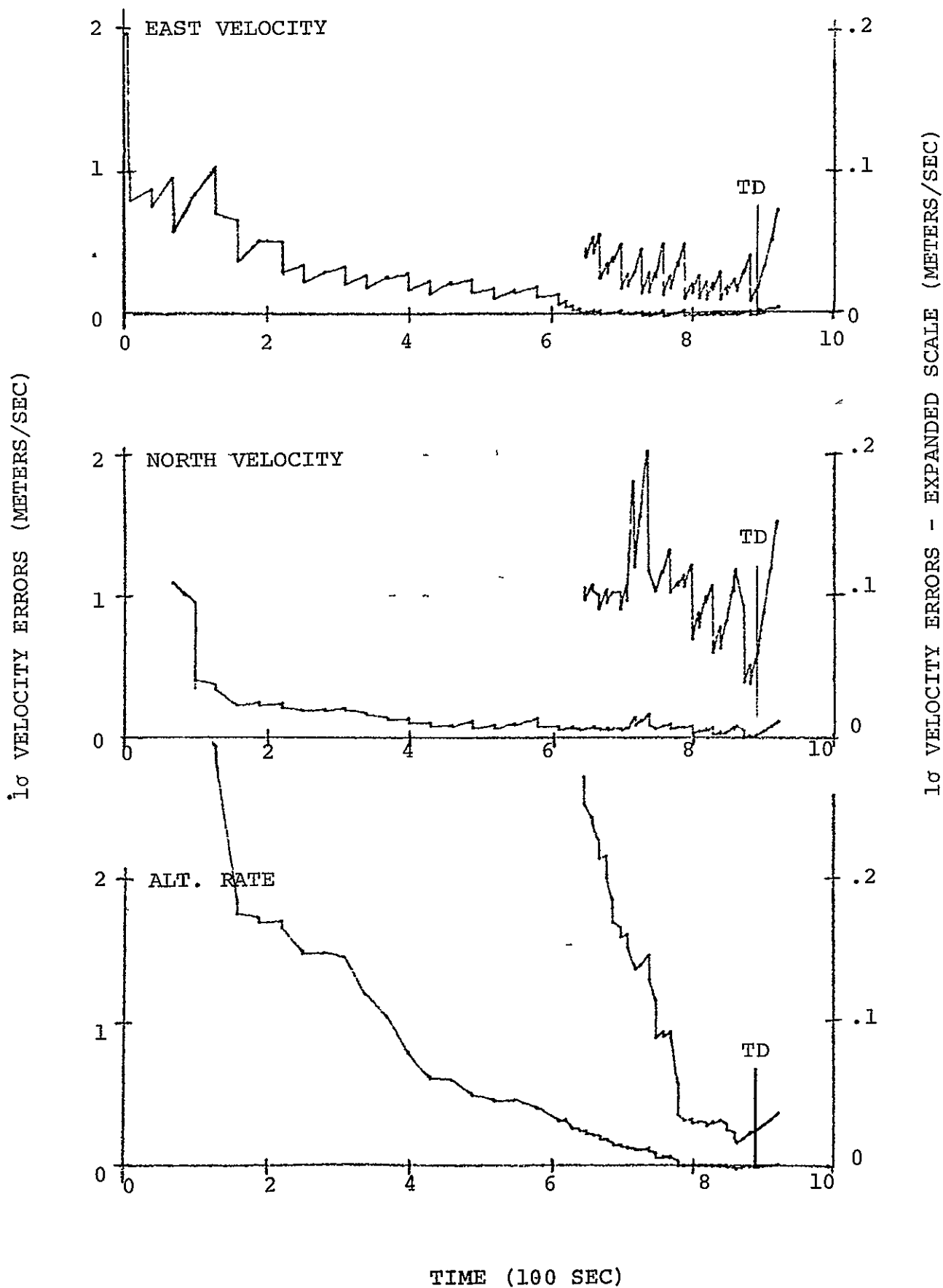


Fig. 4-37 VELOCITY UNCERTAINTY, APPROACH FROM 150 KM TO THE NORTH.

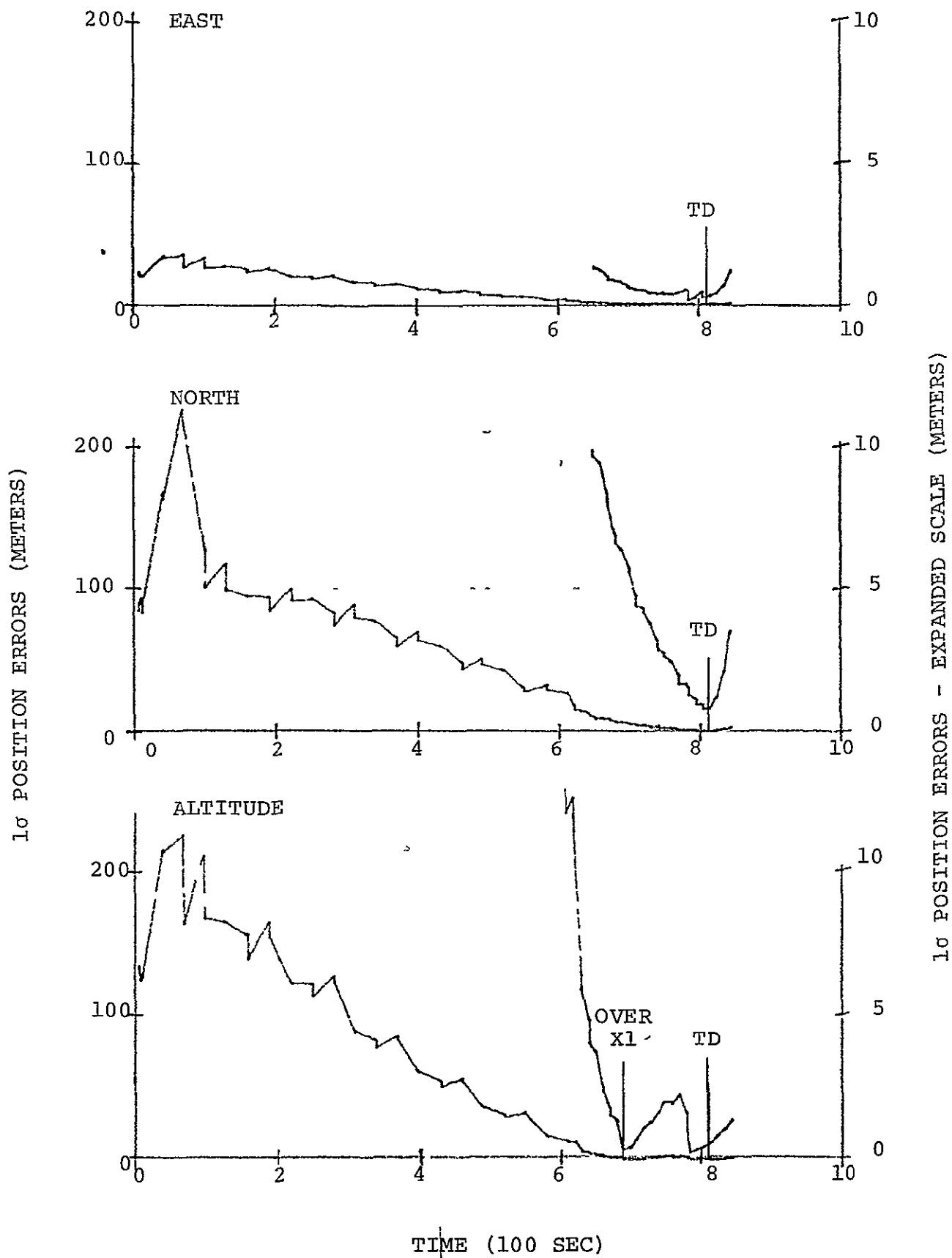


Fig. 4-38 POSITION UNCERTAINTY, STRAIGHT-IN  
APPROACH FROM 150 KM TO THE WEST

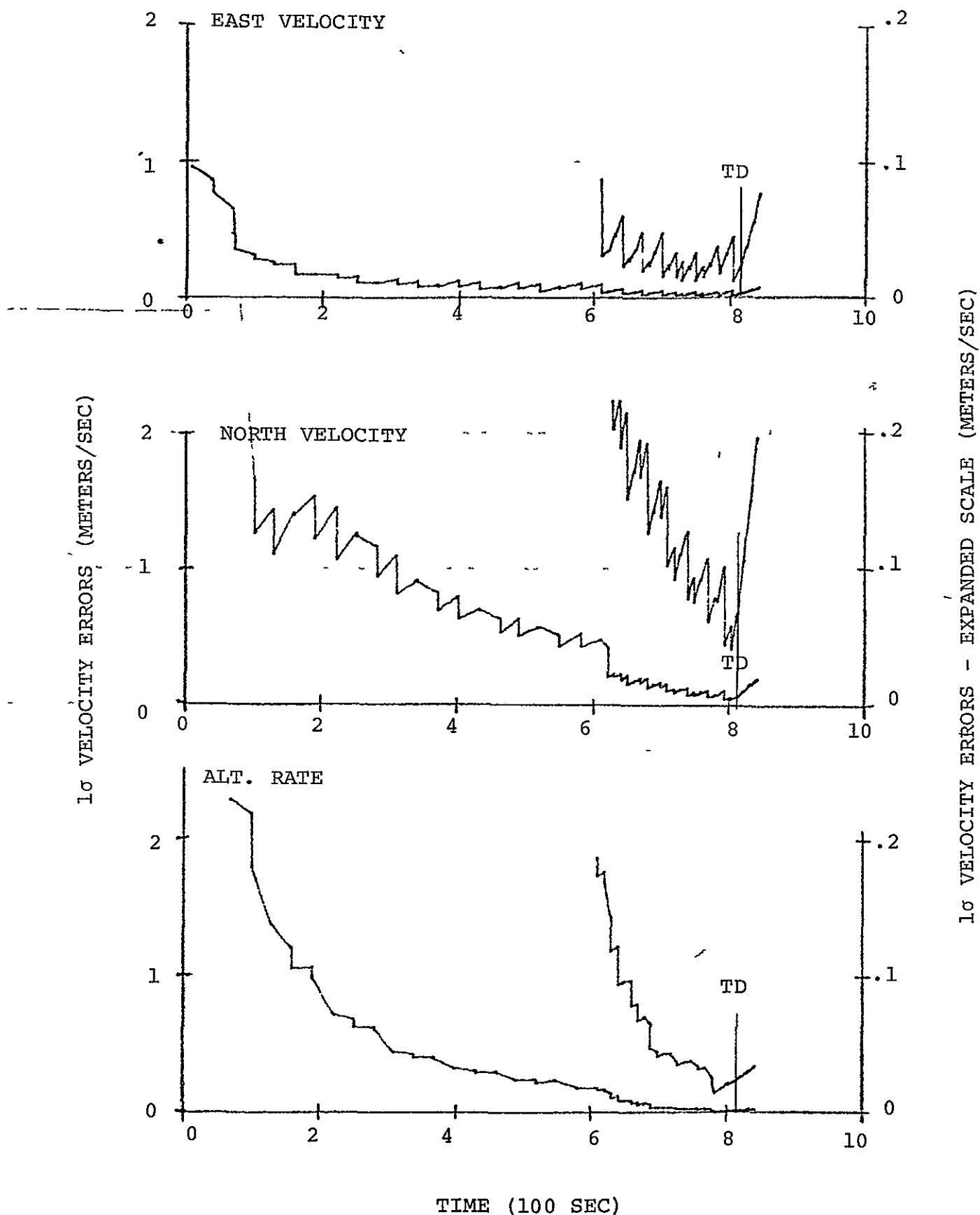


Fig. 4-39 VELOCITY UNCERTAINTY, STRAIGHT-IN APPROACH  
FROM 150 KM TO THE WEST

In both runs, the initial azimuth error was 1.5 milliradian. The run that turns into final approach resulted in an azimuth misalignment at touchdown of 0.1 milliradian. The straight-in approach yielded an azimuth misalignment at touchdown of 0.9 milliradian. Yet in spite of the larger alignment error, the straight-in velocity errors and position errors were as good at touchdown as in the other case.

The significant conclusion is that no additional transponders need be deployed to assist the landing navigation initialization. The terminal area transponders (which have been deployed solely to optimize the final approach and touchdown performance) are sufficient to perform initial updating at a distance of 150 km.

#### 4.5 Effect of Measurement Rate on Performance

4.5.1 Performance With A Measurement Pair Every 5 Sec. In the baseline simulation, one measurement pair (range and delta range) is incorporated every 10 sec. However, the normal measurement sequence and rate is interrupted at the inner-approach transponder to obtain three measurement pairs, two of which have excellent altitude-measurement geometry.

In Figs. 4-40 and 4-41, the results of an alternate simulation are shown where the measurement rate has been increased to one pair every 5 sec. starting at  $t=206$ . That is, the simulation is identical to the baseline simulation until 8 km from touchdown, after which the measurement rate is doubled. Near the inner-approach transponder five measurement pairs are incorporated, two of which have excellent altitude-measuring geometry. Comparing the results with the baseline results shown in Figs. 4-9 and 4-10, it is evident that increasing the measurement rate does little to improve the landing-navigation accuracy. A slight improvement in north velocity accuracy is seen. With  $\Delta t=5$  sec, two measurement pairs to the lateral transponder were obtained after inner-approach-transponder overflight before the  $1^\circ$  elevation-angle cutoff. In the baseline simulation with  $\Delta t=10$  sec only one such measurement pair was obtained.

4.5.2 Recommended Measurement Rates. No single measurement rate is appropriate for all phases of the approach and landing.

When updating of the inertial navigation first begins, three measurement pairs are taken as rapidly as possible to approximate simultaneous range measurements.



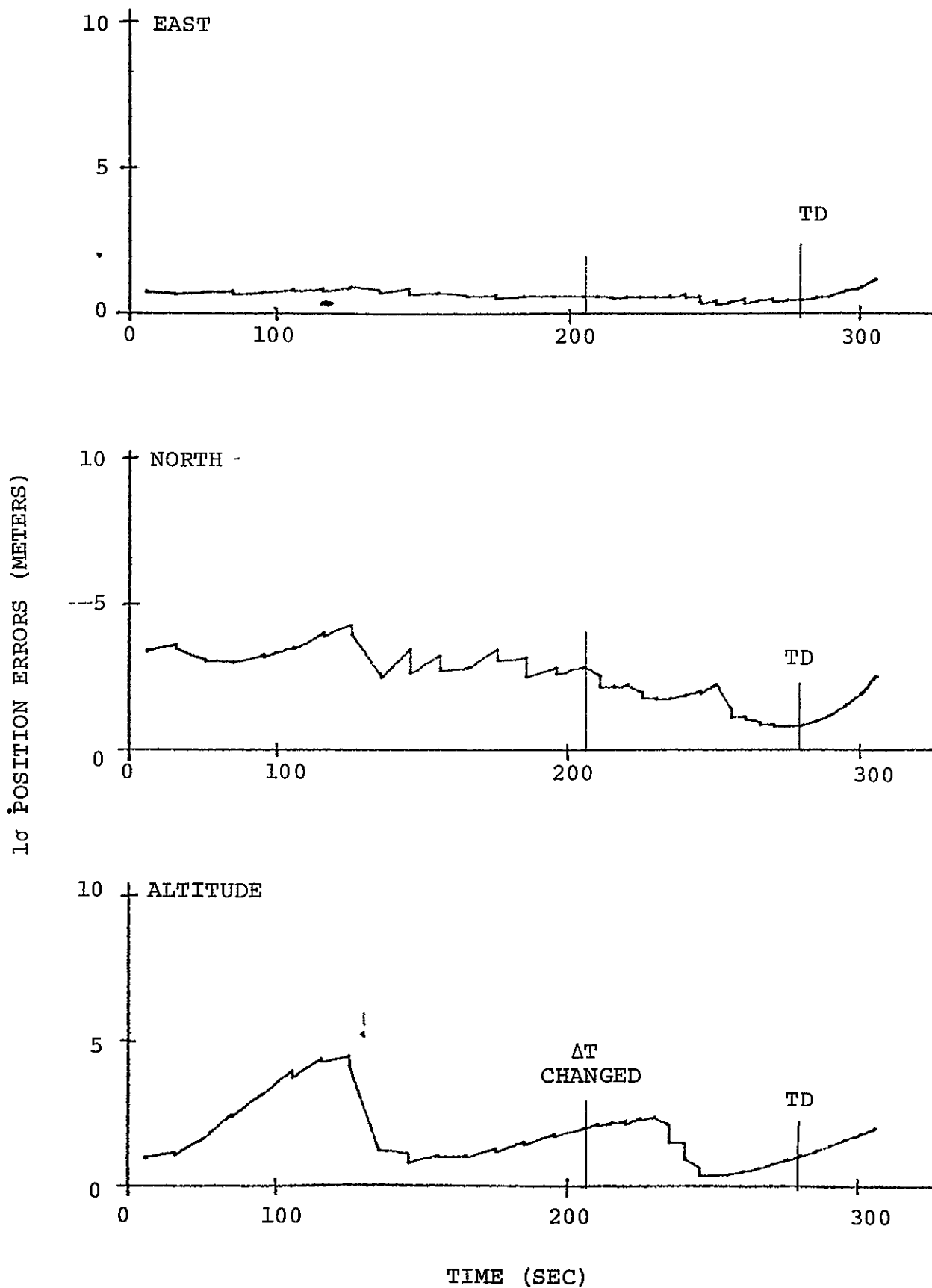


Fig. 4-40 POSITION UNCERTAINTY WITH A MEASUREMENT PAIR EVERY 5 SEC.

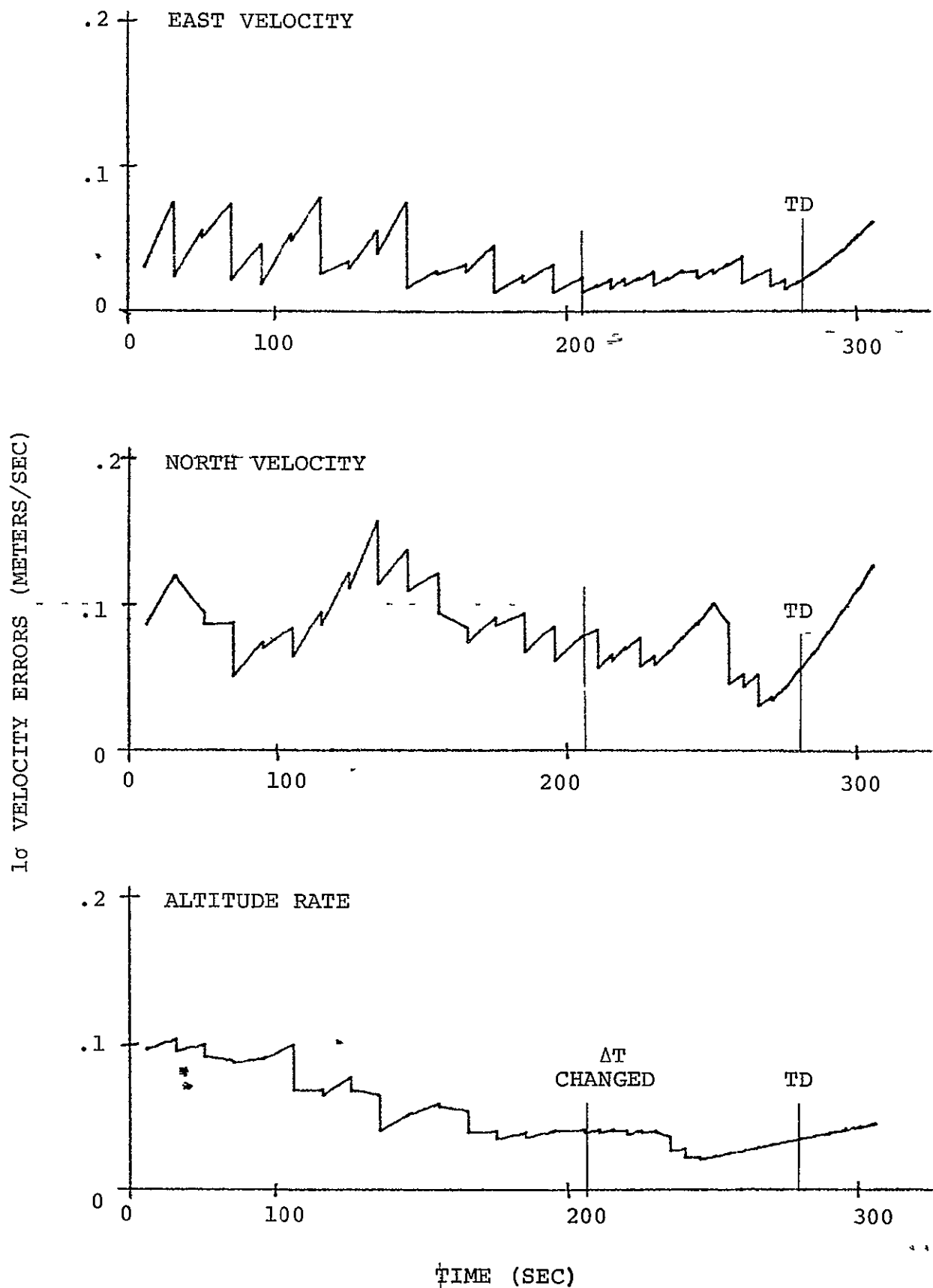


Fig. 4-41 VELOCITY UNCERTAINTY WITH A MEASUREMENT PAIR EVERY 5 SEC.

After the initial position fix, three additional measurement pairs are incorporated to update the velocity. One pair every 2 sec gave satisfactory performance. A slower rate would probably also be satisfactory.

Next follows a long phase during which the vehicle glides from as far as 150 km away to the terminal area. This phase can be as long as ten minutes. The transponder-to-vehicle direction vectors change very slowly during this terminal approach phase. A rapid measurement rate is not only unnecessary but may also be undesirable. A large number of measurements with little or no geometry shift can lead to divergence of the actual errors relative to the onboard-computed uncertainty. A sample rate of one measurement pair every 30 sec gave satisfactory performance.

Before turning onto final approach the measurement rate should be increased to one pair every 10 sec.

Special measurement selection logic must be used on final approach to ensure the best utilization of the transponder geometry. Fig. 4-23 showed the measurement rate required to obtain three measurement pairs within  $20^\circ$  of directly over a transponder on final approach. For the inner approach transponder at 2 km, one pair per 0.6 sec is required (1.5 pairs per sec). For the redundant-inner-approach transponder at 4 km, one pair per 1.2 sec is required (0.8 pairs per sec). For the outer-approach transponders at 9 km and 15 km, correspondingly lower measurement rates are required.

If the data from the lateral transponder is indeed unuseable at very low elevation angles (such as below  $1^\circ$  as assumed in these simulations), then special measurement logic can also be used with the lateral transponder to ensure obtaining several measurement pairs with the best available lateral geometry just before cut-off. However, this is not mandatory to meet the accuracy specification.

#### 4.6 What Range and Delta Range Accuracies Are Required?

4.6.1 Range-Only Performance. One simulation has been run without the delta-range measurements. All conditions are the same as in the baseline simulation, except that only a single range measurement is taken every 10 sec, rather than a

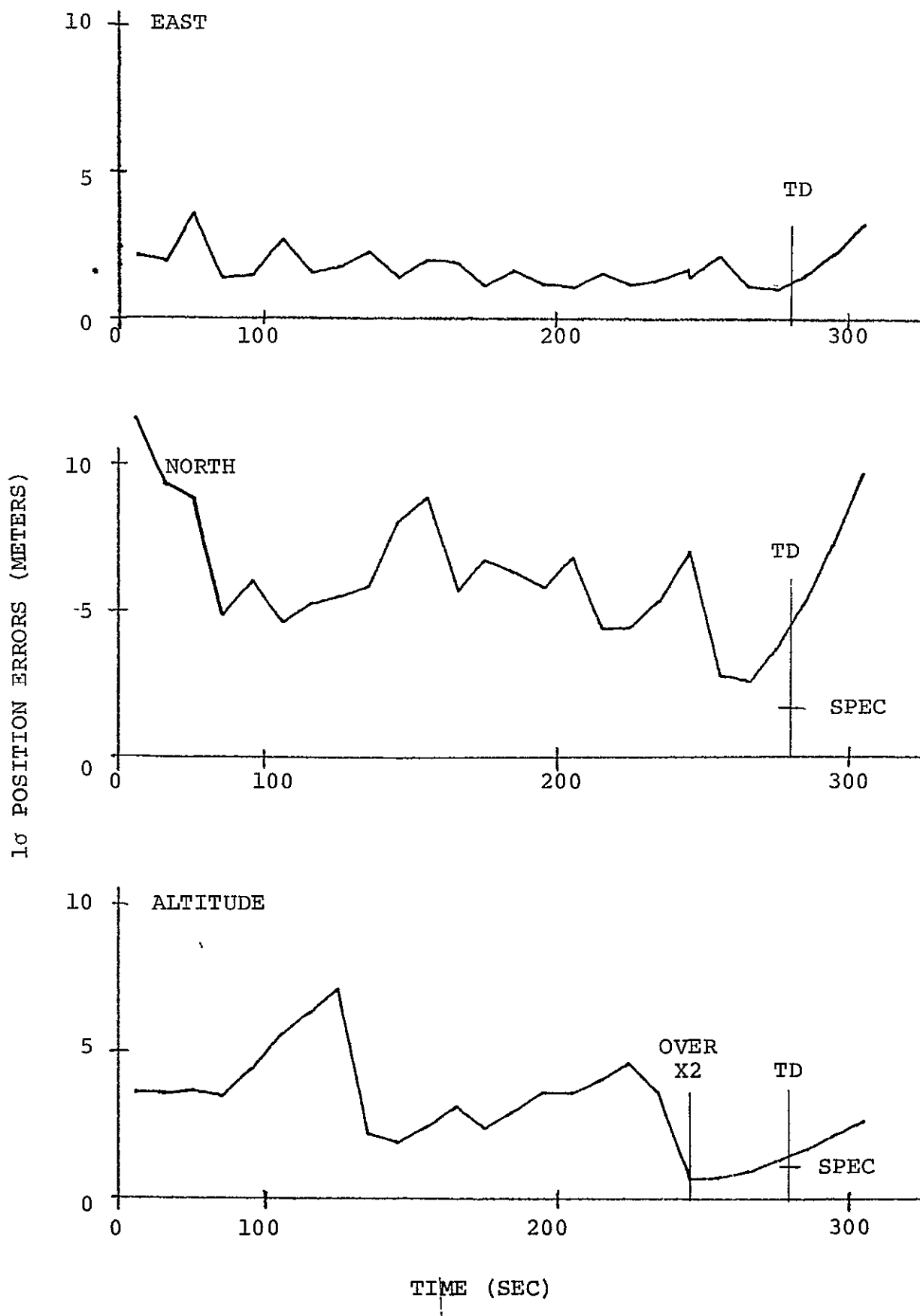


Fig. 4-42 POSITION UNCERTAINTY USING ONLY RANGE MEASUREMENTS

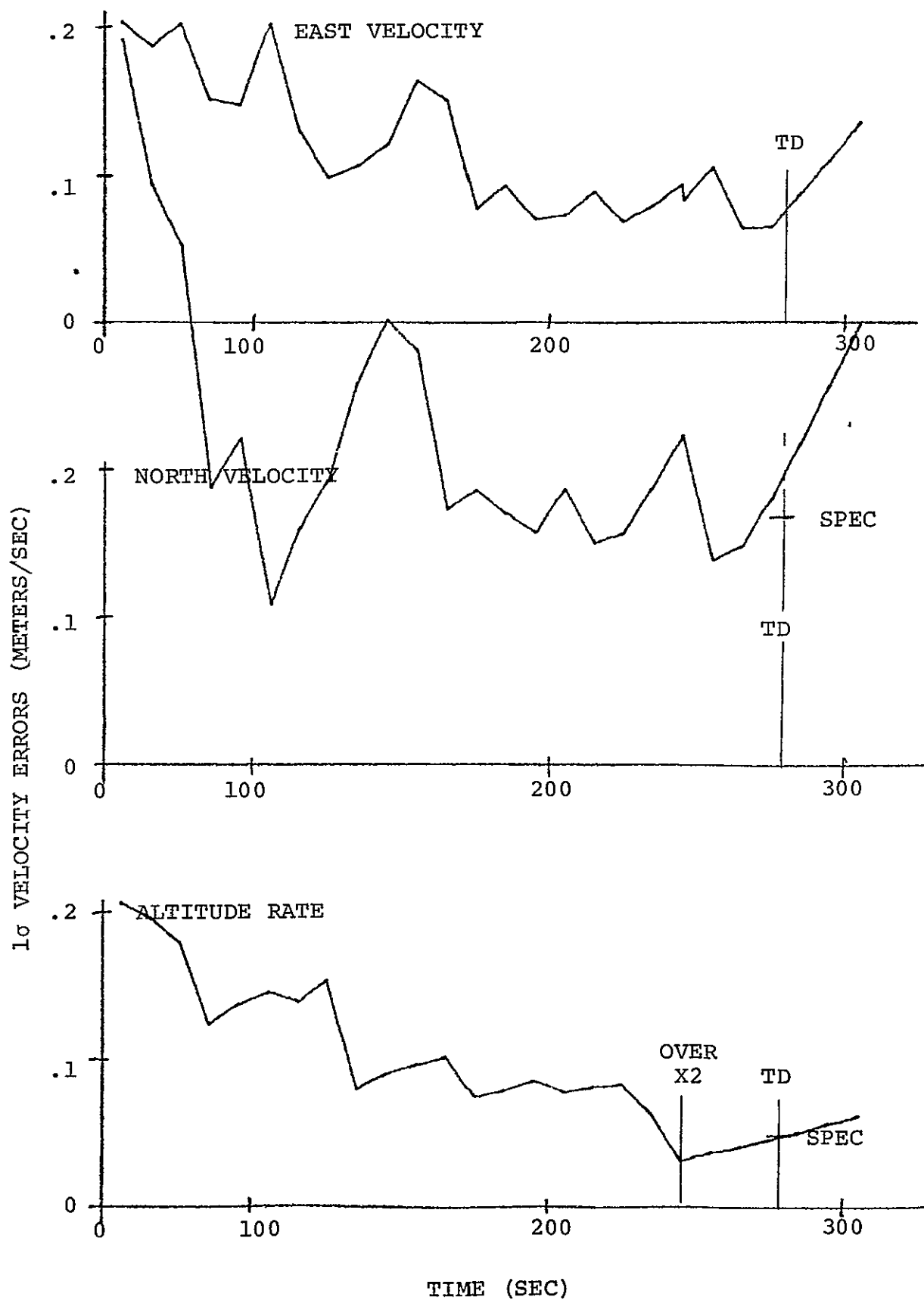


Fig. 4-43 VELOCITY UNCERTAINTY USING ONLY RANGE MEASUREMENTS

range plus delta-range measurement pair. The simulation results are plotted in Figs. 4-42 and 4-43. The performance does not meet the specification. Most noticeable is the north (cross-runway) position error at touchdown of 3.5 meter  $1\sigma$ . The altitude error of 1.1 meter  $1\sigma$  slightly exceeds the specification.

Note, compared with the baseline performance, the north error has quadrupled but the altitude error has only increased by 40%. The relative importance of the delta-range measurement in aiding cross-runway (north) navigation as opposed to altitude navigation is related to the dependence of the range accuracy on elevation angle. The cross-runway measurements are obtained at low elevation angles where the largest multipath error (0.9m  $1\sigma$ ) is likely to occur. The altitude measurements are obtained at high elevation angles for which the multipath error is likely to be negligible. Hence, the altitude navigation has less need for assistance from the more precise delta-range measuring capability (which has been assumed to have a random error of 0.1m  $1\sigma$ , independent of elevation angle).

4.6.2 Performance For Various Range and Delta-Range Accuracies. Several simulations have been run with various levels of range and delta-range random error. The multipath error in the range measurement is maintained at  $0.9 \cos \epsilon$  meter  $1\sigma$ . The propagation error is unchanged at 50 ppm. The transponder biases are unchanged at 0.3 meter  $1\sigma$ . Only the non-multipath random error has been increased from the baseline 0.2 meter  $1\sigma$ . For the delta-range measurements, the random error has been increased from the baseline 0.1 meter  $1\sigma$ . The Kalman filter data is changed to reflect the degraded DME performance. That is, the assumed variance for the DME measurements is consistent with the simulated equipment performance.

The results of these simulations are summarized in Fig. 4-44. The altitude error (h) and the north (cross-runway) error (n) at touchdown are presented. (These are the onboard computed  $1\sigma$  uncertainties.) The values, labeling the figure, for range random error and bias is the root sum square of the  $1\sigma$  non-multipath random error and the  $1\sigma$  bias error. For example, the baseline case is  $(.2^2 + .3^2)^{1/2} = .36$  meter. An arc has been drawn separating those cases which do not meet the specification from those cases that do meet the specification. The time histories of the onboard-computed uncertainties for the 1.0 and 0.3 meter case are presented in Figs. 4-45 and 4-46.

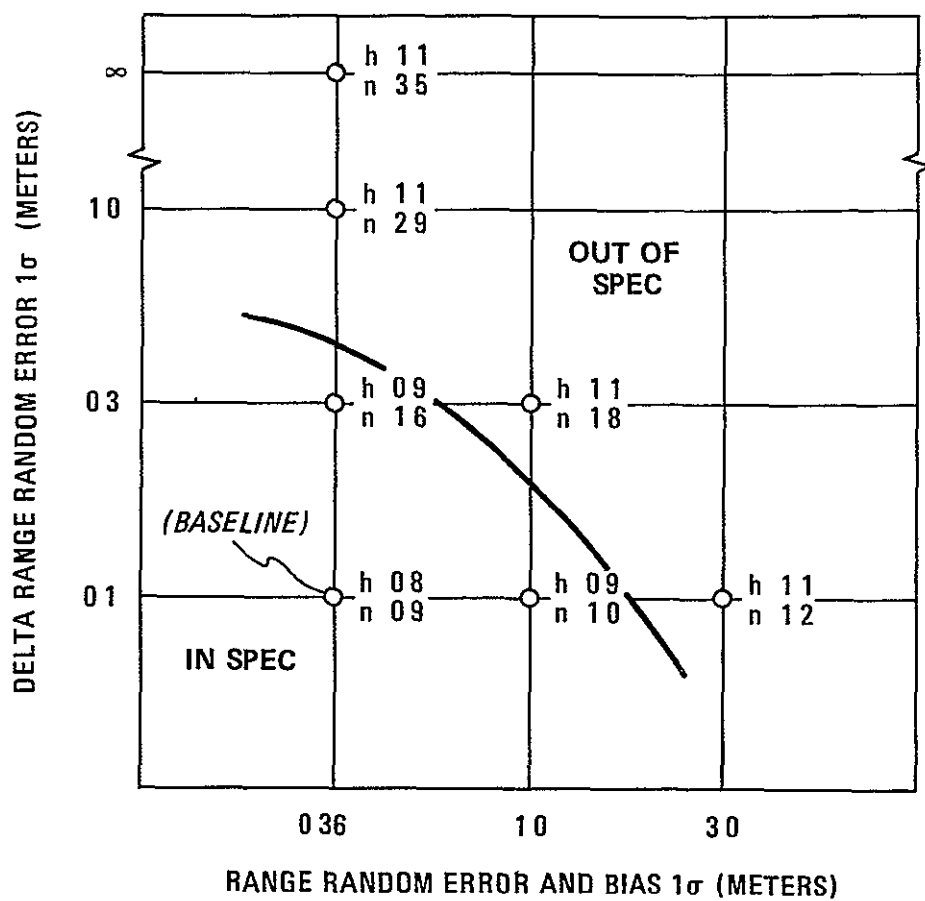


Fig. 4-44 Performance For Various Range and Delta-Range Accuracies

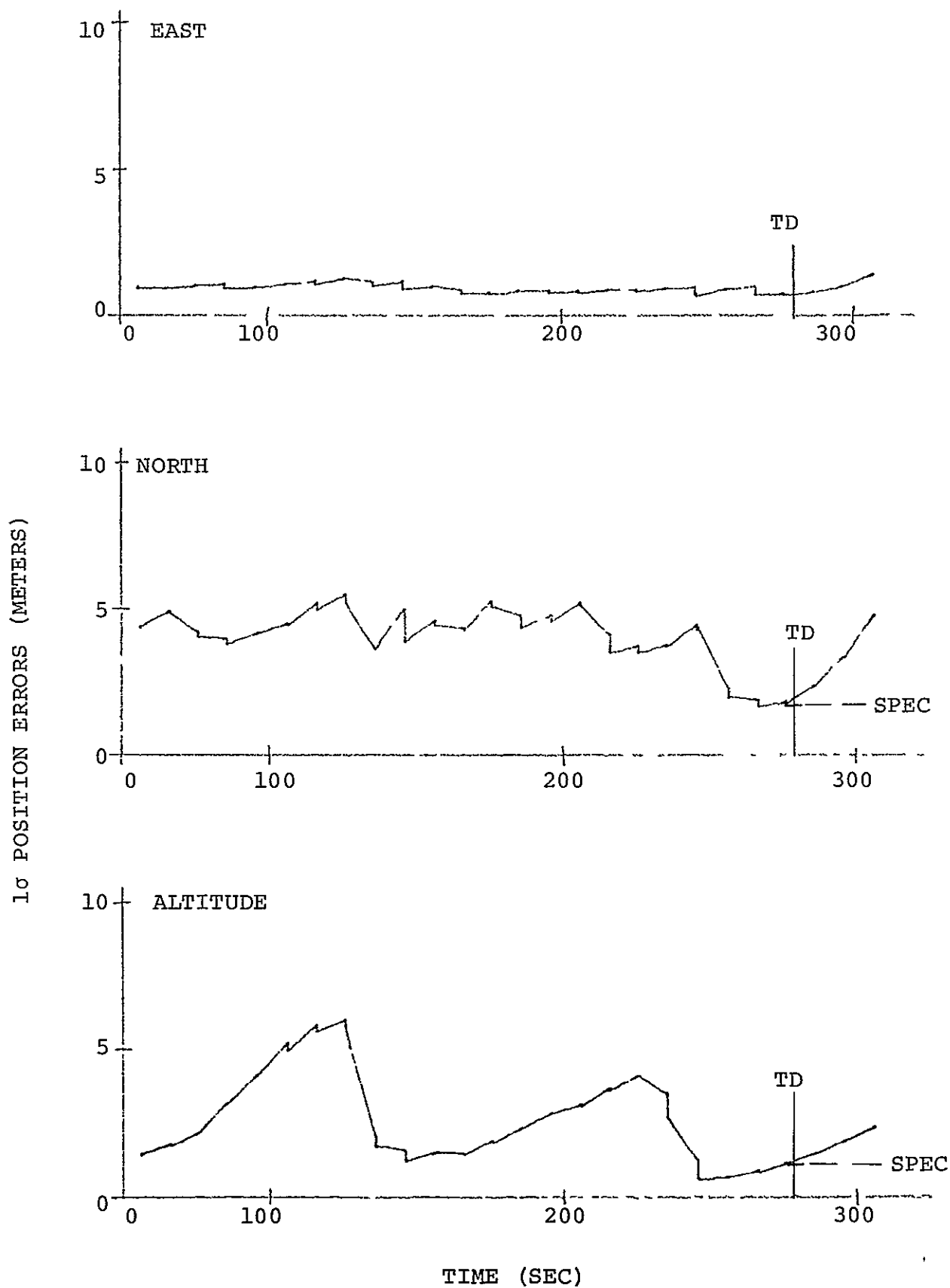


Fig. 4-45 POSITION UNCERTAINTY WITH RANGE AND DELTA-RANGE ERRORS OF 1.0 AND 0.3 METERS  $1\sigma$



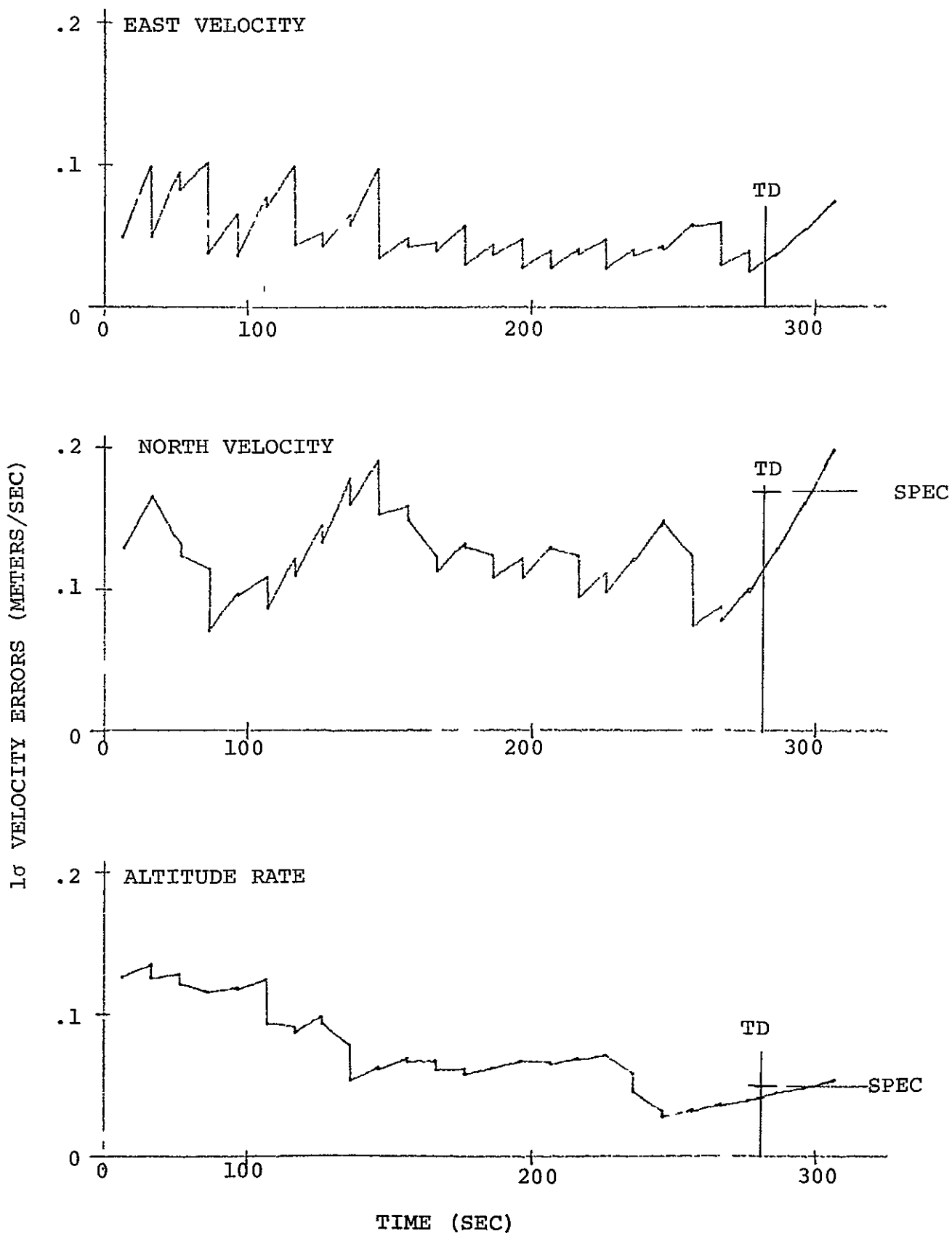


Fig. 4-46 VELOCITY UNCERTAINTY WITH RANGE AND DELTA-RANGE ERRORS OF 1.0 AND 0.3 METERS  $1\sigma$

4.6.3 Should the Delta-Range Be Procured? Including the delta-range measurements does increase the landing navigation accuracy. If one deleted the delta-range measuring capability from the hardware, then additional transponders would have to be deployed to bring the cross-runway and altitude errors within specification. The 10 to 20 percent unit cost saving for the simpler interrogators and transponders would be offset by the increased number of required transponders plus the increased operational costs of more extensive flight inspection and maintenance.

We therefore, recommend that the delta-range measuring capability be included in the landing navigation system for the Space Shuttle.

4.6.4 Recommended Range and Delta-Range Accuracies. Several combinations of range and delta-range accuracies are satisfactory, as was shown in Fig. 4-44. Furthermore, additional tradeoffs exist between DME accuracy and: number of transponders, IMU accuracy, fraction of total GNC touchdown budget allotted to navigation, and so forth. It is clear that specifying DME accuracies is intimately involved with other system design decisions.

An alternate approach is to choose the DME accuracy specifications to be equal to the state-of-the-art and allow other subsystems to benefit from the performance margin. We recommend that this approach be used to establish the range-accuracy specification. But the delta-range accuracy specification may be relaxed, since non-DME sources of error make the available accuracy unuseable. The critical specification numbers are (see Table 2-3): range measurement bias 0.3 meter  $1\sigma$ , multipath range random error  $0.9 \cos \epsilon$  meter  $1\sigma$ , other range random error 0.2 meter  $1\sigma$ , delta-range measurement random error 0.1 meter  $1\sigma$ .

#### 4.7 Transponder Drop-Out Before Touchdown

4.7.1 Simulation Results. In the baseline simulation and all other simulations up to this point it has been assumed that satisfactory range and delta-range measurements can be obtained down to elevation angles as small as  $1^\circ$ . What is the result if this is not the case?

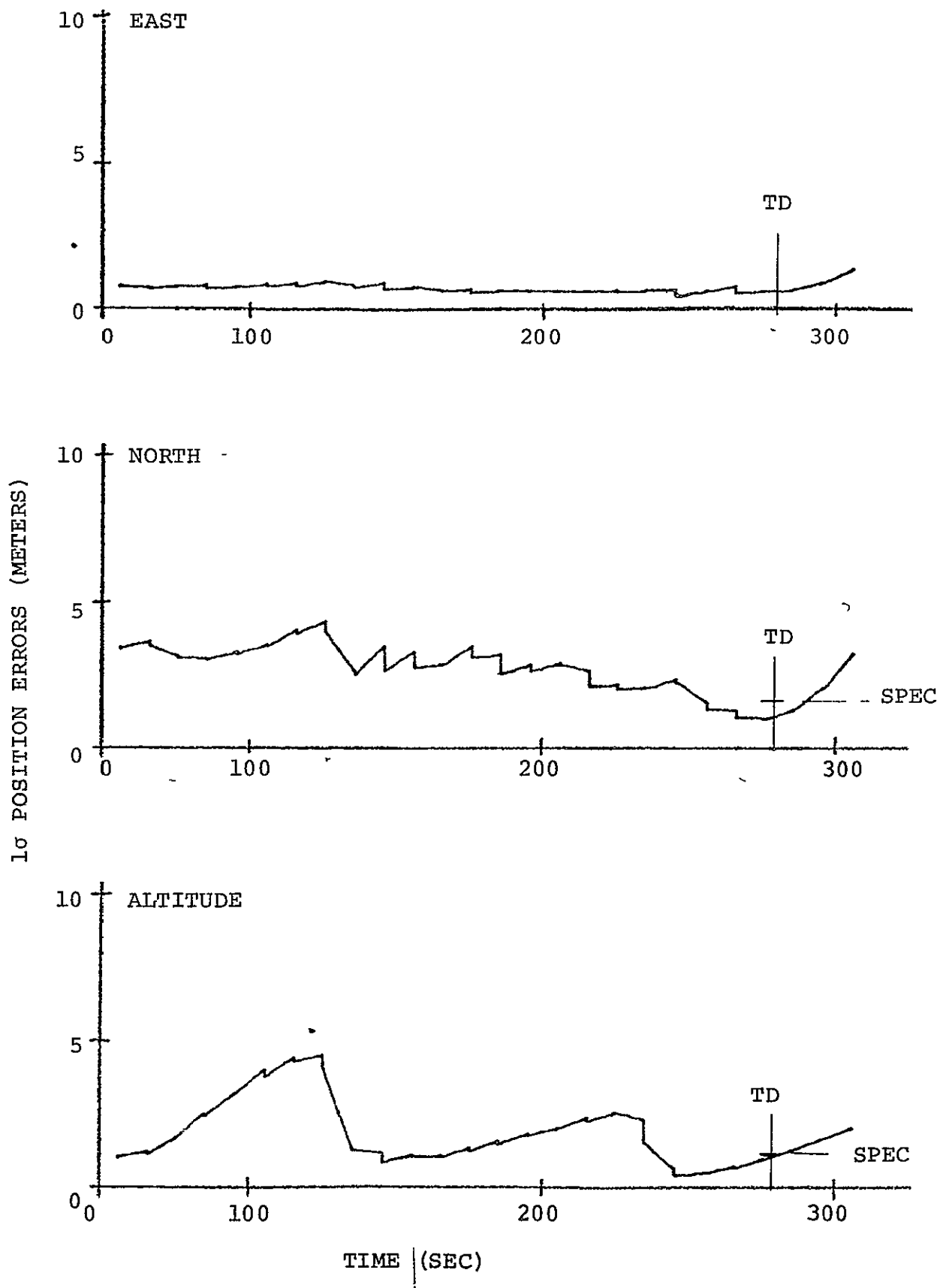


Fig. 4-47 POSITION UNCERTAINTY WITH 2° ELEVATION DME CUT-OFF

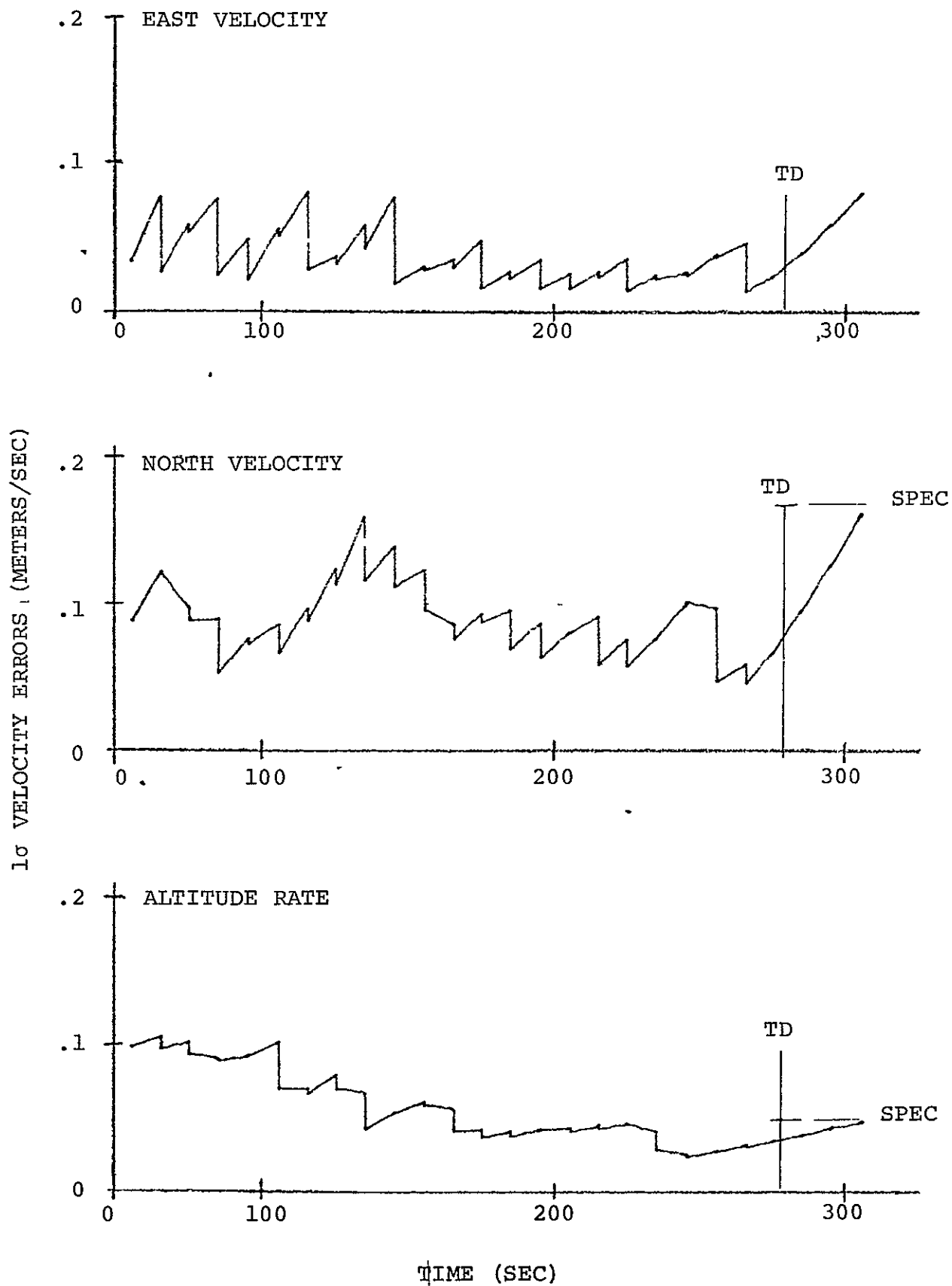


Fig. 4-48 VELOCITY UNCERTAINTY WITH 2° ELEVATION DME CUT-OFF

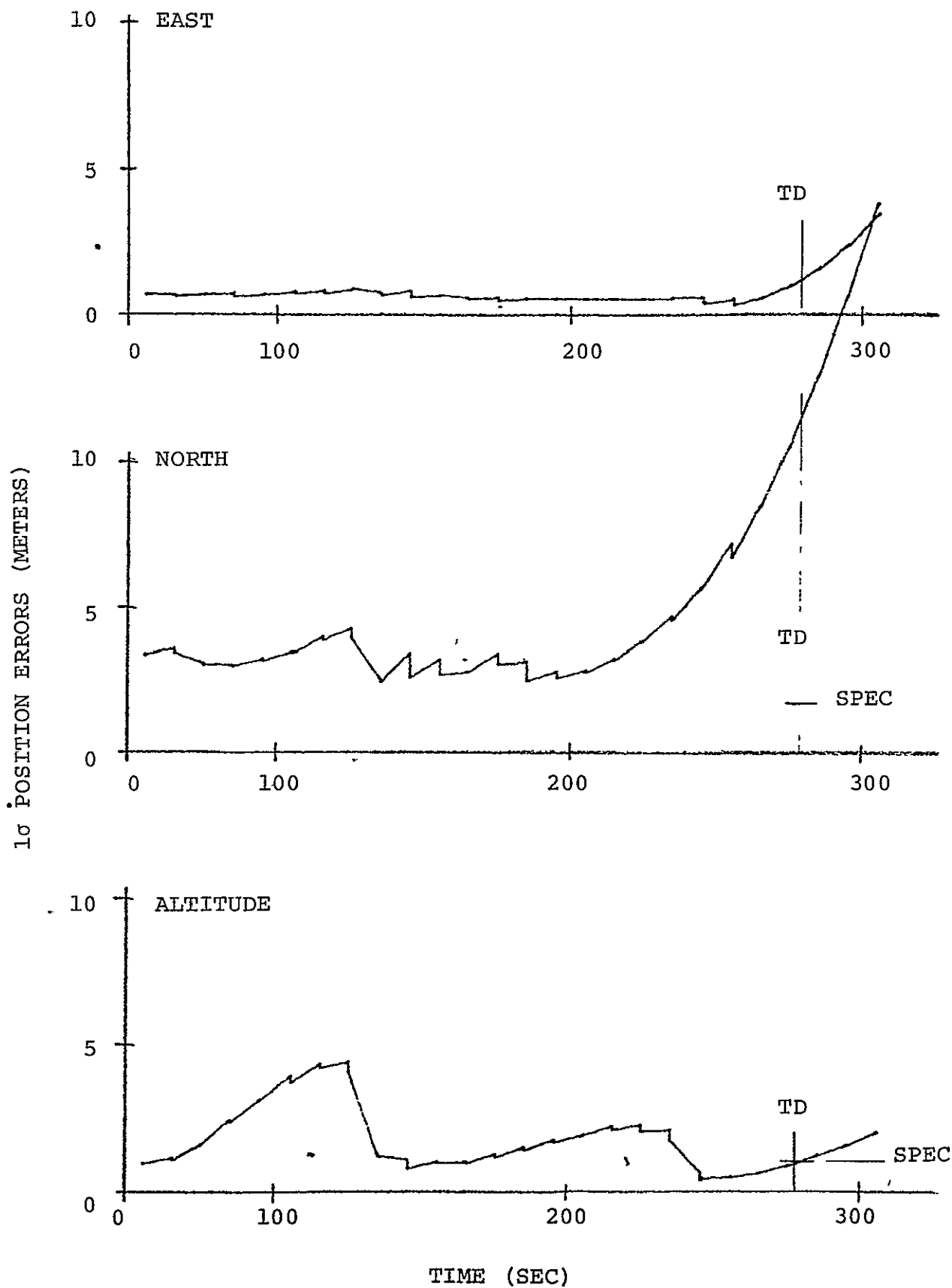


Fig. 4-49 POSITION UNCERTAINTY WITH 5° ELEVATION DME CUT-OFF

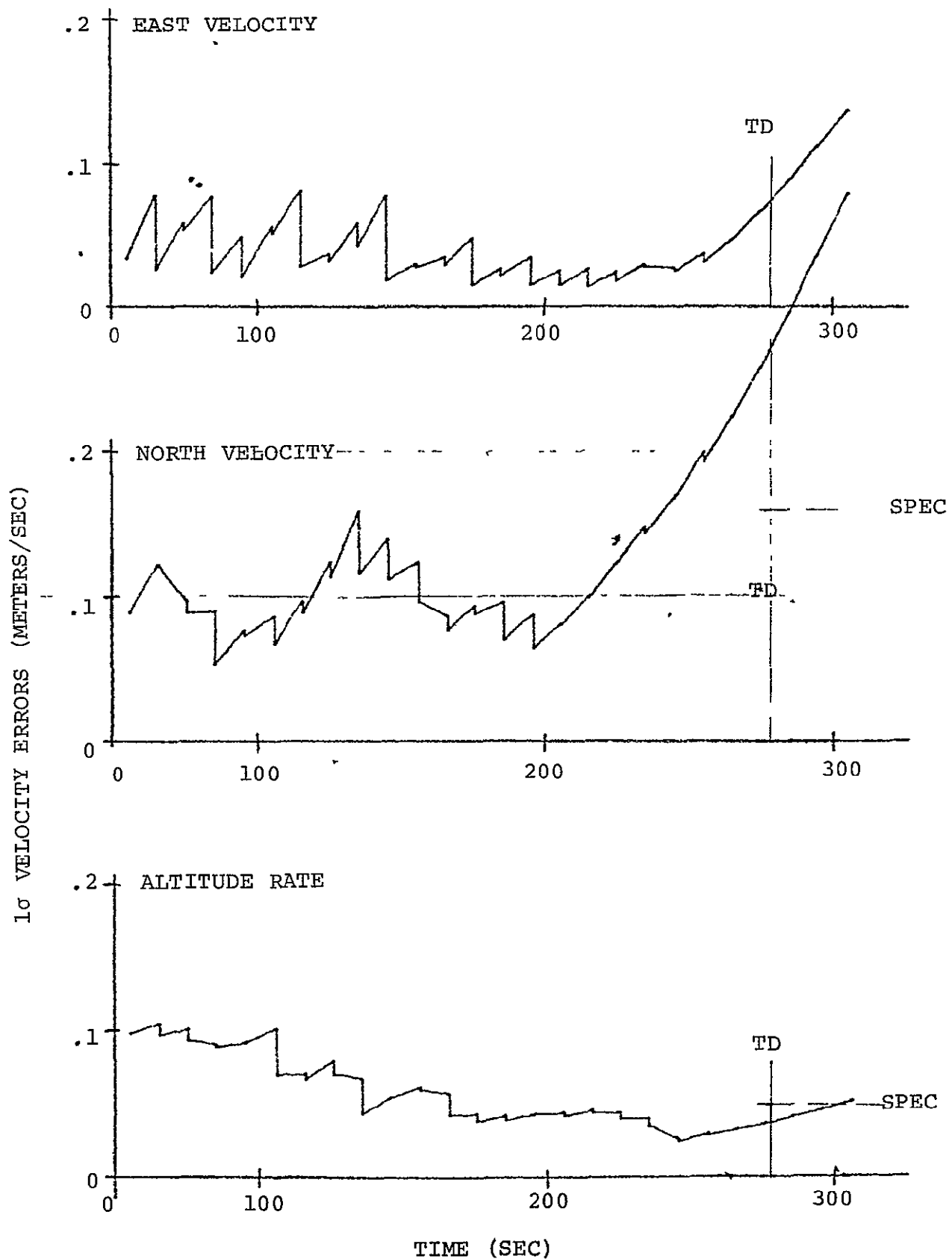


Fig. 4-50 VELOCITY UNCERTAINTY WITH 5° ELEVATION DME CUT-OFF

One simulation has been run with an elevation cut-off angle of  $2^\circ$ . The results are plotted in Figs. 4-47 and 4-48. A second simulation has been run with an elevation cut-off angle of  $5^\circ$ . The results are plotted in Figs. 4-49 and 4-50.

The  $2^\circ$  simulation is almost identical to the  $1^\circ$  baseline simulation. Of the measurements incorporated in the baseline simulation, only the last measurement to the inner-approach transponder at 277 sec is lost with the increased elevation angle. This permits slight increases in the down-runway (east) position and velocity uncertainties. These increases are completely negligible with respect to the specifications.

The  $5^\circ$  simulation exhibits unsatisfactory performance. The cross-runway (north) position and velocity uncertainties are far out of specification. The last measurement to the lateral transponder is obtained 90 sec before touchdown. This is too long an interval for the inertial navigation to extrapolate to touchdown.

If at a particular landing site there would be a  $5^\circ$  elevation angle cut-off at the recommended lateral transponder location, then an alternate transponder placement can be used. The lateral transponder has been moved from the middle of the runway to beside the final approach path as shown in Fig. 4-51.

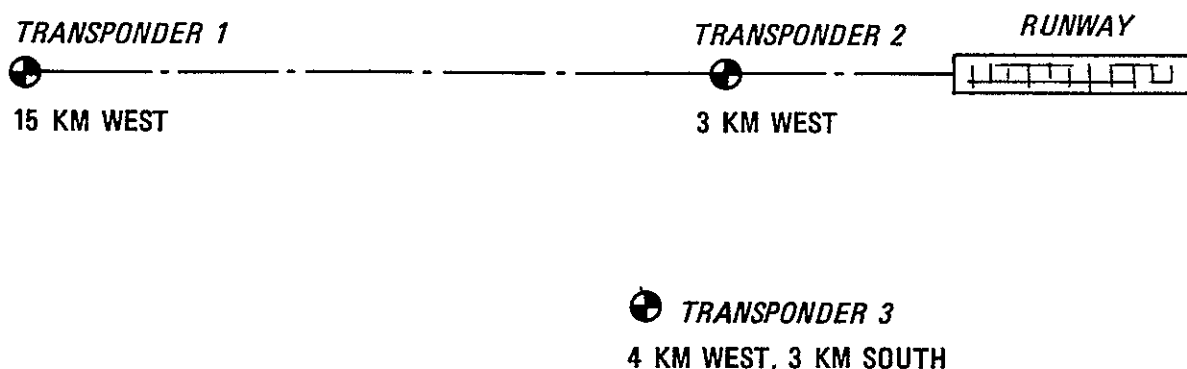


Fig. 4-51 Lateral Transponder Beside Final Approach Path

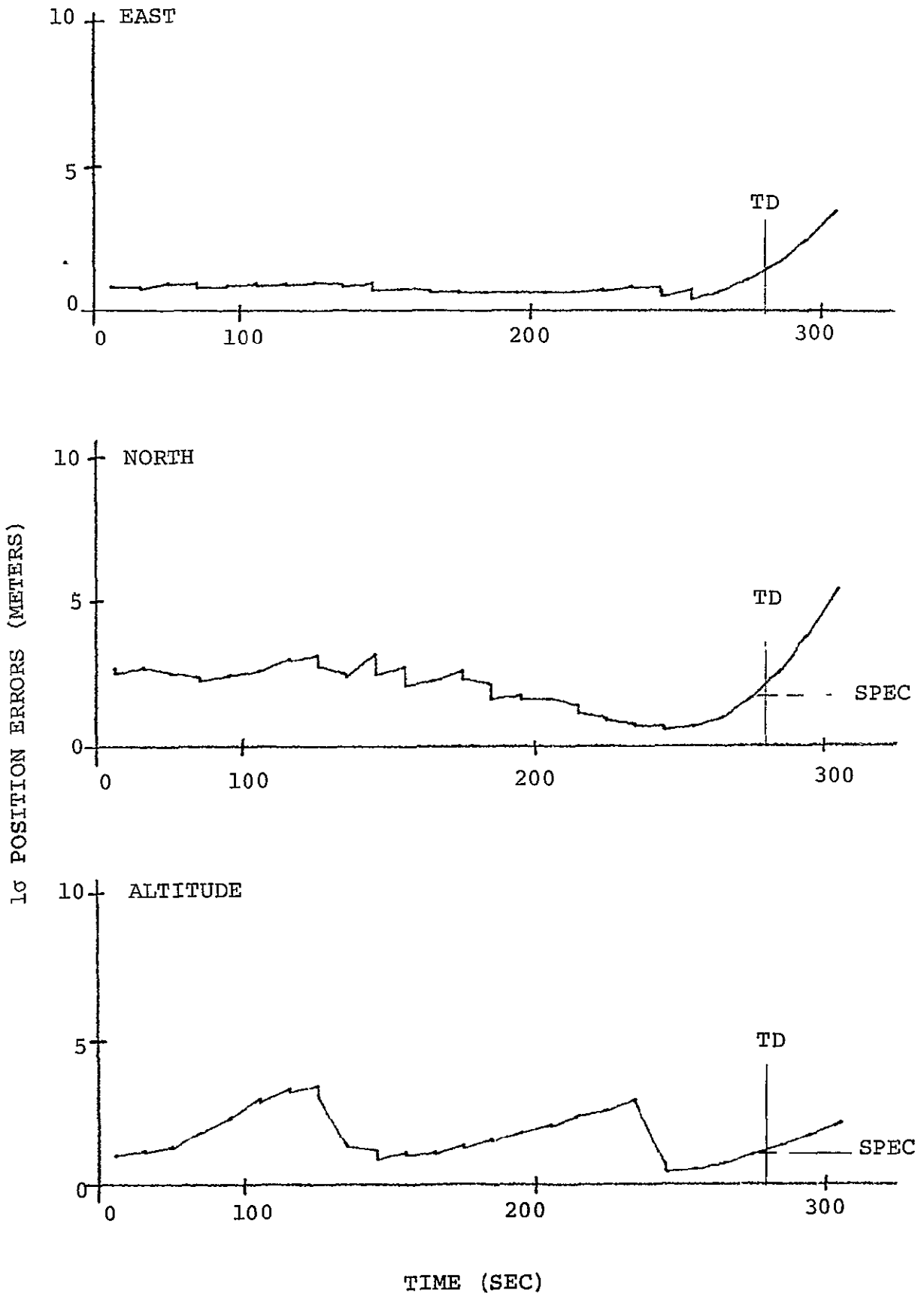


Fig. 4-52 POSITION UNCERTAINTY WITH LATERAL TRANSPONDER  
BESIDE FINAL APPROACH PATH



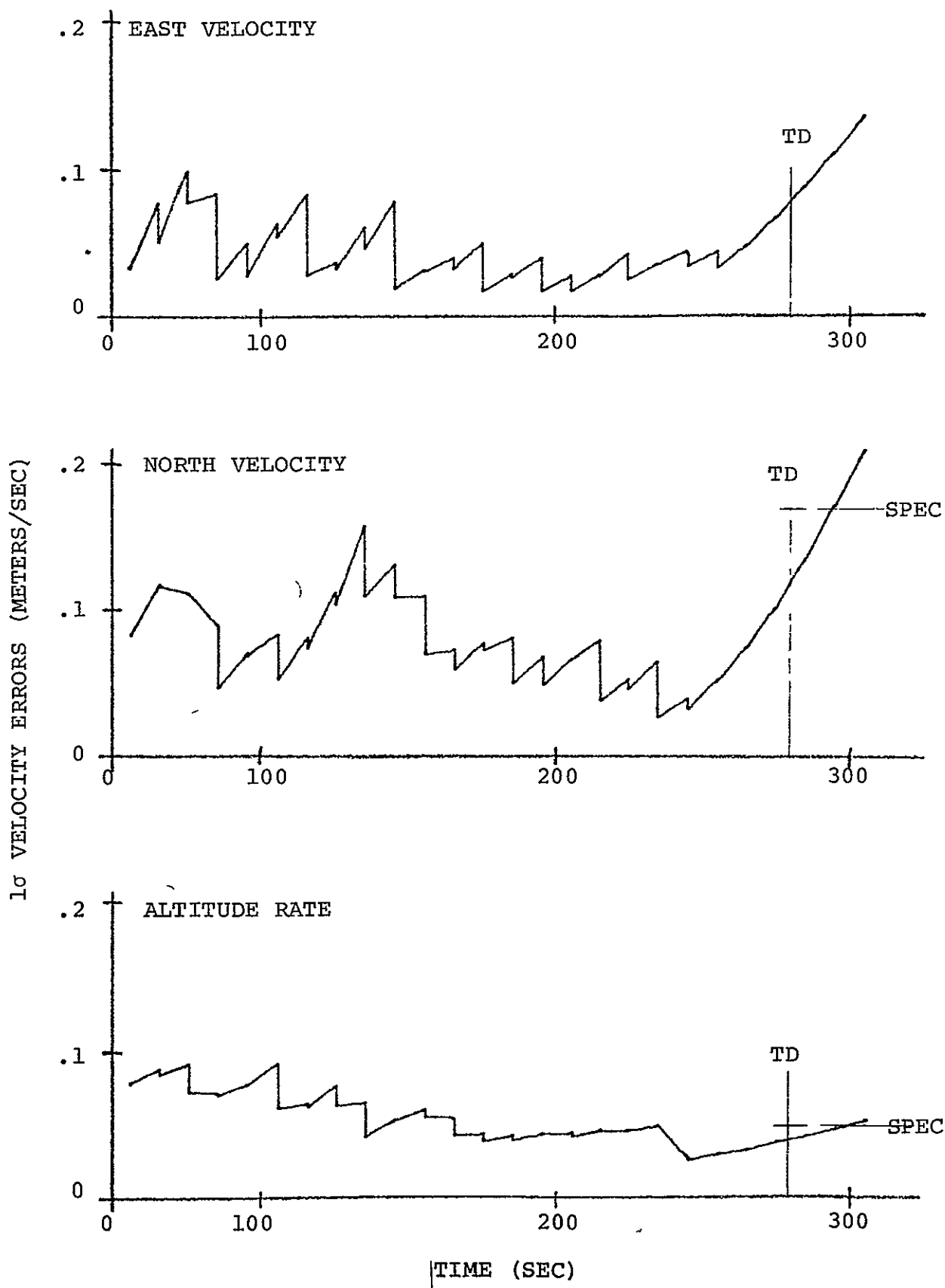


Fig. 4-53 VELOCITY UNCERTAINTY WITH LATERAL TRANSPONDER  
BESIDE FINAL APPROACH PATH

The 5° elevation-angle-cut-off simulation has been repeated with the alternate transponder deployment. The results are presented in Figs. 4-52 and 4-53. The performance almost meets the specification. The last measurement to the lateral transponder occurs 44 sec before touchdown and with excellent cross-runway-measuring geometry.

4.7.2 Recommended Testing. The 1° elevation cut-off angle assumed in the baseline simulation is not based on flight test data. The simulation results indicate that a 2° elevation cut-off angle still permits satisfactory system performance (for the flare altitude-range history simulated). Larger elevation restrictions will require alternate transponder deployment. Clearly, the signal characteristics of the DME must be tested extensively at each instrumented landing site to guarantee satisfactory performance.

It is possible that there is no elevation angle restriction at short ranges with unobstructed line-of-sight. If this is the case, then the recommended lateral transponder placement (3 km to the side of the middle of the runway) provides not only satisfactory touchdown performance but also excellent roll-out lateral navigation. If automatic (Category III-C) roll-out control is a requirement, the DME characteristics at zero altitude should be tested extensively.

#### 4.8 Effect of a Degraded IMU

With three or four IMUs aboard the Space Shuttle, there should be little chance that entry and landing navigation need be conducted with a degraded IMU. Nevertheless, it is of interest to know how sensitive are the performance results to the IMU quality?

One simulation has been run with several IMU errors increased to 3σ values. The three accelerometer biases have been increased to  $1.5 \times 10^{-3}$  meters/sec<sup>2</sup> (150μg). The three g-insensitive gyro drift rates have been increased to  $4.38 \times 10^{-7}$  radians/sec (.09°/hr). The easterly and northerly velocity navigation error after entry have been increased to 30 meters/sec. The platform misalignment after entry about each axis has been increased to 4.5 milliradian. The Kalman filter has not been adjusted to reflect the degraded IMU performance.

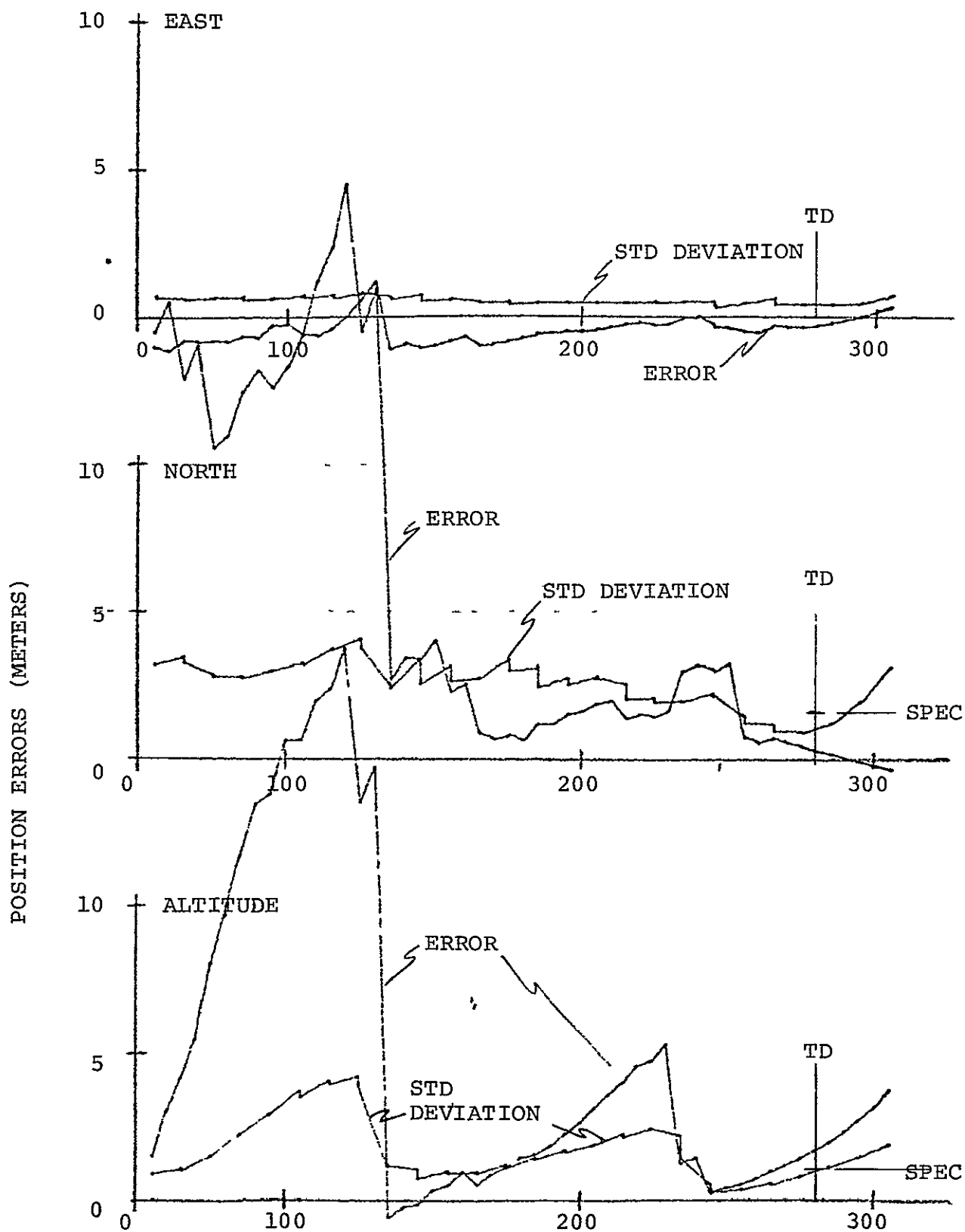


Fig. 4-54 POSITION ERRORS WITH A DEGRADED IMU

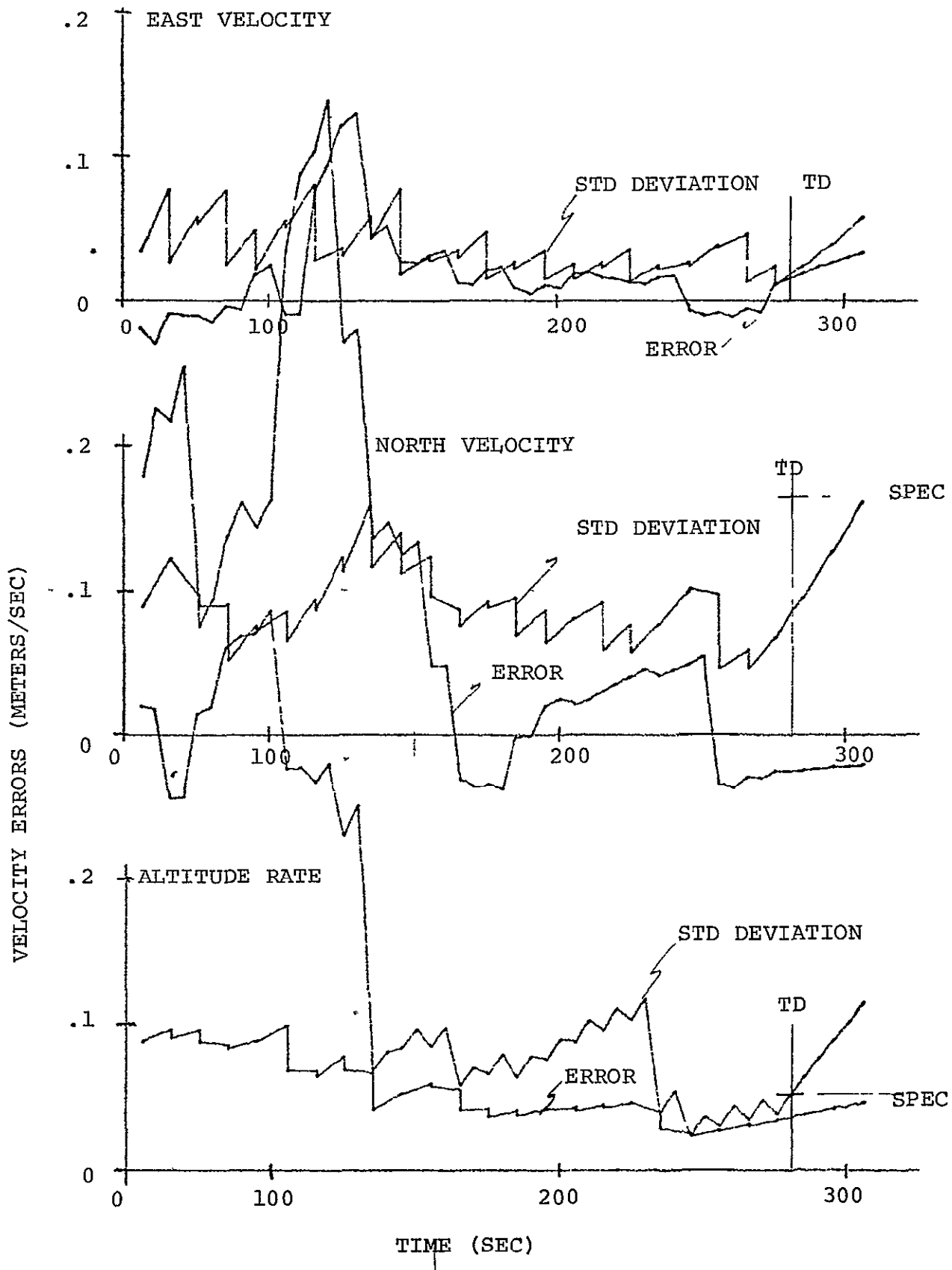


Fig. 4-55 VELOCITY ERRORS WITH A DEGRADED IMU

The simulation results are presented in Figs. 4-54 and 4-55. The curves marked "standard deviation" are the onboard computed 1 $\sigma$  navigation uncertainty. Note these are unchanged from the baseline performance because the Kalman filter is unaware of the degraded IMU. The curves marked "error" are the actual simulated landing navigation errors. It is not surprising that the actual errors generally exceed the onboard computed uncertainty. It is pleasing, however, that the actual performance almost meets the touchdown accuracy specification. Only the altitude is somewhat out-of-spec.

We conclude that the landing navigation system performance is not critically dependent on the assumed IMU performance. A comfortable performance margin exists that can accommodate mildly degraded IMU performance.

## CHAPTER 5

### CONCLUSIONS

Precision DME, aiding the onboard inertial navigation, is all that is required to meet the very stringent Shuttle landing navigation accuracy specification. This can be the same precision DME that is utilized for navigation in other mission phases such as orbital navigation and rendezvous navigation. The commonality of onboard equipment will provide significant cost, weight, volume, and power savings.

An independent source of altitude data is not required. This is a fortunate conclusion, because it was found that barometric altimetry is not sufficiently accurate and radar-altimetry has difficulty with the terrain altitude variation approaching the runway.

The onboard equations for landing navigation have been designed and satisfactory performance has been demonstrated. Initialization logic obtains a DME position fix after the hypersonic entry. The uncertainty in this initial fix is computed as a function of the measurement geometry.

After initialization, a 10-state-variable Kalman filter processes the measured range and delta-range data. It estimates and corrects the errors in indicated position and velocity of the inertial navigation equations. Contributing to the success of the Kalman filter design are the satisfactory choice of a low number of critical state variables, proper treatment of all significant sources of navigation error in modeling these as process and measurement noises, and compensation to avoid difficulties associated with the nonlinear elongation of the measured range.

Satisfactory performance of the Kalman filter has been demonstrated by a five-landing Monte Carlo simulation. The root-mean-squared values of the actual navigation errors are in close agreement with the navigation uncertainty as computed by the onboard Kalman filter. No adjustment of the statistical models used by the filter was necessary to obtain the satisfactory performance. This demonstrates the power of the method of modeling the navigation errors.

Alternate approach patterns have been simulated. With the recommended transponder deployment, the approach pattern has very little influence on the navigation accuracy at touchdown.

Only two transponders can not guarantee satisfactory landing navigation performance. With an unfavorable approach direction the performance can be quite bad.

The minimum number of working transponders necessary to guarantee satisfactory performance is three. Two transponders must be deployed under the final approach path. 1) the inner approach transponder may be placed between 2 km and 4 km from the nominal touchdown location, 2) the outer approach transponder may be placed between 9 km and 15 km from the runway. A third transponder must be placed to the side to provide cross-runway measuring geometry. This lateral transponder can be placed opposite the middle of the runway, the maximum distance to the side that is free of line-of-sight restrictions. This placement permits utilization for either approach direction. A lateral distance of 3 km gives satisfactory performance.

Failure tolerance requires some level of equipment redundancy. Three or four onboard interrogators will be required. Satisfactory transponder-network reliability is obtained by placing a second transponder at each required zone: inner approach, outer approach and lateral. This is a total of six transponders required to instrument a single approach direction and ten transponders required to instrument both approach directions. (The count is not twelve because the lateral transponders serve both approach directions). Separating the redundant transponders provides more geometric diversity. This permits landing navigation performance better than the specification in the normal situation (no failures) and performance equal to the specification in the case of single transponder failures in every critical pair.

Initialization of the landing navigation after a normal deorbit and entry can be delayed safely until the Shuttle is within 150 km of the airport. However, a once-around abort (with no navigation update since launch) could require earlier initialization. There is no problem due to communication blackout or due to radio horizon limitations. The initial position fix can be obtained utilizing the transponders at the airport. No additional transponders need be deployed to insure satisfactory initialization performance. This is another advantage of the precision-DME-aided inertial navigation. Alternate concepts, such as those utilizing the proposed scanning beam microwave landing aid, require additional sources of navigation updating because the terminal area navigation aids

do not have adequate range for the landing navigation initialization.

The highest measurement rate is required during the inner approach transponder overflight. This highest rate is one range-plus-delta-range measurement pair every 0.6 sec, and is within the capability of the CR-100 DME design. Normally on final approach the measurement rate is one pair every 10 sec. During the long glide from the initial position fix to the turn onto final approach, one pair every 30 sec is satisfactory.

If the delta-range circuits are not procured, then additional transponders must be deployed to meet the touchdown navigation accuracy specification. The cost of the additional transponders will more than offset the unit cost savings for a range-only DME design. Therefore the delta-range circuits should be included in the precision DME specification for Shuttle. The DME accuracy required is range-measurement bias 0.3 meter  $1\sigma$ , multipath range random error  $0.9 \cos \epsilon$  meter  $1\sigma$  ( $\epsilon$  is elevation angle), other range random error 0.2 meter  $1\sigma$ , delta-range measurement random error 0.1 meter  $1\sigma$ .

No real-time temperature, pressure, and humidity data need be telemetered to the Shuttle for propagation corrections. Standard-day data will provide a sea-level propagation uncertainty of 50 parts per million, and this is adequate for satisfactory landing navigation performance.

The location of the transponders must be surveyed and stored in the onboard computer. A survey accuracy of 10 parts per million of range from the runway is required.

Satisfactory rollout navigation is provided if a reliable signal can be obtained from the lateral transponder at zero elevation angle. If no signal is available from the lateral transponder below an elevation angle of  $2^\circ$ , the touchdown accuracy is adequate, but the subsequent growth of the cross-runway inertial navigation errors may require that the pilot be able to "see to taxi". If the elevation cut-off is as large as  $5^\circ$ , alternate lateral transponder placement is required.

The landing navigation system performance is not critically dependent on the assumed IMU performance. A comfortable performance margin exists that can accommodate mildly degraded IMU performance.



APPENDIX A

ERROR STATE FORMULATION OF THE ESTIMATION PROBLEM

There are two alternate methods of formulating the state estimation problem, namely:

1. Estimate the total state vector, including the vehicle position and velocity.
2. Estimate the error state vector, including the errors in the indicated position and velocity of the inertial navigation system.

The advantages of the error-state formulation can be seen by a simple single-channel flat-earth example. The vehicle dynamics are modeled by

$$\begin{aligned}\dot{r} &= v \\ \dot{v} &= a \\ \dot{a} &= n_a\end{aligned}\tag{A-1}$$

where  $r$ ,  $v$  and  $a$  are the vehicle position, velocity, and acceleration, and where  $n_a$  is the vehicle jerk. We might model the jerk as white noise. Or we could recognize that the jerk is finite and correlated, and therefore introduce more state variables modeling the vehicle dynamics. This is a modeling decision which must be made using engineering judgement.

An integrating accelerometer is available to measure the vehicle velocity. The measurement  $v_{\text{meas}}$  is modeled by

$$v_{\text{meas}} = v_a + n_v\tag{A-2}$$

where  $v_a$  is the velocity information in the accelerometer and  $n_v$  is the measurement noise (such as due to quantization). The dynamics of the velocity information in the accelerometer are modeled by

$$\begin{aligned}\dot{v}_a &= a_{bias} + a \\ \dot{a}_{bias} &= n_{a_{bias}}\end{aligned}\tag{A-3}$$

where  $a_{bias}$  is the accelerometer bias and  $n_{a_{bias}}$  is a white noise chosen to model the fluctuations in the accelerometer bias.

A radio-derived position measurement  $r_{meas}$  is available. It is modeled by

$$r_{meas} = r + r_{bias} + n_r\tag{A-4}$$

where  $r_{bias}$  is the radio bias and  $n_r$  is the measurement noise. The radio bias is modeled by

$$\dot{r}_{bias} = n_{r_{bias}}\tag{A-5}$$

where  $n_{r_{bias}}$  is a suitable white noise.

In the total state formulation one constructs a Kalman filter to accept the two sources of measurement ( $v_{meas}$  and  $r_{meas}$  and to estimate the elements of the state vector ( $r, v, a, \dots, v_a, a_{bias}, r_{bias}$ ). The dimension of the state vector depends on how many state variables were assigned to modeling the vehicle dynamics. To achieve high accuracy, the velocity measurements must be incorporated frequently.

The alternate formulation is in terms of error quantities. One must add to the system of equations a calculation of accelerometer-derived position. This is simply the integration of the equation

$$\dot{r}_a = v_{meas}\tag{A-6}$$

This calculation is actually performed in the inertial navigation subsystem. One defines the error variables

$$e_{r_a} = r_a - r\tag{A-7}$$

$$e_{v_a} = v_a - v \quad (A-8)$$

For the purpose of filter construction, one considers that there is only one source of measurement. This is the difference between the accelerometer-derived position and the radio-derived position.

$$\Delta r = r_a - r_{\text{meas}} \quad (A-9)$$

This measurement can be expressed in terms of the error state variables as

$$\Delta r = (r + e_{r_a}) - (r + r_{\text{bias}} + n_r) \quad (A-10)$$

$$\Delta r = e_{r_a} - r_{\text{bias}} - n_r$$

Note the difference measurement is not a function of the actual position  $r$  (under the linear assumptions of this simple example).

The differential equations governing the error state variables are:

$$\begin{aligned} \dot{e}_{r_a} &= e_{v_a} + n_v \\ \dot{e}_{v_a} &= a_{\text{bias}} \\ \dot{a}_{\text{bias}} &= n_{a_{\text{bias}}} \\ \dot{r}_{\text{bias}} &= n_{r_{\text{bias}}} \end{aligned} \quad (A-11)$$

In the error state formulation one constructs a Kalman filter to accept the difference measurements ( $\Delta r$ ) and to

estimate the elements of the error state vector ( $e_{ra}$ ,  $e_{va}$ ,  $a_{bias}$ ,  $r_{bias}$ ). Note that the problem of modeling the vehicle dynamics does not exist with the error state formulation.

From this example one can see two significant advantages of the error state formulation over the total state formulation:

1. The vehicle acceleration and its derivatives are not required state variables. Hence one does not need to model and estimate the vehicle acceleration and its derivatives. This reduces the dimension of the required state space.
2. The error state variables are all slowly varying. Hence the computations required to implement the Kalman filter may be performed at a slow sample rate with no significant loss in system accuracy. This eases considerably the computer speed requirement.

While acceleration is not a required state variable, it is an important driving noise, because vehicle acceleration causes the gyros to precess, thus changing the platform alignment. Therefore the power-spectral density of the white noise, which is assumed to be driving the three platform alignment state variables, must be made a suitable non-stationary function of the vehicle acceleration.

## APPENDIX B

### ON TREATING DELTA-RANGE AS A RANGE-RATE MEASUREMENT

A delta-range measurement is sometimes referred to as a range-rate or velocity measurement. Assuming such a measurement is a range-rate measurement, one might design a Kalman filter formulation based on a range-rate difference measurement

$$\dot{z}_r = \dot{r}_{\text{calc}} - \dot{r}_{\text{meas}} \quad (\text{B-1})$$

where  $\dot{r}_{\text{calc}}$  is the expected range-rate based on the indicated velocity of the inertial navigation equations

$$\dot{r}_{\text{calc}} = \underline{b} \cdot \underline{v}_{\text{INS}} \quad (\text{B-2})$$

and  $\dot{r}_{\text{meas}}$  is by definition

$$\dot{r}_{\text{meas}} = \Delta r_{\text{meas}} / \Delta t \quad (\text{B-3})$$

With this approach, a new source of error is introduced, because  $\dot{r}_{\text{meas}}$  is not a true instantaneous range-rate measurement.

To illustrate this point, ignore all the other sources of error. Consider only the finite-measurement-time effect. The range rate is

$$\dot{r} = \underline{b}(t) \cdot \underline{v}(t) \quad (\text{B-4})$$

The change in range during an interval  $\Delta t$  is

$$\Delta r = \int_{-\Delta t/2}^{\Delta t/2} \underline{b}(t) \cdot \underline{v}(t) dt \quad (\text{B-5})$$

where  $t = 0$  is defined to be at the center of the interval.  
If one replaces  $\underline{v}(t)$  and  $\underline{b}(t)$  by their Taylor series expansions

$$\underline{v}(t) = \underline{v}(0) + \underline{a}(0) t + \underline{J}(0) \frac{t^2}{2} + \dots \quad (\text{B-6})$$

$$\underline{b}(t) = \underline{b}(0) + \dot{\underline{b}}(0) t + \underline{b}(0) \frac{t^2}{2} + \dots \quad (\text{B-7})$$

it can be shown that the range change is

$$\Delta r = \underline{b}(0) \cdot \underline{v}(0) \Delta t + [\underline{b}(0) \cdot \underline{v}(0) + 2\dot{\underline{b}}(0) \cdot \underline{a}(0) + \underline{b}(0) \cdot \underline{J}(0)] \Delta t^3 / 24 + \text{higher order terms} \quad (\text{B-8})$$

It is evident that  $\Delta r / \Delta t$  (as an estimate of range rate at  $t=0$ ) is in error by a velocity

$$\dot{e}_r = [\underline{b}(0) \cdot \underline{v}(0) + 2\dot{\underline{b}}(0) \cdot \underline{a}(0) + \underline{b}(0) \cdot \underline{J}(0)] \Delta t^2 / 24 \quad (\text{B-9})$$

An estimate of the maximum values of each of the three error terms may be computed by assuming that the vehicle is 1000 meters from the transponder, flying at a velocity with components of 100 m/sec perpendicular and parallel to the line-of-sight, accelerating at  $1g$  as in a  $45^\circ$  banked turn ( $10 \text{ m/sec}^2$ ), and having a roll rate of  $0.1 \text{ radian/sec}$ . The three terms within the brackets of Eq. (B-9) are then

$$\underline{b} \cdot \underline{v} = v^3 / r^2 = 1 \text{ m/sec}^3 \quad (\text{B-10})$$

$$2\dot{\underline{b}} \cdot \underline{a} = 2g v / r = 2 \text{ m/sec}^3 \quad (\text{B-11})$$

$$\underline{b} \cdot \underline{J} = \dot{\phi} g = 1 \text{ m/sec}^3 \quad (\text{B-12})$$

Thus, a maximum value for the sum of the three terms could be  $4 \text{ m/sec}^3$ . From Eq. (B-9), the resulting range-rate measurement would have an error, depending on the choice of  $\Delta t$ , as shown in Table B-1.

$\Delta t(\text{sec})$	$e_{\dot{r}} \text{ (m/sec)}$
.3	0.02
1.0	0.17
3.0	1.50
10.0	16.7

Table B-1 Maximum range-rate-measurement error due to vehicle and line-of-sight kinematics.

Clearly, to suppress these kinematic errors, the delta-range measurement interval  $\Delta t$  should be chosen small. However, choosing  $\Delta t$  small amplifies the random error of the range-rate measurement

$$e_{\dot{r}} = e_{\Delta r} / \Delta t \quad (\text{B-13})$$

With a delta-range random error  $e_{\Delta r}$  of 0.1 meter and  $\Delta t = 1$  sec, the range-rate error is .1 m/sec. With  $\Delta t = 0.3$  sec the range-rate error is .3 m/sec. An appropriate value for  $\Delta t$  appears to be in the range 0.3 to 1.0 sec.

One practical advantage of the range-rate-measurement formulation is that the range-rate calculated from the velocity of the inertial navigation equations, as in Eq. (B-2), is easily calculated to a precision of 0.1 meter/sec. It will be more difficult to calculate the change in range, as in Eq. (3-102), to an accuracy of 0.1 meter.

The disadvantage of the range-rate formulation is the inability to select a large delta-range interval  $\Delta t$  to improve the measurement "signal-to-noise ratio".

# APPENDIX C

## COMPENSATION FOR NONLINEAR ELONGATION OF MEASURED RANGE

The equations for utilizing a range measurement to improve the state vector estimate can be written in the following form: The basic range difference measurement is

$$z_r = r_c - r_m \quad (C-1)$$

where  $r_c$  is the calculated range based on the estimated position and  $r_m$  is the range measured by the DME. The measurement gradient vector is

$$\underline{h}_r = \begin{bmatrix} \underline{b}_E \\ 0 \end{bmatrix} \quad (C-2)$$

where  $\underline{b}_E$  is the estimated direction from the transponder to the vehicle and  $0$  indicates that all other elements of the  $\underline{h}$  vector are zero. The assumed measurement-error variance is calculated as

$$r_r = \sigma_b^2 + r_c^2 \sigma_p^2 f^2(h) + \sigma_m^2 \cos^2 \epsilon + \sigma_r^2 \quad (C-3)$$

The standard deviations of transponder bias  $\sigma_b$ , propagation error  $\sigma_p$ , multipath random error  $\sigma_m$ , and other random error  $\sigma_r$  are the error contributors accounted for in Eq. (C-3).

Given the calculated values of  $z_r$ ,  $\underline{h}_r$ , and  $r_r$ , the Kalman filter incorporates the measurement according to

$$\underline{k} = P^- \underline{h} / (\underline{h}^T P^- \underline{h} + r) \quad (C-4)$$

$$\hat{\underline{x}}^+ = \hat{\underline{x}}^- + \underline{k} (z - \underline{h}^T \hat{\underline{x}}^-) \quad (C-5)$$



$$P^+ = (I - \underline{k} \underline{h}^T) P^- (I - \underline{k} \underline{h}^T)^T + \underline{k} r \underline{k}^T \quad (C-6)$$

However, if the measurement variance  $r$  is very small compared with the position estimate covariance, nonlinear effects can prevent proper filter convergence. Consider the geometry and coordinate axes shown in Fig. C-1.

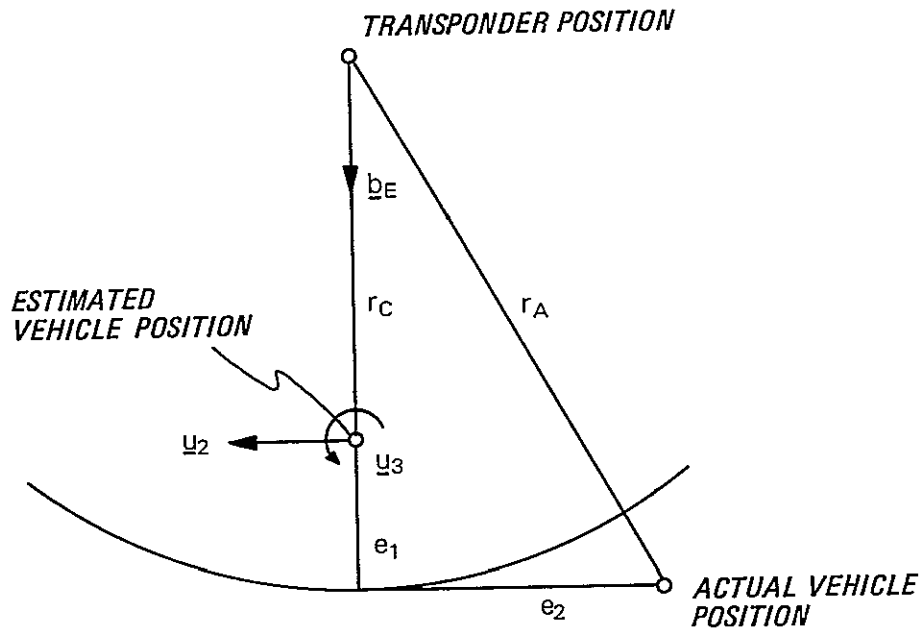


Fig. C-1 Nonlinear elongation of measured range

The actual range  $r_A$  may be expressed in terms of the estimated range  $r_C$  and the estimate error components  $e_1$ ,  $e_2$ ,  $e_3$  as

$$r_A = [(r_C + e_1)^2 + e_2^2 + e_3^2]^{1/2} \quad (C-7)$$

This may be expanded in a Taylor series. Retaining only the linear and quadratic terms yields

$$r_A = r_C + e_1 + (e_2^2 + e_3^2)/2r_C \quad (C-8)$$

The measurement difference is

$$z_r = r_C - (r_A + e_r) \quad (C-9)$$

$$z_r = -e_r - e_1 - (e_2^2 + e_3^2)/2r_C \quad (C-10)$$

where  $e_r$  is the error in the range measurement.

In many applications with very precise DME ( $e_r$  of the order of 1 meter), the quadratic term can easily be the largest contributor to the measurement difference. Consider a position error  $e_2$  of 4 km and a range  $r_C$  of 200 km. The quadratic term equals

$$e_2^2/2r_C = 40 \text{ meters} \quad (C-11)$$

It is clear that if such a 40 meter measurement difference were assumed to be evidence of a 40 meter error  $e_1$ , then the subsequent filter performance would be unpredictable, to say the least. Such an assumption underlies the linear Kalman filter implementation, Eqs. (C-1) through (C-6).

We have developed a satisfactory remedy to this problem. Assume the random measurement error  $e_r$  has mean zero and variance  $r_r$ . Similarly, assume that the components of the estimation error have mean zero and standard deviations  $\sigma_1, \sigma_2, \sigma_3$ . The mean value of the measurement difference Eq. (C-10) is then

$$E[z_r] = -(\sigma_2^2 + \sigma_3^2)/2r_C \quad (C-12)$$

Note in spite of the unbiased estimate errors and measurement error, the measurement difference is biased by the quadratic term. This nonlinear bias should be subtracted from the basic measurement difference. That is, a modified measurement difference  $z_r'$  should be utilized in Eq. (C-5).

$$z_r' = z_r + (\sigma_2^2 + \sigma_3^2)/2r_C \quad (C-13)$$

The random measurement error  $e_r$  is assumed to be statistically independent of the position-estimate-error components  $e_1, e_2, e_3$ . Therefore, the mean square value of the measurement difference Eq. (C-10) is

$$E[z_r^2] = r_r + \sigma_1^2 + E[e_1(e_2^2 + e_3^2)]/r_C + E[(e_2^2 + e_3^2)^2]/4r_C^2 \quad (C-14)$$

To evaluate the indicated expectations, an assumption about the probability distribution of the error vector  $[e_1, e_2, e_3]$  must be made. Assume a Gaussian distribution consistent with the mean zero and component standard deviations  $\sigma_1, \sigma_2, \sigma_3$  already assumed. Under the Gaussian assumption, the first expectation term can be shown to be zero, leaving

$$E[z_r^2] = r_r + \sigma_1^2 + E[e_2^4 + 2e_2^2 e_3^2 + e_3^4]/4r_C^2 \quad (C-15)$$

Assume the  $\underline{u}_2$  and  $\underline{u}_3$  directions have been chosen so that  $e_2$  and  $e_3$  are uncorrelated. Under the Gaussian assumption, uncorrelated also implies  $e_2$  and  $e_3$  are statistically independent. Therefore, the expectation of the product  $e_2^2 e_3^2$  is the product of the expectations. Also under the Gaussian assumption the expectation of the fourth powers of  $e_2$  and  $e_3$  can be evaluated in terms of the standard deviations. As a result it can be shown

$$E[z_r^2] = r_r + \sigma_1^2 + (3\sigma_2^4 + 2\sigma_2^2 \sigma_3^2 + 3\sigma_3^4)/4r_C^2 \quad (C-16)$$

The variance of the measurement difference is

$$\text{Var}[z_r] = E[z_r^2] - (E[z_r])^2 \quad (C-17)$$

$$\text{Var}[z_r] = r_r + \sigma_1^2 + (\sigma_2^4 + \sigma_3^4)/2r_C^2 \quad (C-18)$$

The variance  $\sigma_1^2$  may be expressed in terms of the covariance  $P$  and measurement gradient  $\underline{h}$  as

$$\sigma_1^2 = \underline{h}^T P \underline{h} \quad (C-19)$$

$$\text{Var}[z_r] = \underline{h}^T P \underline{h} + r_r + (\sigma_2^4 + \sigma_3^4)/2r_C^2 \quad (C-20)$$

The desired effect of the a priori variance  $r_r$  utilized in the standard filter Eq. (C-4) and Eq. (C-6) is the prevention of a high weighting  $\underline{k}$  from being placed on errors in the measurement

difference  $z$  not related to the linear geometry represented by the  $\underline{h}$  vector. The desired effect can be accomplished by adding the variance of the nonlinear effect to the variance  $r_r$  of the DME errors. That is, a modified variance  $r'_r$  should be utilized in Eqs. (C-4) and (C-6)

$$r'_r = r_r + (\sigma_2^4 + \sigma_3^4)/2r_C^2 \quad (C-21)$$

It was assumed that the  $\underline{u}_2$  and  $\underline{u}_3$  directions were chosen so that  $e_2$  and  $e_3$  are uncorrelated. The variances of  $e_2$  and  $e_3$  may be computed in terms of the covariance matrix  $P_{rr}$  of the position estimate in the following manner: One pair of orthogonal unit vectors both orthogonal to the estimated transponder-to-vehicle direction  $\underline{b}_E$  is

$$\underline{u}_a = \text{unit } (\underline{b}_E \times \underline{r}_{VE}) \quad (C-22)$$

$$\underline{u}_b = \underline{u}_a \times \underline{b}_E$$

where  $\underline{r}_{VE}$  is the estimated vehicle position. The two-dimensional covariance matrix  $P'$  in the space spanned by  $\underline{u}_a$  and  $\underline{u}_b$  is

$$P' = \begin{bmatrix} P_{aa} & P_{ab} \\ P_{ab} & P_{bb} \end{bmatrix} \quad (C-23)$$

where

$$\begin{aligned} P_{aa} &= \underline{u}_a^T P_{rr} \underline{u}_a \\ P_{ab} &= \underline{u}_a^T P_{rr} \underline{u}_b \\ P_{bb} &= \underline{u}_b^T P_{rr} \underline{u}_b \end{aligned} \quad (C-24)$$

The variances  $\sigma_2^2$  and  $\sigma_3^2$  of the uncorrelated errors  $e_2$  and  $e_3$  are the eigenvalues of  $P'$ . Solving the eigenvalue problem, one finds

$$\sigma_2^2, \sigma_3^2 = (P_{aa} + P_{bb} \pm [(P_{aa} - P_{bb})^2 + 4P_{ab}^2]^{1/2})/2 \quad (C-25)$$

In summary, to compensate for the nonlinear elongation of the measured range, insert Eqs. (C-22), (C-24), (C-25), (C-13), and (C-21) between standard Eqs. (C-3) and (C-4).

A summary of these compensation equations is presented in Table C-1.

Estimated line-of-sight coordinates

$$\underline{u}_a = \text{unit } (\underline{b}_E \times \underline{r}_{VE})$$

$$\underline{u}_b = \underline{u}_a \times \underline{b}_E$$

Position covariance normal to estimated line-of-sight

$$P_{aa} = \underline{u}_a^T P_{rr} \underline{u}_a$$

$$P_{ab} = \underline{u}_a^T P_{rr} \underline{u}_b$$

$$P_{bb} = \underline{u}_b^T P_{rr} \underline{u}_b$$

Eigenvariances of normal covariance

$$\sigma_2^2, \sigma_3^2 = (P_{aa} + P_{bb} \pm [(P_{aa} - P_{bb})^2 + 4 P_{ab}^2]^{1/2})/2$$

Modified range difference measurement

$$z_r' = z_r + (\sigma_2^2 + \sigma_3^2)/2r_C$$

Modified assumed measurement error variance

$$r_r' = r_r + (\sigma_2^4 + \sigma_3^4)/2r_C^2$$

Table C-1 Compensation for Nonlinear Elongation of Measured Range

## REFERENCES

- 1-1 T.S. Bettwy, "Integration of RF Functions for Navigation, Voice and Data Communication", presented at the Space Shuttle Integrated Electronics Technology Conference, NASA/MSC, 12 May 1971.
- 1-2 D.G. Krenz, M.B. Cronkhite, F. Lisenbe, C. Mehr, "CR-100 Implementation Study for Space Shuttle", Final Technical Report 16-1, Cubic Corp., San Diego, California, 24 June 1971.
- 1-3 C.W. Clark and D.A. Dyer, "Shuttle Touchdown Requirements", NASA/MSC Internal Note EG-71-10, 30 April 1971.
  
- 2-1 D.G. Krenz, M.B. Cronkhite, F. Lisenbe, C. Mehr, "CR-100 Implementation Study for Space Shuttle", Final Technical Report 16-1, Cubic Corp., San Diego, California, 24 June 1971.
- 2-2 W. L. Swingle, "IMU Error Models for Shuttle", NASA/MSC Memo EG5-71-69, 22 March 1971.
- 2-3 E.M. Copps, N.A. Carlson, J.P. Green, F.H. Martin, H.R. Morth, W.S. Widnall, et al, "Design of the Completely Integrated Reference Instrumentation System (CIRIS)", Contract Final Report, Intermetrics, May 1970.
- 2-4 S.P. Livingston and W. Gracy, "Tables of Airspeeds, Altitude and Mach Number Based on the Latest Values for Atmospheric Properties and Physical Constants", NASA TN D-822, August 1961.
- 2-5 O.G. Sutton, The Challenge of the Atmosphere, Harper & Brothers, New York, 1961.
- 2-6 M. Kayton and W.R. Fried, eds., Avionics Navigation Systems, Chapter 11, "Air-Data Systems", John Wiley & Sons, New York, 1969.
- 2-7 W.A. Baker, "Air Data System and Altimetry Errors", Boeing Coordination Sheet 6-8201-109, 15 May 1969.
- 2-8 C.Q. Cook, Deputy Chief Engineer, Flight Guidance & Control, McDonnell-Douglas, Long Beach, Calif., private communication, 2 June 1971.

- 2-9 T. Mathison, Supervisor, Boeing Flight Test, Seattle, Wash., private communication, 26 May 1971.
- 2-10 W. Irwin, Boeing Flight Test, Seattle, Wash., private communication, 27 May 1971.
- 2-11 D. J. Bourque, "Evaluation of Barometric Altimetry at Low Altitude," Final Report, N65-23770, FAA, Atlantic City, N.J., January 1965.
- 2-12 "Radio Altimeter", ARINC Characteristic 552, Aeronautical Radio, Inc., Annapolis, Md., issued 1 November 1962, reprinted with supplements 1-4, 8 January 1970.
- 2-13 D. Maurer, Bendix Avionics, Ft. Lauderdale, Fla., private communication, 25 May 1971.
- 2-14 J. Maynard, Honeywell, Inc., Minneapolis, Minnesota, private communication, 27 May 1971.
- 2-15 G.B. Litchford, "The 100 ft. Barrier", Aeronautics and Astronautics (AIAA), July 1964.
  
- 3-1 P.D. Joseph, "Automatic Rendezvous, Part II: On-board Navigation for Rendezvous Missions", Course notes for "Space Control Systems - Attitude, Rendezvous, and Docking", UCLA Engineering Extension, Los Angeles, 1964.
- 3-2 R.E. Kalman, "A New Approach to Linear Filtering and Prediction Problems", Trans. ASME, Series D. Journal of Basic Engineering, Vol. 82, March, 1960.
- 3-3 R.H. Battin, Astronautical Guidance, McGraw-Hill, New York, 1964.
- 3-4 S.F. Schmidt, "A Square Root Formulation of the Kalman Filter with Random Forcing Functions", Sect. 3 of "Final Report for Missions Analysis Guidance Study", Report 68-23 by Analytical Mechanics Assoc. Inc. for Goddard Space Flight Center, January, 1969.
- 3-5 P.G. Kaminski, A.E. Bryson, and S.F. Schmidt, "Discrete Square Root Filtering: A Survey of Current Techniques", submitted for publication in IEEE Transactions on Automatic Control, 1971.

- 3-6 C. Broxmeyer, Inertial Navigation Systems, McGraw-Hill, New York, 1964
- 3-7 G.R. Pitman, etc., Inertial Guidance, John Wiley & Sons, New York, 1962.
- 3-8 E.M. Copps, N.A. Carlson, J.P. Green, F.H. Martin, H.R. Morth, W.S. Widnall, et al, "Design of the Completely Integrated Reference Instrumentation System (CIRIS)", Contract Final Report, Intermetrics, May 1970.
- 3-9 W.L. Swingle, "IMU Error Models for Shuttle", NASA/MSC Memo EG5-71-69, 22 March 1971.
- 3-10 N.A. Carlson, "Position From Three Simultaneous Range Measurements", unpublished notes, Intermetrics, 27 April 1970.
  
- 4-1 R. Morth and W.S. Widnall, "Space Guidance Development, Approach and Landing Study Results", Contract Final Report, Intermetrics, 26 March 1971.
- 4-2 D. Moore, "Terminal Area Subsonic Guidance", presented at the Guidance and Control Division Space Shuttle Task Review Meeting, NASA/MSC, 15 April 1971.
- 4-3 L.A. McGee, G.L. Smith, D.M. Hegarty, R.B. Merrick, T.M. Carson, and S.F. Schmidt, "Navigation for Space Shuttle Approach and Landing Using an Inertial Navigation System Augmented by Various Data Sources", presented at the Space Shuttle Integrated Electronics Technology Conference, NASA/MSC, 11 May 1971.
- 4-4 C.R. Price, "Space Shuttle Terminal-Area Navigation Accuracy Versus Onboard Antenna Coverage and Ground Transponder Location", Internal Note MSC-EG-71-14, NASA/MSC, 26 May 1971.
- 4-5 B.R. Bean, "Tropospheric Refraction", Chapter in Advances in Radio Reserach, Vol. 1, Academic Press, London, 1964.